Exceptional Events Study: Final Report

Utah Department of Environmental Quality Research Grant
Project Period: July 15th, 2014 to January 14th 2016
Principle Investigator: John C. Lin (University of Utah)
Contributors: Derek V. Mallia, Adam Kochanski

Courtesy of Derek Mallia, University of Utah

1. Introduction

Biomass burning is known to be responsible for releasing large quantities of carbon monoxide (CO), particulate matter (PM), precursors of ozone (O_3), and other species relevant for air quality into the atmosphere. Effects of biomass burning not only affect the area local to the fire, but may also impact the air quality of regions downwind from the fire. The 2012 western U.S. wildfire season was characterized by significant wildfire activity across much of the American West, with potential adverse impacts on Utah's air quality. Previous studies have already shown that enhancement in CO, $PM_{2.5}$, and O_3 concentrations can occur at sites downstream of the wildfires [*DeBell et al.*, 2004; *Dempsey*, 2013; *Jaffe et al.*, 2013; *Jaffe and Wigder*, 2012; *Sapkota et al.*, 2005].

In addition to biomass burning, the emission and transport of dust can cause degraded air quality in Utah. *Hahnenberger and Nicoll* [2012] found that "dust events produced elevated PM_{10} concentrations exceeding the Environmental Protection Agency's (EPA) National Ambient Air Quality Standards (NAAQS) on 16 days since 1993, or 0.9 per year". *Steenburgh et al.* [2012], combining meteorological and satellite datasets, produced a climatology of dust events for the Wasatch Front. Both studies pointed to the southwestern U.S. as the origin of dust for the population centers along the Wasatch in northern Utah, but these studies did not develop a modeling framework capable of quantifying the exact impact each event had on PM concentrations in northern Utah.

Elevated concentrations of O_3 and PM can cause significant health problems, especially to the elderly, young children, and people with lung and heart diseases [*Gauderman et al.*, 2004; *Weinmayr et al.*, 2010]. Exposure to adverse air quality caused by dust events and wildfires is expected to continue into the foreseeable future, due to rapid population rise taking place in Utah [*Utah Foundation*, 2014] combined with a general increase in wildfire activity across the western U.S. [*Dennison et al.*, 2014] from climate change [*Westerling et al.*, 2006]. This trend is anticipated to continue, with the average maximum air temperature increasing for these regions even under the IPCC's moderate emission scenario [*IPCC*, 2007]. Dust production in the future will also likely increase, due to a combination of shifting climate [*Munson et al.*, 2011] and heightened anthropogenic activities (e.g., agriculture, energy exploration/development, recreation) [*Field et al.*, 2009; *Neff et al.*, 2008], which would arise from the increased population dust source regions. The U.S. Census has clearly identified western U.S. as the region of the most rapid population growth in the nation [*U.S. Census Bureau*, 2010].

Despite advances in the published literature mentioned above, these studies generally lacked the ability to provide a *quantitative assessment* of the impact of wildfires or dust events on air quality, instead relying upon statistical or qualitative approaches . Here we present and expand upon a modeling framework that will allow us to quantitatively assess the impacts of wildfire and dust events on air quality, along with ability to identify the exact source regions of emissions that are responsible for degrading air quality during these events.

2. Methodology

In order to quantify the impacts of wildfires and dust events, we coupled the Weather Research and Forecasting model [*Skamarock* et al., 2008] with the Stochastic Time-Inverted Lagrangian Transport model [*Lin et al.*, 2003] (WRF-STILT). WRF is a Eulerian non-hydrostatic atmospheric mesoscale model, which can simulate a variety of meteorological phenomena. Backward trajectory ensembles, which are used to simulate concentrations of air quality relevant species, were generated from STILT, which is driven by wind fields provided by WRF (Fig. 1). STILT backward trajectories incorporate the effects of turbulent dispersion within the planetary boundary layer via stochastic processes. This modeling framework has been use for the interpretation of CO_2, CO and other trace gases, while also being applied to chemically active species. Careful coupling between WRF and STILT has been carried out, with an emphasis towards physical consistency and mass conservations [*Nehrkorn et al.*, 2010]. Technical details about STILT can be found in *Lin et al.*, [2013].

Using a receptor-orientated framework, information from the STILT trajectories, combined with wildfire emission inventories or a dust parameterization can be used to determine the direct influences of upwind wildfire and dust emissions on the receptor. This makes STILT a valuable tool for interpreting atmospheric concentrations at observation sites. In order to determine the upwind source regions, the STILT calculates the surface flux footprint $f(\mathbf{x}_r, \mathbf{t}_r|x_i, y_j, t_m)$ for a receptor at location $\mathbf{x}_r$ and time $\mathbf{t}_r$ to an upwind source at (x_i, y_j) and prior time t_m can be estimated from the WRF-STILT backward trajectories [*Lin et al.*, 2003; *Skamarock* et al., 2008]. The footprint is simply the measure of the upwind surface influences for a receptor as determined by the STILT backward trajectories. The footprint has units of mixing ratio per unit surface flux and is a function of the number of Lagrangian particles within the planetary boundary layer (PBL) for some upwind location, as seen in the equation below:

$$f\left(\boldsymbol{x_r}, \boldsymbol{t_r}\middle|x_i, y_j, t_m\right) = \frac{m_{air}}{h\bar{\rho}(x_i, y_j, t_m)} \frac{1}{N_{tot}} \sum_{p=1}^{Ntot} \Delta t_{p,i,j,k} \qquad \text{(Eq. 1)}$$

where m_{air} is the molecular weight of air, h is the height of the volume in which the surface fluxes are diluted over (surface influence volume), ρ is the average density for all particles, N_{tot} is the total number of particles, and $\Delta t_{p,i,j,k}$ is the amount of time a particle p spends within the surface influence volume at location (x_i, y_j) and time t_m [*Lin et al.*, 2003; *Wen et al.*, 2012; *Kim et al.*, 2013; *Lin et al.*, 2013]. Any surface fluxes that occur within the PBL are assumed to be rapidly mixed within the surface influence volume, which is taken to extend from the surface to a height of 0.5 z_i (one half of the PBL height). Previous studies have indicated that simulated STILT footprints were insensitive to the exact value of the column height *"h"* as long as h was between 10 and 100% of the PBL height [*Lin et al.*, 2003]. By combining the footprint with a flux source, STILT can determine the atmospheric concentration contribution of that source.

A potential limitation of the STILT framework arises from the fact that the emitted tracers are treated as chemically inert and do not undergo any chemical transformations in the atmosphere while being transported. In order to mitigate this problem the STILT framework has

been extended to include chemical transformations ("STILT-Chem") [*Wen et al.*, 2012]. STILT-Chem runs in "receptor-oriented" or "time-reversed" mode simulates the air parcel ensembles starting from the receptor location and track them backward in time, elucidating upstream influences on the receptor. Due to nonlinearities in the chemical transformations, they are then applied to the air parcels in a forward-time sense.

The Lagrangian modeling framework presented here could make for a valuable tool for understanding events exceeding NAAQS levels and yield quantitative evidence for demonstrating exceptional events.

3. Results

The objective of the Exceptional Events project was to construct and apply a modeling framework that combines Lagrangian atmospheric modeling with emission inventories and dust parameterizations in order to determine the contributions of wildfires and dust emissions to the air quality of the population centers of northern Utah.

3.1 Quantifying the effects of wildfires on CO and $PM_{2.5}$ concentrations along the Wasatch Front

The first objective of the Exceptional Events project was to model primary $PM_{2.5}$ and CO concentrations along the Wasatch Front during the 2012 western U.S. wildfire season in order to determine whether enhanced concentrations and exceedances in NAAQS could be attributed to upwind wildfires. As discussed in section 2, we used the WRF-STILT modeling framework in order to determine the contributions of wildfires towards enhancements and exceedances of air quality relevant species along the Wasatch Front. An initial analysis for Salt Lake City (SLC) resulted in a peer-reviewed scientific publication attached with this report [*Mallia et al.*, 2015], which quantified the impacts of fire emissions on CO and $PM_{2.5}$ concentrations at SLC. This study represents a first step towards formulating a Lagrangian modeling framework that could quantify the impacts of fire emissions on air quality in a major urban center. Technical details behind the modeling CO and $PM_{2.5}$ concentrations, emission inventories used, along with model validation of WRF and STILT can be found in *Mallia et al.*, [2015].

The summer of 2012 was an active wildfire season for the western U.S., with over 6 Tg of CO and 80 Tg of CO_2 emitted, which was nearly double the average emission for a typical wildfire season. Significant wildfire activity during the 2012 wildfire season was generally focused across central Idaho, Utah, northern California, and Washington, which are all areas comprising potential upwind source regions of SLC (Fig. 2). There was also increased local wildfire activity within Utah that was not seen in previous wildfire seasons. Simulations of CO and $PM_{2.5}$ were carried out for June through September, which encompassed the majority of the wildfire activity seen in Fig. 3.

Simulations for the 2012 wildfire season showed frequent wildfire impact on elevated CO and CO_2 concentrations at SLC (Fig. 3a). There were three distinct episodes of prolonged wildfire impacts for June 24th-July 5th, August 6th-24th, and September 19th-24th. Similar trends

were also seen in $PM_{2.5}$ concentrations at Hawthorne (Fig. 4). The mean CO enhancement from non-negligible episodes (≥5 ppb) was 28.6 ppb, with a median of 17.2 ppb. This was greater than the 2007 western U.S. wildfire season, which reported a mean and median of 23.4 and 12.6 ppb, respectively. The most intense wildfire episodes (>95% percentile) were characterized by median values of 122.3 ppb (Fig. 5).

Fig. 6a shows the WRF-STILT model footprint, which shows the potential upwind source regions for air arriving at SLC. As expected, the majority of these source regions are located to the west of Utah as a result of the predominant flow from mid-latitude westerlies. The footprint strength decreases the further away from SLC, as air parcels disperse and mix upward and away from the surface. Wildfires in Idaho had the largest contributions towards wildfire CO concentrations in SLC, with 39.1% of the contributions coming from this particular source region in 2012 (Fig. 7). The majority of these contributions in Idaho came from 3 large complex fires (Mustang, Halstead and Trinity fires) located in the Salmon River Mountains (Fig. 6b). Wildfires across Utah also played a significant role towards contributions in SLC at 33.5%, with contributions predominantly coming from 5 fires in central Utah (Fig. 6b and 7). Wildfire in California+Nevada played a moderate role (19.2%) while wildfires in the Pacific Northwest and the eastern Rockies played a minimal role with only 4.5% and 3.3% of the contributions coming from these regions, respectively (Fig. 7). Contributions from the southwestern U.S. were considered negligible with contributions under 1%. $PM_{2.5}$ simulations showed similar contributions by source region as Fig. 7.

WRF-STILT simulations for CO performed reasonably well when compared against observed values in SLC for August and September (Fig. 3b and 3c). There was increased wildfire activity starting around August 6th and was fairly persistent through August 25th (Fig. 3a and 3b). The daily-averaged $PM_{2.5}$ concentrations (both modeled and observed) are shown in Fig. 4 and 8a for SLC. As seen in the 3-hourly CO plots, there were increased wildfire contributions from August 7th - 25th and September 12th – 23rd for the daily averaged plots for $PM_{2.5}$ (observations were missing between August 22nd and September 6th). The enhancements seen in the observed concentrations of $PM_{2.5}$ generally match up well with the STILT-modeled wildfire contributions seen in Fig 4 and 8a.

While the WRF-STILT model seemed acceptable in resolving periods of increased wildfire contributions for August and September 2012 when compared to the observations, additional verification was looked at to confirm model results. Speciated particulate matter data from Hawthorne was used as an additional data source to verify days of wildfire contributions, as previous work has shown that biomarkers such as organic carbon and potassium are useful for identifying wood burning.

The increased wildfire contribution as suggested by the WRF-STILT matches up, in general, with the elevated concentrations of speciated organic carbon and potassium ions (Fig. 8b) between August 8th –25th, and for September 13th – 23rd. The general agreement between modeled $PM_{2.5}$ from wildfires against the observed $PM_{2.5}$, organic carbon and potassium ions suggests that the modeled wildfire contributions is likely realistic in a qualitative sense.

However, the exact contributions suggested by the WRF-STILT to enhancements of $PM_{2.5}$ cannot be regarded as quantitative, due to the lack of consideration of secondary formation processes and chemical reactions that affect $PM_{2.5}$. This could also explain the discrepancies between the modeled wildfire contributions and the observed $PM_{2.5}$ contributions.

In addition to the work presented above, other observation sites along the Wasatch Front were looked at to see if the results were consistent with *Mallia et al.*, [2015]. The WRF-STILT simulations below follow the same framework discussed in *Mallia et al.*, [2015]. Technical details behind these model simulations can also being found in this paper.

The large impacts of wildfires on observed $PM_{2.5}$ concentrations extended beyond SLC, which included Logan, Provo, Brigham City, Ogden, and Tooele (Fig. 9). Logan had the largest enhancements, especially during the months of August and September (Fig. 10). This is likely the result of Logan's closer proximity to the Idaho fires, which was one of the dominants area of fire activity during these months (Fig. 11). It should be noted that the observed enhancements seen at Logan match well with the modeled wildfire contributed $PM_{2.5}$ concentrations. While the timing of the observed and modeled enhancements of $PM_{2.5}$ correlate well, there is a slight underestimation of $PM_{2.5}$ concentrations during the middle of September. As of right now its unclear whether this discrepancy is the result of transport error, lack of plume rise formulation, lack of chemistry, and/or an underestimation in the emission fields.

Provo, which was the southern most site in our study, showed the largest enhancements of $PM_{2.5}$ concentrations during the month of June and July from wildfires in central Utah (Fig. 12). This is likely a result of Provo being closer to the central Utah wildfires, which peaked in intensity during the months of June and July. The magnitude of the observed $PM_{2.5}$ enhancements roughly matched with the modeled wildfire contributed $PM_{2.5}$ concentrations, though there was an underestimation of 10 $\mu g/m^3$ during the middle of September, which was present at all of the observation sites discussed previously. As a whole, the extended work presented here was consistent with the results found in *Mallia et al.*, [2015].

From this study we were able to conclude that the STILT model can (1) reasonably resolve CO and $PM_{2.5}$ concentrations within the Salt Lake Valley and along the Wasatch Front, (2) wildfires can have large, episodic impacts on $PM_{2.5}$ and CO concentrations, and (3) the WRF-STILT model was able capture the timing and magnitude of wildfire contributions when compared to observations. However, there were some underestimations in model results during the month of September, which may be related to a lack of a plume rise parameterization in the WRF-STILT modeling framework. Ultimately, this work also lays the groundwork for future back-trajectory wildfire studies, which will need to include wildfire plume rises. This study also lays the groundwork for state agencies to prove exceptional events to EPA when the NAAQS is violated.

3.2 Simulations of O_3 concentrations using STILT-Chem

We have completed a month-long simulation of chemically active pollutants, with Salt Lake City as the receptor (Fig. 13). The comparison suggests that STILT-Chem is capable of

capturing both the timing and diurnal cycle of pollution plumes even in the middle of a highly urbanized region likely Salt Lake City. However, we also see that this simulation fails to capture peaks in the observed O_3. We suspect that this is due to the lack of fire emissions in this simulation. At least part of the "missing O_3" in the simulation is due to the contribution from fires, which were especially active during Aug 2012.

3.3 Quantifying the effects wind-blown dust along the Wasatch Front

Until recently, it has been difficult to directly quantify the impacts of dust events on Utah's air quality as it requires the ability to explicitly separate dust from anthropogenic sources. Based on WRF-STILT, we developed a modeling framework that can separate the effects of natural dust sources from anthropogenic sources. A similar methodology that was employed in *Mallia et al.*, [2015] was used here to separate anthropogenic produced $PM_{2.5}$ from natural dust sources during high-wind events. The events chosen here (March 30th and April 27-28th 2010) were considered severe, with $PM_{2.5}$ concentrations exceeding > 200 μg/m^3 with visibility that was reduced to less than ¼ 1-km [*DAQ* 2010a; *DAQ* 2010b].

Currently, no dust emission inventory exists for the Great Basin. Thus, an existing dust model was needed to generate dust emissions for the times of interest. *Tong et al.* [2011] recently developed a dust emission model (FENGSHA), which was used to estimate dust emissions across the U.S. and is currently used within the latest version of CMAQ (CMAQ 5.0) (http://www.camq-model.org). The vertical flux of dust (gm^{-2} s^{-1}) can be calculated by the following equation:

$$F = \sum_{i,j} K \times A \times \frac{\rho}{g} S_i \times SEP \times u_* \times \left(u_*^2 - u_{*ti,j}^2\right) \times E_i \quad \text{for } u_* > u_{*_t} \quad \text{(Eq. 2)}$$

where i is the landuse type, j is the soil type. The various components of Eq. 2 are explained below: K represents the ratio of the vertical flux to horizontal sediment, which is dependent on the clay content (%) and calculated as the following [*Tong et al.*, 2010; *Fu et al.*, 2014]:

$$K = \begin{cases} 10^{.136[clay\,\%]-6} & for\ clay\% < 20\% \\ .0002 & for\ clay\% \geq 20\% \end{cases} \quad \text{(Eq. 3)}$$

A is the particle supply limitation (set to value of 3 following recommended value in CMAQ), ρ is the air density, g is the gravitational constant, S is the area of landuse type i. SEP is the soil erodibility factor, which is defined as the following:

$$SEP = 0.08 \times clay\% + 1.00\ x\ silt\% + 0.12 \times sand\% \quad \text{(Eq. 4)}$$

u_* is the friction velocity, and u_{*_t} is the threshold friction velocity which determines the intensity and the onset of dust emissions. u_{*_t} can be defined as the following:

$$u_{*t} = u'_{*t} \times f_d \times f_m \qquad \text{(Eq. 5)}$$

where u'_{*t} is the threshold friction velocity for loose fine-grained soil with low surface roughness. This variable depends on soil type and varies from .3 to .7, which based on dust studies in the Mojave Desert [*Gillette et al.*, 1980]. f_d is the soil moisture while f_m is the snow cover. Finally, *E* represents the land erodability fraction, which depends on whether the area landuse is classified as barren, cropland, shrubland, or shrubgrass; otherwise *E* is considered to be 0. For this study, we assigned regions of playa as barren, which has the highest erodability factor (.75). It should be noted that the majority of central and western Utah were classified under one of these 4 categories, with the exception of urbanized areas along the Wasatch Front, the Great Salt Lake, and areas associated with rugged terrain (Fig. 14). Clay, silt, and sand %s were obtained from the Soil Information for Environmental Modeling and Ecosystem Management (http://www.soilinfo.psu.edu/index.cgi?soil_data&index.html), instead of using assumed percentages found soil lookup tables.

WRF output, which contains information for landuse and soil types, air density, friction velocity, soil moisture, and snow cover, was used to drive the dust emission model. It should be noted that previous work has shown that the WRF default USGS database (1994) is insufficient for providing realistic landuse and soil type information across much of western Utah [*Massey et al.*, 2014] (Fig. 15). To rectify this issue, WRF was recompiled with the National Landuse Cover 2006 Database (NLCD 2006), which also has a much more realistic representation of landuse and soil type data across western Utah. In addition, a soil and landuse category was added for playa, which covers a significant portion of western Utah (Fig. 15).

Once the dust emission model was run for the March 30th and April 27-28th case studies, the WRF-STILT modeling framework was used to determine the direct contributions towards observed $PM_{2.5}$ concentrations along with validity of the dust emission model employed in the above. In additional, a gravitational settling scheme by *Zender et al.* [2003] was adopted in addition to dry and wet deposition. More information on dry and wet depositions schemes used in the WRF-STILT modeling framework can be found in *Mallia et al.* [2015].

i. April 27th 2010

The first case that investigated in this study was the April 27th 2010 high wind event. This event was characterized by strong winds that preluded the passage of a strong frontal system, which is fairly typical for wind-blown dust. Strong southwesterly winds were widespread across most of western Utah, with wind gusts exceeding 25 m/s along the Wasatch Front. Daily $PM_{2.5}$ concentrations at Rose Park, Hawthorne (SLC), and Cottonwood all exceeded the EPA NAAQS 24-hour standard of 35 μg/m^3 by > 10 μg/m^3.

Prior to the passage of the storm system at 1200 UTC, winds were relatively light (5 m/s) and out of the southeast with no dust emissions occurring across Utah (Fig. 16a). However, as the day progressed, afternoon heating promoted the mixing of strong mid-level winds downward with the approaching storm system at 1800 UTC (Fig. 16b). At this point, the dust

emission model indicated that wind blown dust was being kicked up over the Escalante Desert and Skull Valley. By 2300 UTC, the winds associated with the storm frontal passage had strengthened further with sustained southwesterly winds averaging between 10-15 m/s across much of central and western Utah (Fig. 16c). At this time, dust emissions were maximized across much of central Utah with hotspots including the Escalante Desert, the Lake Sevier (intermittent endorheic lake), and Milford Flats (Fig. 16c). STILT model footprints suggest that air arriving at SLC was likely originating from some of the aforementioned hot spots (Fig. 17). These hot spots were consistent with *Hahnenberger and Nicoll* [2012], who concluded that these areas were major sources of dust according to satellite observations during major high wind events. By 0300 UTC, the lower atmosphere began to decouple from the free atmosphere resulting in a weakening of surface winds across much of Utah (5-10 m/s). In response to the weakening surface winds, dust emissions decreased rapidly across much of Utah (Fig 16d).

The emission model shown in Fig 16 was coupled with the WRF-STILT model to see if our modeling framework could reproduce the elevated observed $PM_{2.5}$ concentrations at Hawthorne during this event. Initial results show that in the most part, the WRF-STILT model was able to replicate the magnitude and duration of April 27th 2010 dust event (Fig. 18). Observations (Fig. 18) indicated that wind-blown dust started being observed around 2100 UTC, which coincided with the initial increase of STILT dust contributed $PM_{2.5}$ concentrations. The dust event within the WRF-STILT model reached its peak intensity at around 0100 UTC the next day with concentrations >250 $\mu g/m^3$, while the observed $PM_{2.5}$ concentrations lagged between 1-2 hours before finally ramping considerably at 0300 UTC the next day. Once the event reached its peak intensity, observed concentrations of $PM_{2.5}$ dropped off significantly, and dropped back down to typical background levels by 1000 UTC. WRF-STILT dust contributed $PM_{2.5}$ showed a similar signature, with $PM_{2.5}$ concentrations dropping off considerably after an hour of reaching its highest concentration. Modeled concentrations of $PM_{2.5}$ dust dropped off completely by 1300 UTC, which was several hours after the final drop off in observed $PM_{2.5}$ concentrations.

Fig. 17a shows that the WRF-STILT footprint was oriented through the SSW relative to SLC, indicate that the southwesterly flow associated with pre frontal passage resulted in air that was originating from central and southwestern Utah. The orientation of the footprint generally remained the same throughout most of the event. WRF-STILT modeled dust $PM_{2.5}$ contributions were relatively low at 2300 UTC (Fig. 19a), which was the likely result of weaker surface winds 4-5 hours back, which is when the backward trajectories would have been crossing central Utah where dust emissions were being (Fig. 16b). At 0300 UTC the next day, dust $PM_{2.5}$ contributions picked up significantly across central and southwestern Utah (Fig.19b). At this "receptor time", trajectories were crossing over these regions at 2200-2300 UTC the previous day, which is when surface winds were the strongest resulting in a greater dust emissions of $PM_{2.5}$ (Fig 16c). The areas with the largest dust $PM_{2.5}$ contributions seen in Fig. 19 were centered over the Sevier Desert, Sevier Lake, and Milford Flats, which were pointed out by *Hahnenberger and Nicoll* [2012] as being hotspots for wind-blown dust.

ii. March 30th 2010

The second case study we investigated was the March 30th 2010 high wind event, which was responsible for multiple exceedances in EPA's NAAQS along the Wasatch Front with $PM_{2.5}$ concentrations averaging > 50 $\mu g/m^3$ over the course of the day. As with the April case study, this event was characterized by strong southerly winds out ahead of a frontal system that was moving in from the northwest, which cleared the Wasatch Front by 0100 UTC on April 28th.

The morning of March 30th at 1400 UTC saw light winds across the northern Wasatch Front, with winds coming out of the south at 5-8 m/s (Fig. 20a). However, as the day progressed (1800 UTC), afternoon heating allowed for the coupling of the free troposphere with the PBL, which mixed down stronger mid-level winds ahead of the frontal system. Due to afternoon mixing, 10-m surface winds accelerated to 10-15 m/s with the flow predominantly coming out of the SW (Fig. 20b) across much of central and western Utah. As a result, dust emissions increased in magnitude across Escalante Desert, the Lake Sevier, and the Milford Flats regions. Surface winds continued to accelerate through 2100 UTC where dust emissions were maximized across the aforementioned regions at 100-250 $\mu g/m^2 s$ (Fig. 20c). By 0100 UTC the next day, the cold frontal passage pushed through SLC steering the surface winds out of the northwest (Fig. 20d). At the same time, winds across central and western Utah began to decelerate as the PBL began to decouple from the free troposphere resulting in a weakening of dust emission across much of Utah.

According to observations at Hawthorne (Fig. 21), concentrations of $PM_{2.5}$ began to increase at ~1800 UTC, which coincides with an increase of surface winds and dust emissions seen in Fig. 20b. $PM_{2.5}$ at Hawthorne continued to rise sharply through 2200 UTC reaching a peak concentration of ~250 $\mu g/m^3$. Modeled concentrations of $PM_{2.5}$ from dust emissions failed to increase significantly during the duration of the event with contributions barely exceeding 10 $\mu g/m^3$ between 1700 – 0100 UTC the next day. After 2300 UTC, observed concentrations for $PM_{2.5}$ decreased sharply through 0100 UTC. STILT modeled $PM_{2.5}$ concentrations remained slightly elevated at 10 $\mu g/m^3$ from 0100 -1900 UTC the next day, which was not reflected in the observations since the observed concentrations of $PM_{2.5}$ at Hawthorne returned to its background concentrations of 5-10 $\mu g/m^3$ by 0100 UTC, which coincides with the passage of the aforementioned frontal system.

WRF-STILT footprints indicated that the synoptic flow was out of the southwest at the start of the event, which is typical before the passage of a frontal system (Fig. 22). However, as the event persisted, winds start to shift towards the W and WNW by 2300 UTC as indicated by the footprint orientated to the west relative to SLC. This coincides with the passage of the frontal system seen in observations Fig. 23, which is also reflected in the surface winds maps from WRF (Fig 20c), though the frontal system lags by approximately 40-km. At 1800 UTC, the STILT footprints indicated that $PM_{2.5}$ should have been picked up across central Utah as emissions were maximized around this time (Fig.22b). However, the trajectories on average take about 3-4 hours to reach central and southwestern Utah (~1400 UTC), which is when dust emissions were at a

relative minimum due weaker surface winds (Fig. 24). This is also reflected in the $PM_{2.5}$ contribution maps, which shows no appreciable amount of dust emissions anywhere (Fig. 25a-b).

At 2300-0300 UTC, the STILT footprint was crossing over western Utah (Salt Flats) (Fig. 22c and d); however, there were no significant amounts of dust being emitted over this region at any point (Fig 20). Surface observations from Mesowest showed that winds were generally out of the NW (Fig. 23), which generally agrees with the footprint shift in direction seen in Fig. 22c-d. WRF-STILT modeled dust $PM_{2.5}$ contributions for this time period showed little $PM_{2.5}$ contributions across the Salt Flats with the exception of gridcell just west of the Great Salt Lake (Fig. 25d). The WRF-STILT footprints and Mesowest surface analysis suggest that the major source region for dust during the March 30 event was likely W and NW of SLC, potentially over the Salt Flats. However, due to possible underestimations of emissions of $PM_{2.5}$ by the dust model, this event was not well captured by WRF-STILT model.

Additional analyses were done on the March 30th 2010 high-wind event in order to determine potential causes of underestimations in dust across the Salt Flats. The first step was to compare soil moisture between the Salt Flats and central Utah where dust emissions were maximized. Previous work in *Massey et al.*, [2014] suggested that WRF has a tendency to overestimate soil moisture by a factor of 2 across the Salt Flats as a result of significant positive biases found in NOAA's reanalysis products, which are generally used as initial boundary conditions for WRF. Correction factors from *Massey et al.*, [2014] were applied to soil moisture across the Salt Flats within this dust emission model; however, no observable differences in emissions were seen in the aforementioned area (not shown). As a result, soil moisture biases within the model could not explain the lack of emissions across the Salt Flats.

However, u'_{*t}, which control u_{*t} , was twice as high for the playa than for central Utah. u'_{*t} was original calculated in CMAQ v5.0 based on a lookup table which determines the strength of u'_{*t} based on the clay % of the soil from *Gillette et al.* [1980]. However, *Tong et al*., [2010] determined that the u'_{*t} calculated by *Gillette et al.* [1980] was overestimated, and opted to go with lower values of u'_{*t}. *Tong et al.* [2011]'s reasoning was that the originally calculated u'_{*t} in *Gillette et al.* [1980] were from dust samples from the Mojave desert, which may not be applicable to other regions across the globe. As a result, we decided to apply the *Tong et al.*, [2011] and *Fu et al*., [2014] u'_{*t} values, which averaged closer to .3 instead of .7.

The new u'_{*t} was applied to the dust emission model, which resulted in greater $PM_{2.5}$ dust emissions over Salt Flats (Fig. 26) for the March 30th 2010 high wind event that was not previously seen before the modification. This modified dust emission model was then coupled with WRF-STILT trajectories in order to generate new simulated concentrations of $PM_{2.5}$ for Hawthorne (Fig. 27). Overall, there were some improvements in the simulated concentrations of $PM_{2.5}$, albeit some underestimation still existed within the modeled results by ~100 $\mu g/m^3$. The duration of the event was sufficiently modeled (4 vs 5 hours), although timing issues still existed. The simulated results missed the timing of the peak observed concentrations by 2-3 hours. Looking at the WRF-STILT dust $PM_{2.5}$ contribution maps reveals (Fig. 28) that modifying the dust emission model resulted in larger contributions from the Salt Flats when compared with the

original run (Fig. 25 and 28b). However, the timing issue seen in Fig. 27 indicates that there may potentially be a timing issue with the WRF-STILT trajectories.

A possible explanation behind the errors seen in the simulated results may be attributed to the orientation of the WRF-STILT footprint at 2300 UTC (Fig. 22c). At this time the WRF-STILT footprint was oriented out in the WSW, even after the passage of the frontal system seen in the MesoWest surface analysis (Fig. 23). MesoWest observations across SLC and western Utah indicate a more NW flow associated with the passage of the frontal system. These differences between the observations and modeled results can be seen in the WRF surface wind fields at 2300 UTC (Fig. 20c) where winds were still coming out of the west, with the cold front lagging over the Great Salt Lake. This suggests that WRF may have some timing issues with passage of the cold front, since WRF did not push the front through until 0000 UTC the next day (Fig. 29). This timing difference in the passage of the frontal system between WRF and MesoWest observations may be a crucial factor behind the lag of increased wind blown $PM_{2.5}$ concentrations in the model with the observed concentrations of $PM_{2.5}$, since the majority of the dust emissions over the Salt Flats were located to the west of SLC, and not to the SW where there was a large gap in emissions between central and western Utah. This can be seen in the dust contributions maps in Fig. 28 where there were only modest contributions over the Salt Flats at 2300 UTC (Fig. 28a), however, as the footprints shifted further north the contributions across the Salt Flats increased significantly (Fig. 28b, 29a, and b). Additional work will likely be needed to improve the timing of the cold frontal passage within the WRF wind fields. This highlights the significance of having very accurate meteorology fields inputted into STILT when dealing potentially distant sources.

4. Conclusions

Presented in this study is a Lagrangian modeling framework that is capable of resolving several exceptional events as defined by the NAAQS. In this study, WRF-STILT model performed adequately in capturing wildfire activity for the summer of 2012 along with the April 27-28 wind-blown dust event. The modeling framework incorporated a variety of sources/sinks for each species in order to determine the wildfire and dust contributions relative to the other sources.

CO concentrations from WRF-STILT compared reasonably against observations in SLC, with the diurnal cycle within SLC being well resolved. However, CO contributions from wildfires were relatively minimal when compared to local anthropogenic contributions and background concentrations. Wildfire influences on $PM_{2.5}$ concentrations along the Wasatch Front were much more significant, with contributions exceeding 15 $\mu g/m^3$ on multiple occasions during the summer of 2012. There were several instances where the EPA's NAAQS were exceeded at Logan according to observations during this period. WRF-STILT simulations were able to replicate periods of elevated concentrations of $PM_{2.5}$, suggesting that wildfires played a major role in exceedances in the NAAQS, which would classify these events as being "exceptional" as defined by the EPA. The WRF-STILT modeling framework also replicated

other wildfire enhancements across the Wasatch Front, further proving the validity of these simulations. The majority of these wildfire influences can be attributed to fires across in Idaho, which accounted for up to 33% of the wildfire contributions, despite being non-local. Contributions from Idaho were especially significant during the months of August and September.

The WRF-STILT modeling framework also did a sufficient job when modeling dust events at SLC. The April 27-28th event was well resolved by WRF-STILT, as the model was able to capture the magnitude and duration of the event. However, the model did show a noticeable lag by about 1-2 hours. The model had a bit more difficulty during the March 30th wind-blown dust event as it was unable to replicate observed concentrations at any point during the event. The orientation of the footprint along with a suspicious lack of emissions over the Salt Flats, which has been identified as a hot spot for dust emissions in previous work, suggested a potential issue with the emission model used within this study. A thorough analysis of the dust emission model suggested that the u'_{*t} was set too high for the salt flats, resulting no dust being emitted across this region. Using the approach discussed in *Fu et al*., [2014], we set the average u'_{*t} to .3 which resulted in greater emissions cross the Salt Flats, while showing no appreciable increases across other regions in Utah. This modification resulted in improvements in the WRF-STILT modeled results, though the simulation had timing issues that can be attributed to a lag in the passage of the frontal system by approximately 1-hour. Regardless, this modification should improve future $PM_{2.5}$ dust simulations over SLC, especially when the source region located over the Salt Flats.

Acknowledgments

This study was made possible by funding from the Utah Department of Environmental Quality and NOAA grant NA130AR4310087. We would like to thank the Utah Department of Environmental Quality for carrying out observations at the Hawthorne site (downloaded from http://www.epa.gov/ttn/airs/airsaqs/) and for providing emission data used in this study. We also would like to specifically thank Chris Pennell and Whiney Oswald for providing us soil type data used for the dust emission modeling. We would also like to thank Shawn Urbanski for providing an emissions inventory for wildfires. D. Mallia gratefully acknowledges the support of the University of Utah's Global Change and Sustainability Center Graduate Fellowship during his first year of graduate studies. The authors also thank Joshua Benmergui for providing scripts that calculate depositional loss and valuable input from Erik Crosman, Deyong Wen, and the University of Utah WRF Users Group. The support and resources from the Center for High Performance Computing at the University of Utah are gratefully acknowledged. The data used to produce the results in this study are available from the corresponding author upon request.

5. References

DeBell, L. J., R. W. Talbot, J. E. Dibb, J. W. Munger, E. V. Fischer, and S. E. Frolking (2004), A major regional air pollution event in the northeastern United States caused by extensive forest fires in Quebec, Canada, *Journal of Geophysical Research-Atmospheres*, *109*(D19).

Dempsey, F. (2013), Forest fire effects on air quality in Ontario: evaluation of several recent examples, *Bulletin of the American Meteorological Society*, *94*, 1059-1064.

Dennison, P. E., S. C. Brewer, J. D. Arnold, and M. A. Moritz (2014), Large wildfire trends in the western United States, 1984–2011, *Geophysical Research Letters*, 2928-2933, doi:doi://10.1002/2014GL059576.

Division of Air Quality (DAQ) (2010a), PM_{10} and $PM_{2.5}$ Exceptional Event –High wind, March 30th 2010. [Available online at http://www http://deq.utah.gov/ProgramsServices/programs/air/exceptionalevents/docs/2013/07Jul/highwindmarch302010.pdf.].

Division of Air Quality (DAQ) (2010b), PM_{10} and $PM_{2.5}$ Exceptional Event –High wind, April 27th, 2010. [Available online at http://www http://deq.utah.gov/ProgramsServices/programs/air/exceptionalevents/docs/2013/07Jul/highwindapril272010.pdf.].

Field, J. P., J. Belnap, D. D. Breshears, J. C. Neff, G. S. Okin, J. J. Whicker, T. H. Painter, S. Ravi, M. C. Reheis, and R. L. Reynolds (2009), The ecology of dust, *Frontiers in Ecology and the Environment*, *8*(8), 423-430, doi:10.1890/090050.

Fu, X., S. X. Wang, Z. Cheng, J. Xing, B. Zhao, J. D. Wang, and J. M. Hao (2014), Source, transport and impacts of a heavy dust event in the Yangtze River Delta, China, in 2011, *Atmos. Chem. Phys.*, *14* 1239–1254.

Gauderman, W. J., E. Avol, F. Gilliland, H. Vora, D. Thomas, and K. Berhane (2004), The effect of air pollution on lung development from 10 to 18 years of age, *New England Journal of Medicine*, *351*, 1057-1067.

Gillette, D.A., J. Adams, A. Endo, D. Smith, and R. Kihl (1980), Threshold velocities for input of soil particles into the air by desert soils. *Journal of Geophysical Research 85. doi: 10.1029/JC085iC10p05621*

Hahnenberger, M., and K. Nicoll (2012), Meteorological characteristics of dust storm events in

the eastern Great Basin of Utah, U.S.A., *Atmospheric Environment*, *60*, 601-612.
IPCC (2007), *IPCC Fourth Assessment Report: Climate Change 2007 (AR4)*, Cambridge University Press.

Jaffe, D. A., N. Wigder, N. Downey, G. Pfister, A. Boynard, and S. B. Reid (2013), Impact of Wildfires on Ozone Exceptional Events in the Western U.S., *Environmental Science & Technology*, *47*, 11065-11072.

Jaffe, D. A., and N. L. Wigder (2012), Ozone production from wildfires: A critical review, *Atmospheric Environment*, *51*, 1-10.

Kim, S., D. Millet, L. Hu, M. Mohr, T. Griffis, D. Wen, J.C. Lin, S. Miller, and M. Longo, (2013) Constraints on carbon monoxide emissions in the United States based on tall tower measurements, *Environmental Science and Technology*, *47*, 8316-8324, doi:10.1021/es4009486.

Lin, J. C., C. Gerbig, S. C. Wofsy, A. E. Andrews, B. C. Daube, K. J. Davis, and C. A. Grainger (2003), A near-field tool for simulating the upstream influence of atmospheric observations: the Stochastic Time-Inverted Lagrangian Transport (STILT) model, *J. Geophys. Res.*, *108*(4493), D003161, doi: 10.1029/2002JD003161.

Lin, J. C., D. Brunner, C. Gerbig, A. Stohl, A. Luhar, and P. Webley (2013), Lagrangian Modeling of the Atmosphere, *AGU Geophysical Monograph*, 200, 349 pp.

Mallia, D. V., J. C. Lin, S. Urbanski, J. Ehleringer, and T. Nehrkorn (2015), Impacts of upwind wildfire emissions on CO, CO_2, and $PM_{2.5}$ concentrations in Salt Lake City, Utah, *Journal of Geophysical Research-Atmospheres*, *120*, 147–166.

Massey, J. D., W. J. Steenburgh, S. W. Hoch, and J. C. Knievel (2014), Sensitivity of Near-Surface Temperature Forecasts to Soil Properties over a Sparsely Vegetated Dryland Region. *J. Appl. Meteor. Climatol.*, **53**, 1976–1995.

Munson, S. M., J. Belnap, and G. S. Okin (2011), Responses of wind erosion to climate-induced vegetation changes on the Colorado Plateau, *Proceedings of the National Academy of Sciences*, *108*(10), 3854-3859, doi:10.1073/pnas.1014947108.

Neff, J. C., A. P. Ballantyne, G. L. Farmer, N. M. Mahowald, J. L. Conroy, C. C. Landry, J. T. Overpeck, T. H. Painter, C. R. Lawrence, and R. L. Reynolds (2008), Increasing eolian dust deposition in the western United States linked to human activity, *Nature Geoscience*, *1*(3), 189-195, doi:10.1038/ngeo133.

Nehrkorn, T., J. Eluszkiewicz, S. C. Wofsy, J. C. Lin, C. Gerbig, M. Longo, and S. Freitas (2010), Coupled Weather Research and Forecasting–Stochastic Time-Inverted Lagrangian Transport (WRF–STILT) model, *Meteorology and Atmospheric Physics, 107,* 51–64.

Sapkota, A., J. M. Symons, J. Kleissl, L. Wang, M. B. Parlange, J. Ondov, P. N. Breysse, G. B. Diette, P. A. Eggleston, and T. Buckley (2005), Impacts of the 2002 Canadian forest fires on

particulate matter air quality in Baltimore City, *Environmental Science and Technology*, *39*(1), 24-32.

Skamarock, W., J. B. Klemp, J. Dudhia, D. O. Gill, D. M. Barker, M. G. Duda, X. Y. Huang, W. Wang, and J. G. Powers (2008), A description of the Advanced Research WRF Version 3, *NCAR Technical Note,* 126-126.

Steenburgh, W. J., J. D. Massey, and T. H. Painter (2012), Episodic Dust Events of Utah's Wasatch Front and Adjoining Region, *Journal of Applied Meteorology and Climatology*, *51*, 1654-1669.

U.S. Census Bureau (2010), United States Census 2010. Geographic products and information, edited.

Tong, D. Q., G. E. Bowker, S. He, D. W. Byun, R. Mathur, and D. A. Gillette (2011), Development of a Windblown Dust Module within the Community Multi-scale Air Quality (CMAQ) Model: Description and Preliminary Applications in the Continental United States, *submitted J. Geophys. Res*.

Utah Foundation (2014), A snapshot of 2050: An Analysis of the projected population change in Utah*Rep. 721*, 19 pp, Utah Foundation, Salt Lake City, UT.

Wen, D., J. C. Lin, D. Millet, A. Stein, and R. Draxler (2012), A backward-time stochastic Lagrangian air quality model, *Atmospheric Environment*, *54*, 373–386, doi:10.1016/j.atmosenv.2012.02.042.

Westerling, A. L., H. G. Hidalgo, D. R. Cayan, and T. W. Swetnam (2006), Warming and earlier spring increase western U.S. forest wildfire activity, *Science*, *313*, 940-943.
Zender, C. S., H. Bian, and D. Newman (2003), Mineral dust entrainment and deposition (DEAD) model: description and 1990s dust climatology, *Journal of Geophysical Research*, *108*(4416), doi:10.1029/2002JD002775.

Zender, C. S., H. S. Bian, and D. Newman (2003), Mineral Dust Entrainment and Deposition (DEAD) model: Description and 1990s dust climatology, *J. Geophys. Res.-Atmos.*, *108*, 4416, doi:10.1029/2002JD002775.

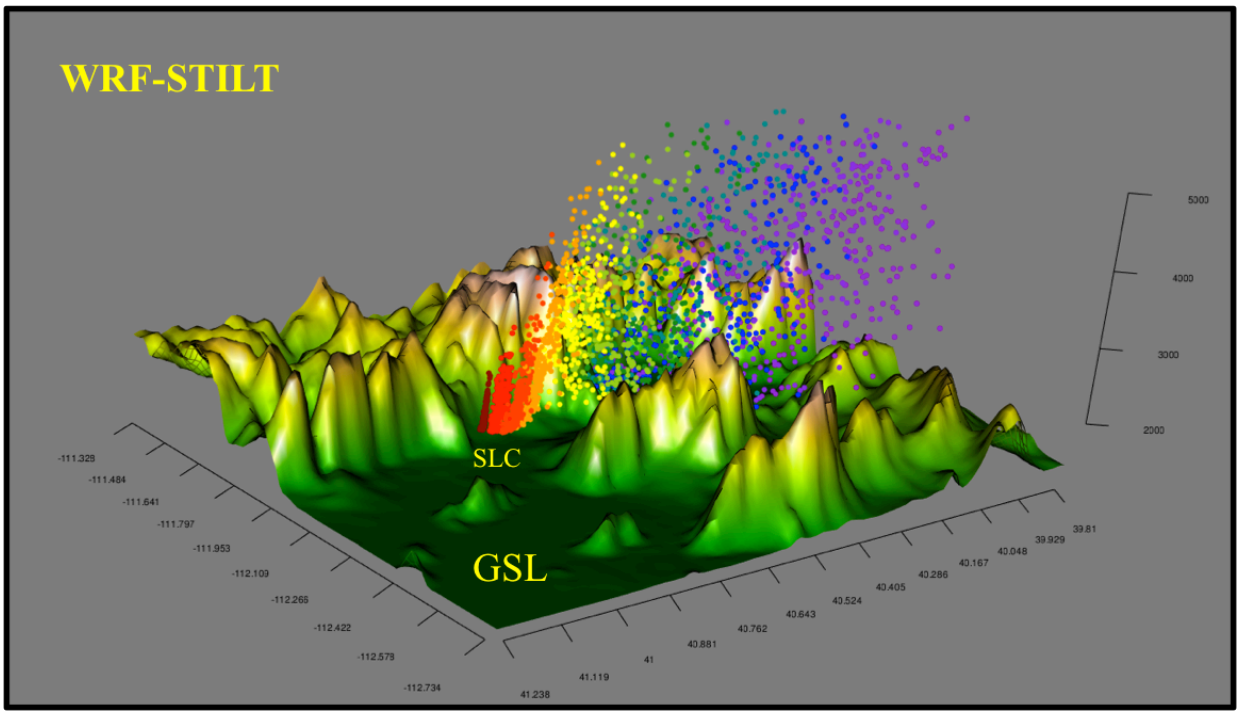

Figure 1. WRF-STILT simulation for July 17th 2012 at 0000 UTC for the Salt Lake area. Cooler colored particles indicate STILT air parcels travelling further back in time from the receptor (located in the Sugarhouse area of Salt Lake City). Trajectories in the particular simulation go backwards in time for 3 hours (purple).

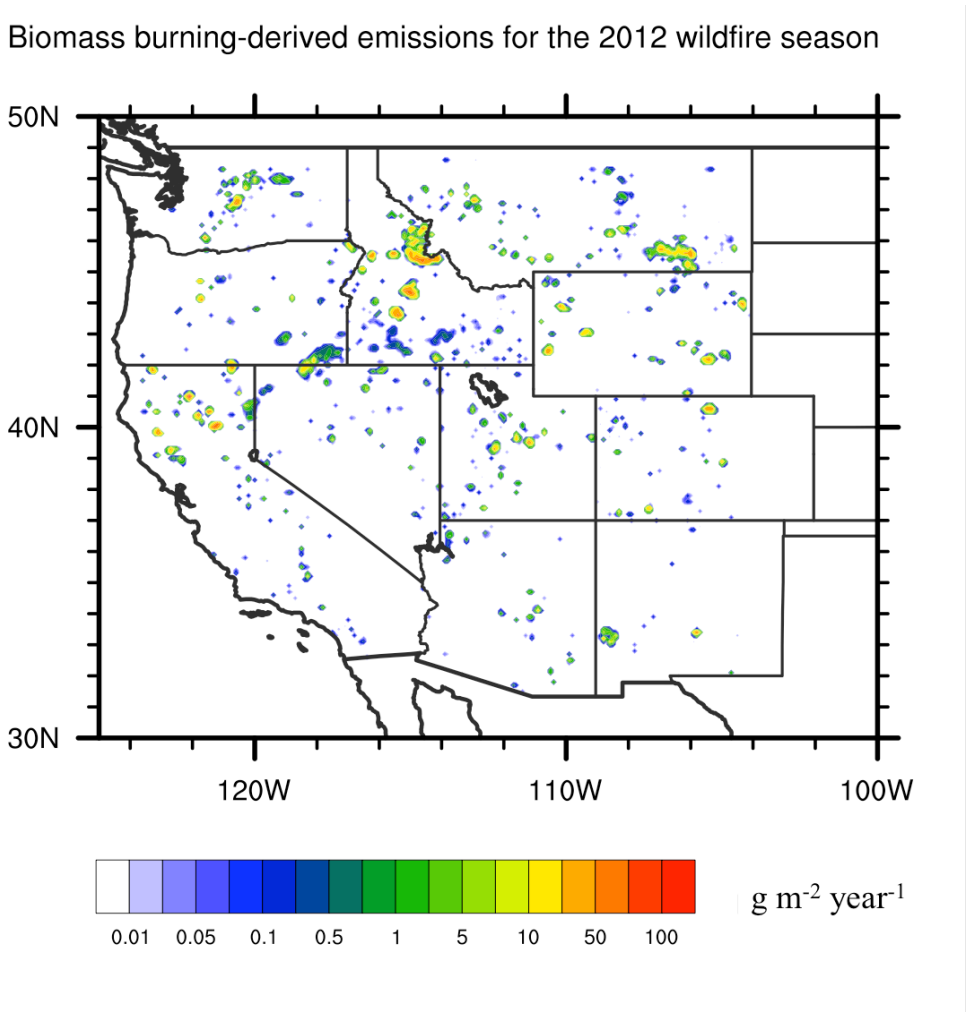

Figure 2. Total wildfire emissions for the 2012 wildfire seasons from the Wildland Fire Emissions Inventory.

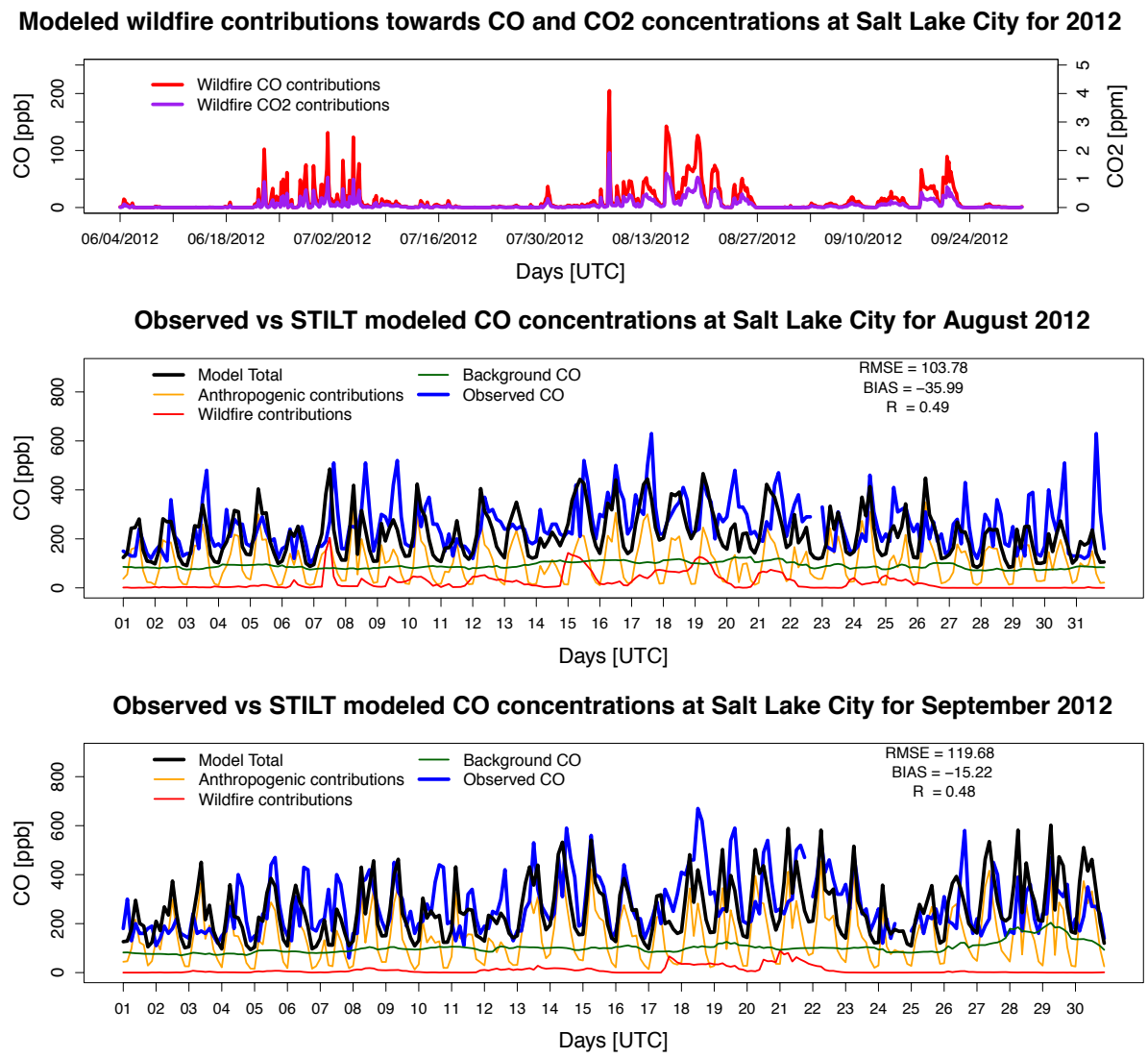

Figure 3. (a) Modeled wildfire CO contributions for the entire 2012 western U.S. wildfire season. (b and c) STILT-simulated and observed CO concentrations for SLC, zoomed in on August and September 2012. The black line is model total while the orange, red, and dark green lines are contributions from anthropogenic and fire emissions and the background CO, respectively. The blue line is the observed CO concentrations for SLC.

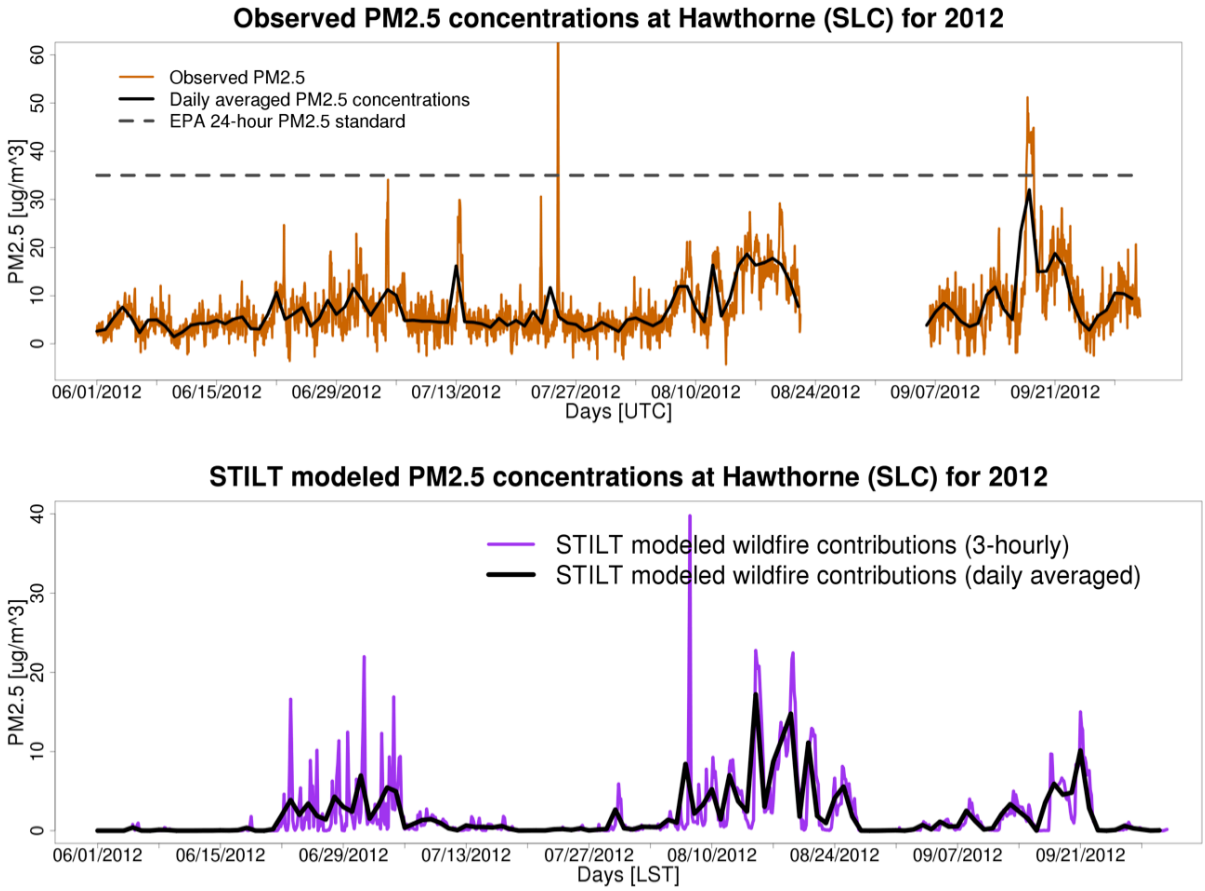

Figure 4. Observed concentrations of $PM_{2.5}$ (a) vs. modeled wildfire contributed $PM_{2.5}$ concentrations (b) at SLC.

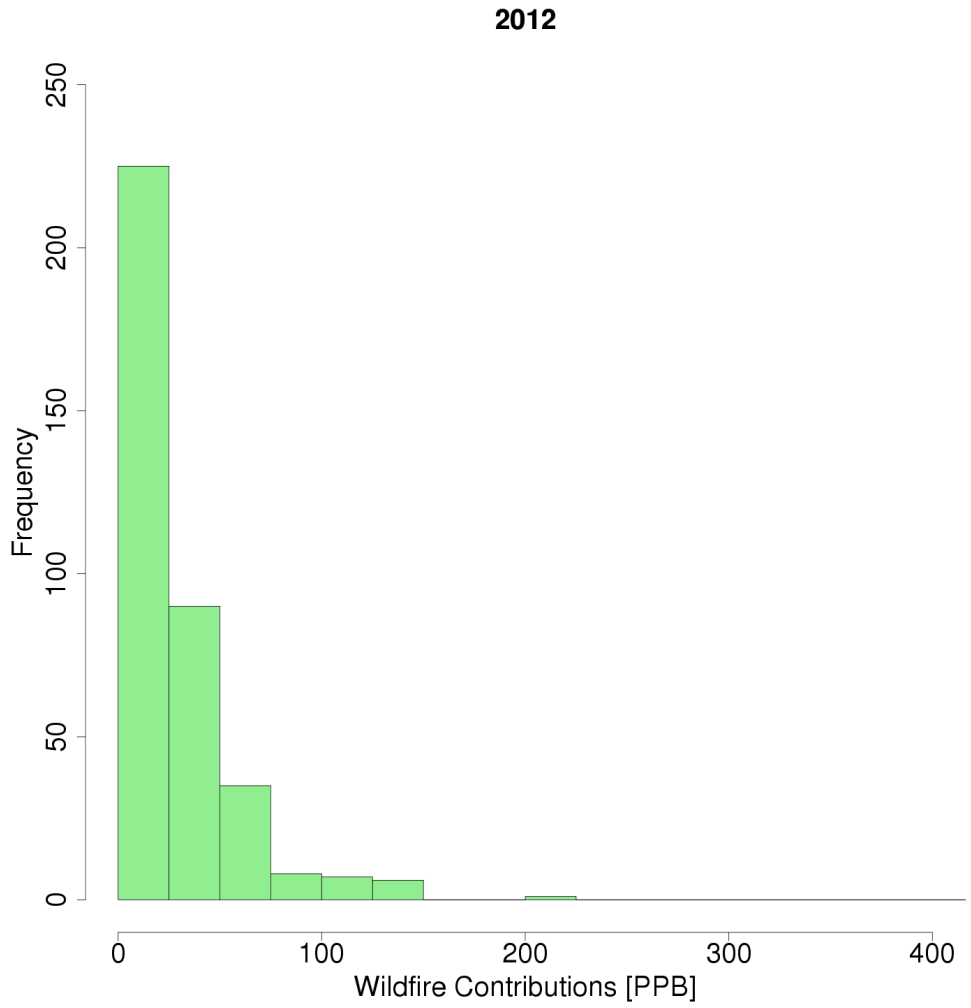

Figure 5. Frequency of 3-hourly wildfire contributions to SLC CO concentrations for the 2012 western U.S. wildfire season. Wildfire contributions ≥5 ppb are included in the lowest bin.

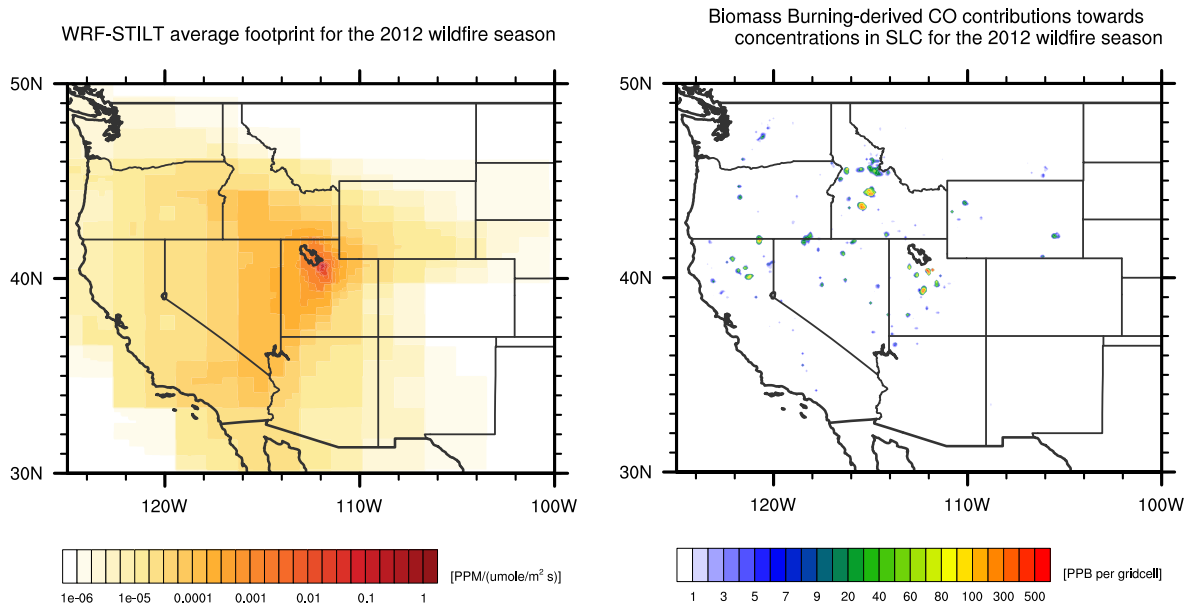

Figure 6. (a) STILT-generated average footprints for the 2012 wildfire season for SLC. (b) Wildfire-derived contributions to CO concentrations at SLC, integrated over the 2012 wildfire season.

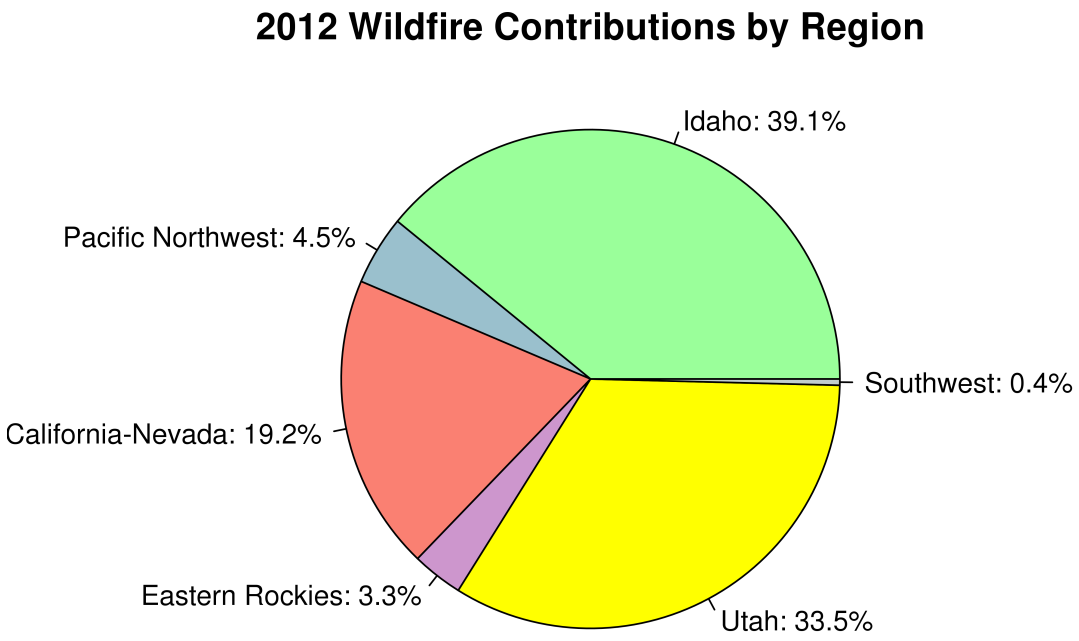

Figure 7. The contribution from each of the source regions to wildfire-derived CO enhancements at SLC for the 2012 western U.S. wildfire season.

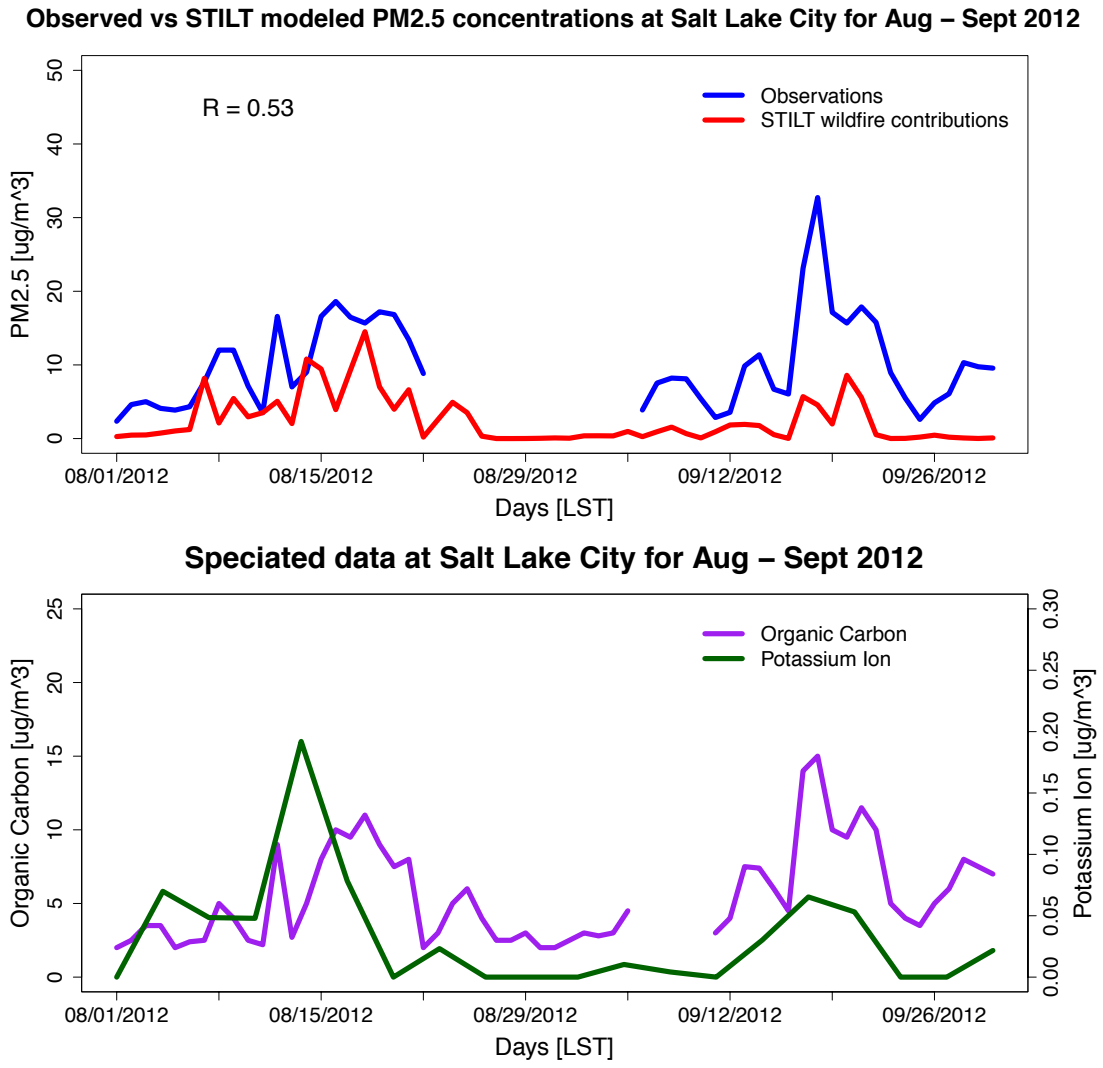

Figure 8. (a) Modeled and observed daily averaged $PM_{2.5}$ concentrations at SLC. (b) Measured values of organic carbon (daily) and speciated potassium ion concentrations (every 3 days) at SLC.

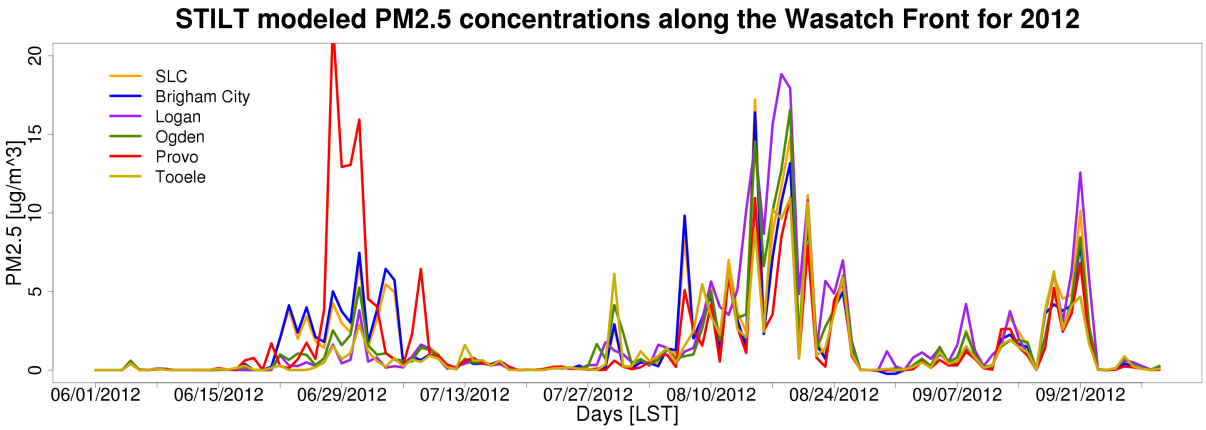

Figure 9. Modeled wildfire-contributed primary $PM_{2.5}$ concentrations at all sites along the Wasatch Front for the summer of 2012.

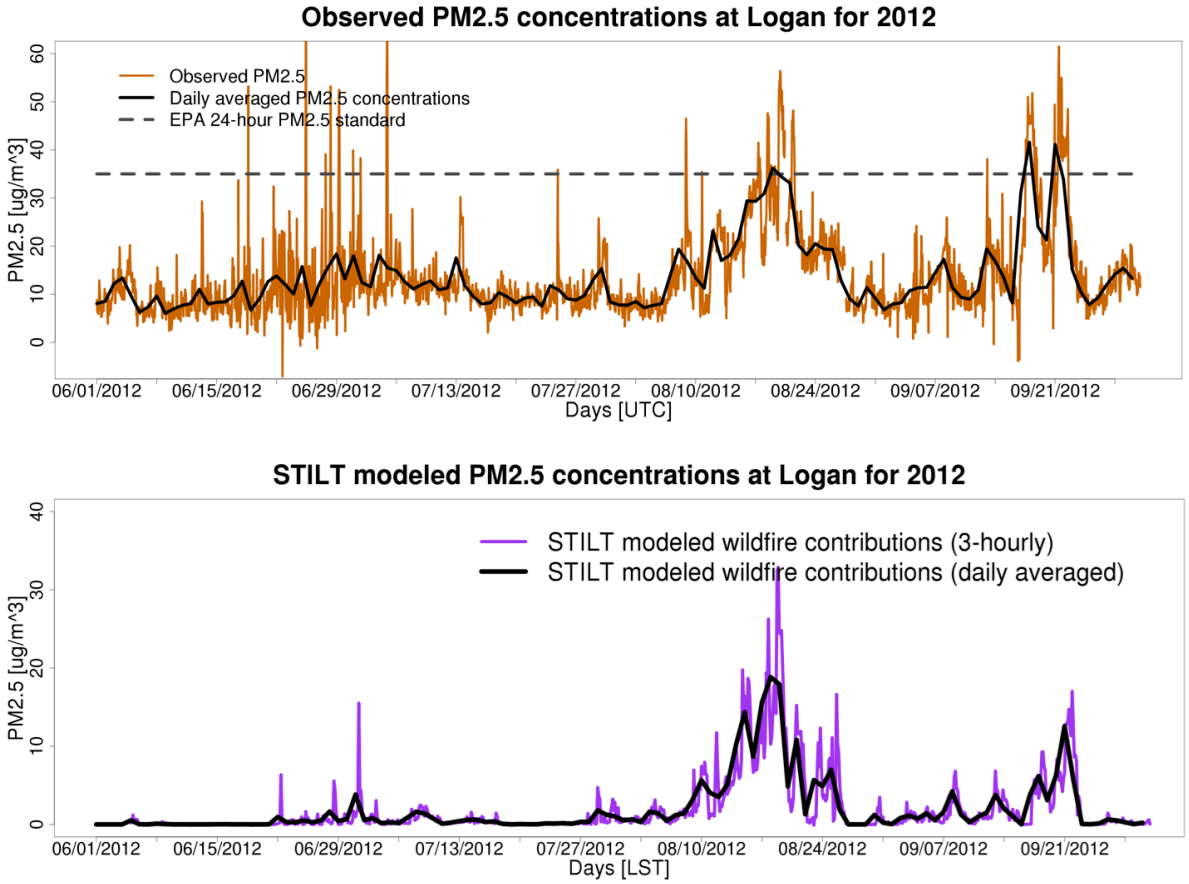

Figure 10. Observed concentrations of $PM_{2.5}$ (a) and modeled wildfire contributed $PM_{2.5}$ concentrations (b) at Logan.

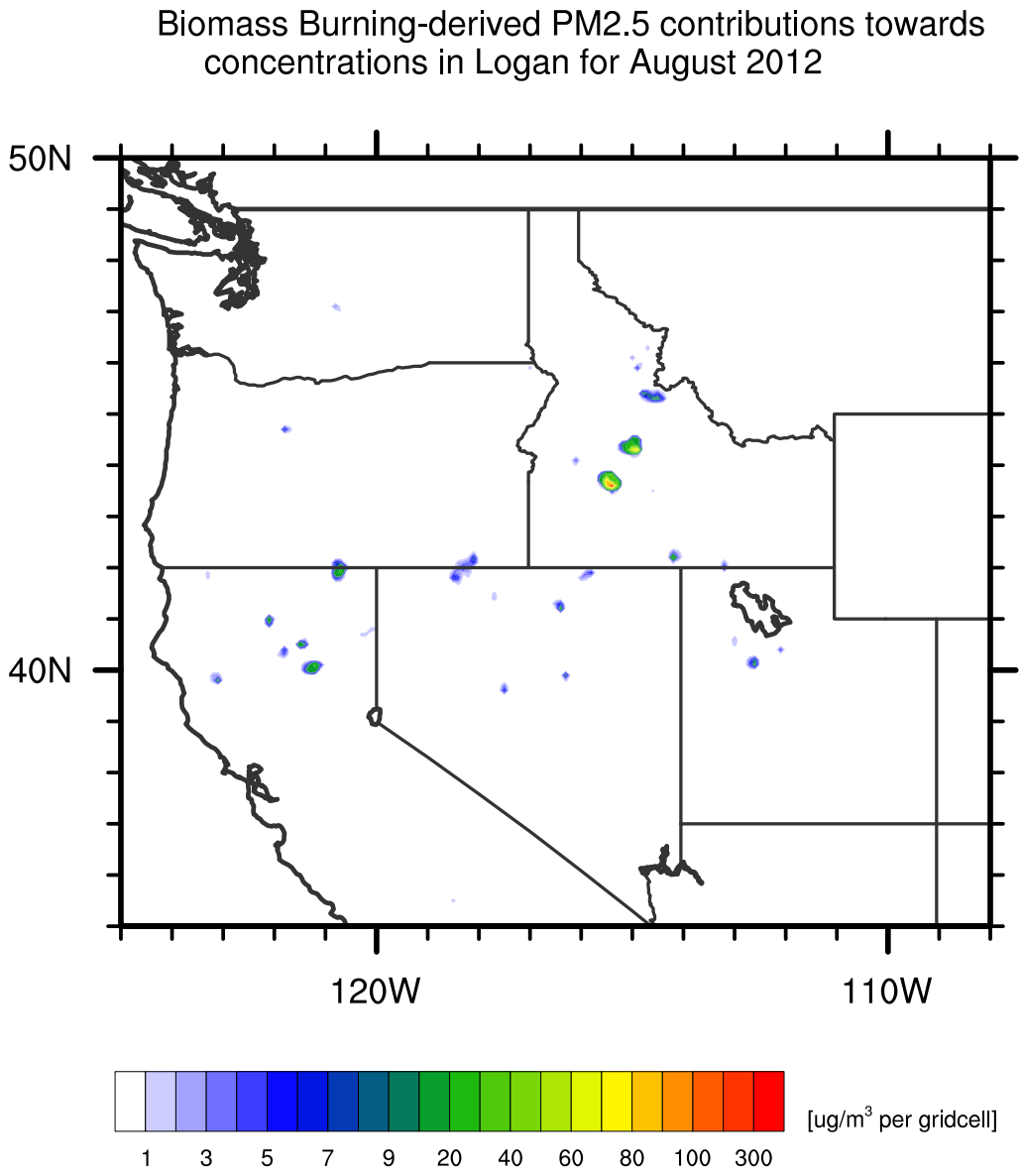

Figure 11. Modeled wildfire $PM_{2.5}$ contributions towards concentrations at Logan.

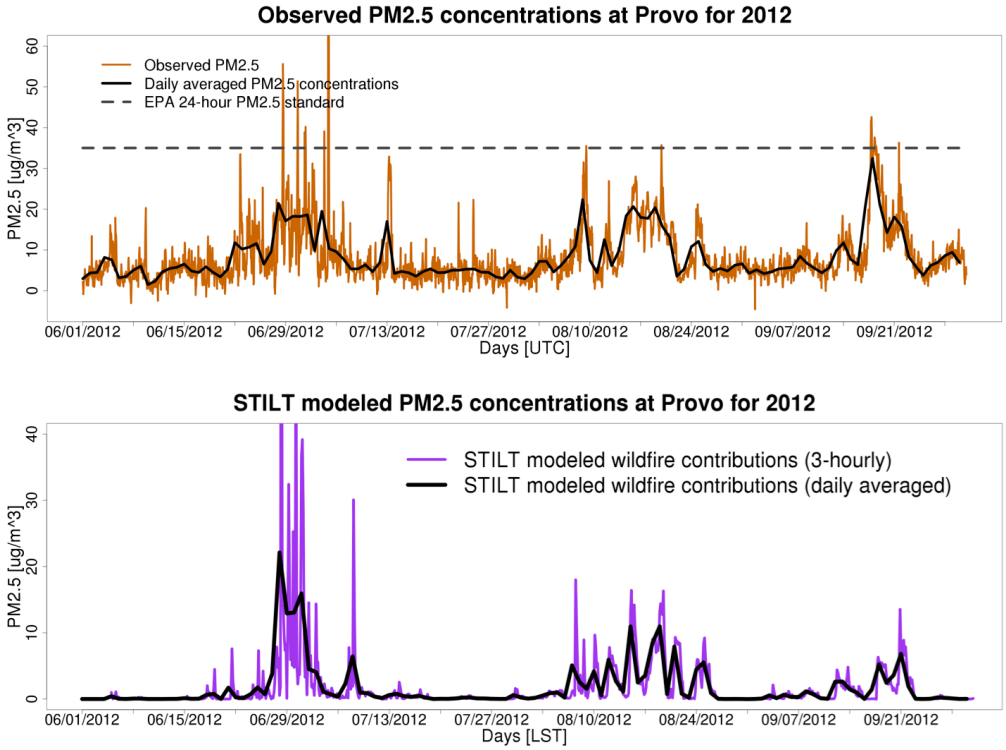

Figure 12a). Observed concentrations of $PM_{2.5}$ (top) and modeled wildfire contributed $PM_{2.5}$ concentrations (bottom) at Provo.

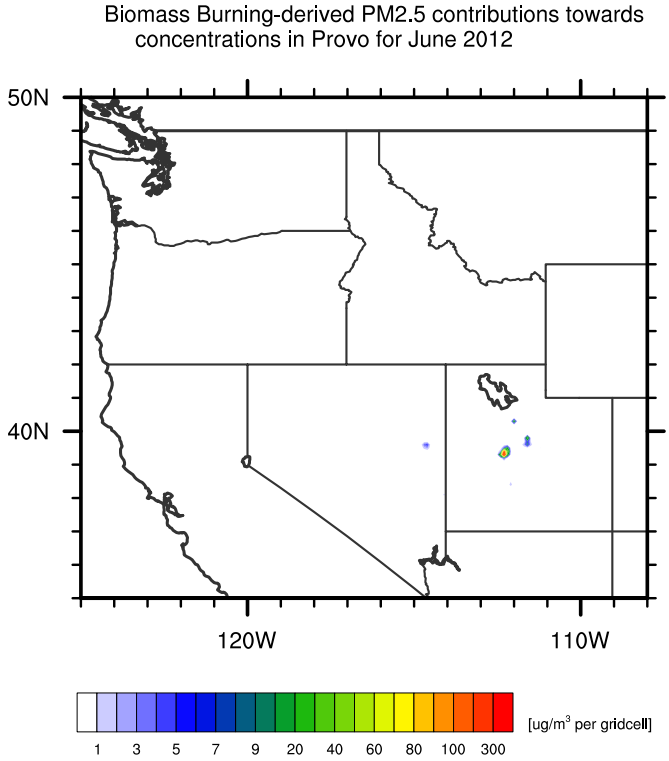

Figure 12b). Modeled wildfire $PM_{2.5}$ contributions towards concentrations at Provo.

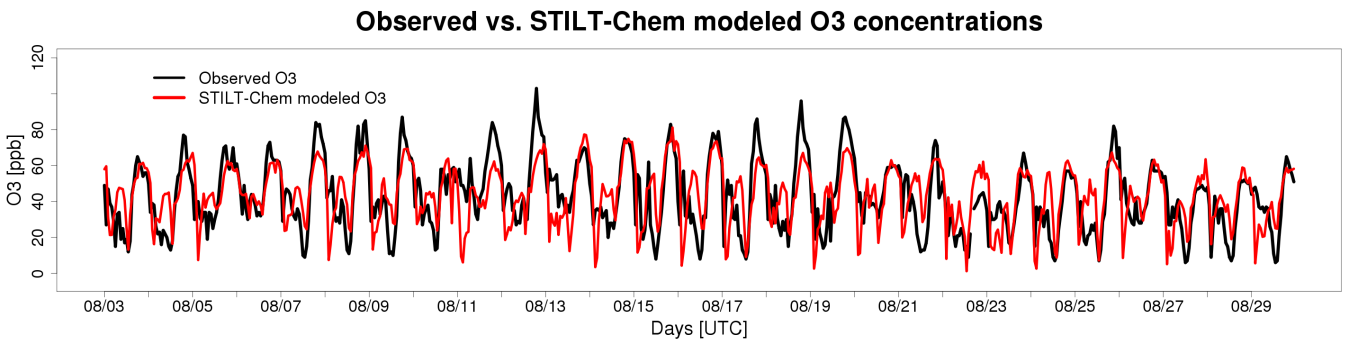

Figure 13. Ozone concentrations in Salt Lake City, Utah, during August 2012 as simulated by STILT-Chem (red) and observed by the Utah Division of Air Quality (black).

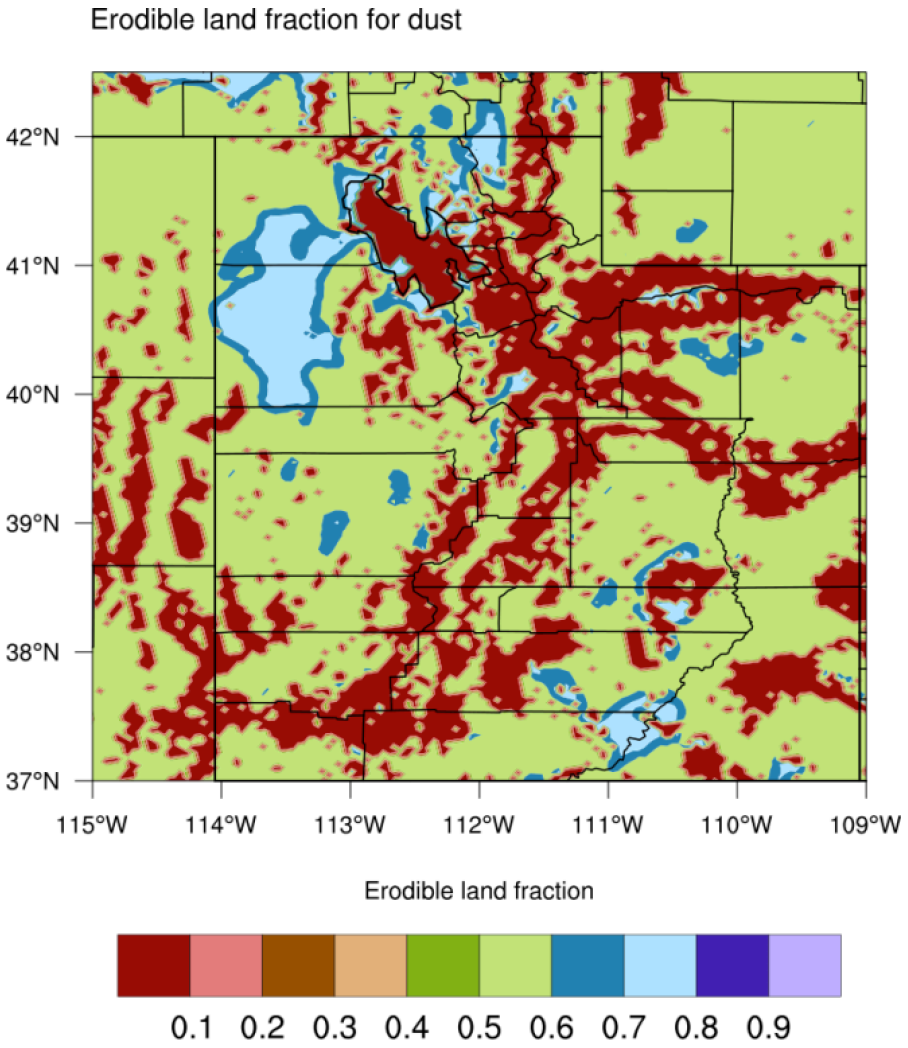

Figure 14. Erodible land fraction for dust emissions across Utah.

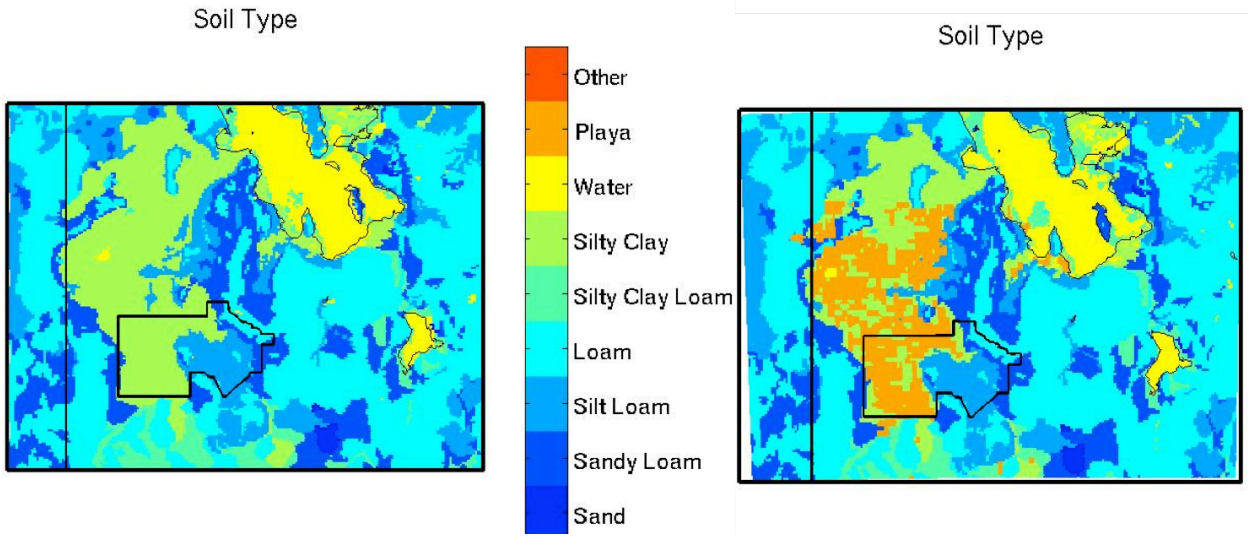

Figure 15. Figure of soil type changes within WRF. The left shows the WRF soil categories using the default USGS data set while the updated WRF (right) uses the NLCD 2006 database, which now includes a playa category. Source: *Jeff Massey*

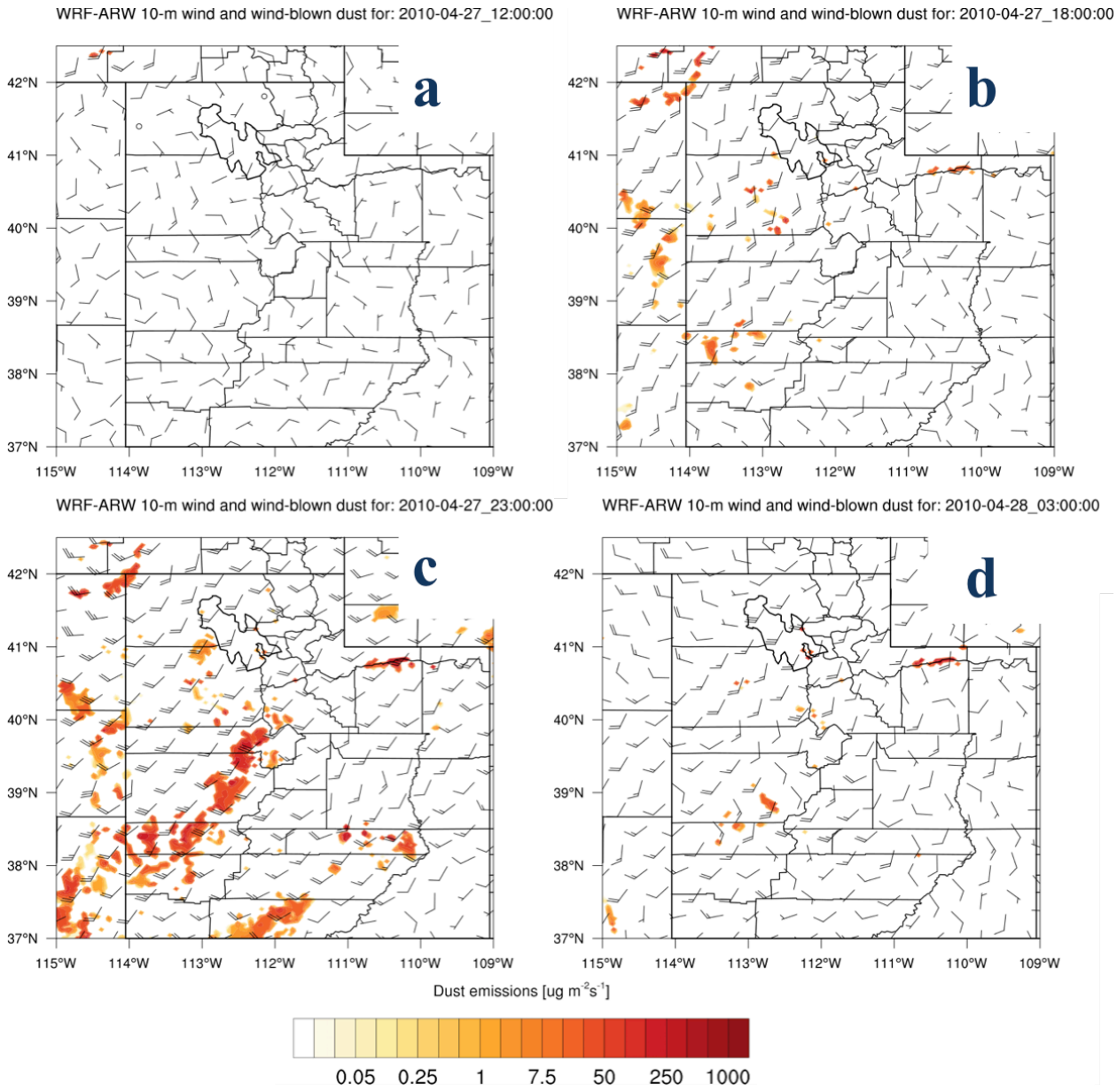

Figure 16. Dust emissions of $PM_{2.5}$ and WRF-simulated 10-m surface winds (kts) for the April 27-28th 2010 high wind event. Simulations for (a) 1200 UTC, (b) 1800 UTC, (c) 2300 UTC, and (d) 0300 UTC.

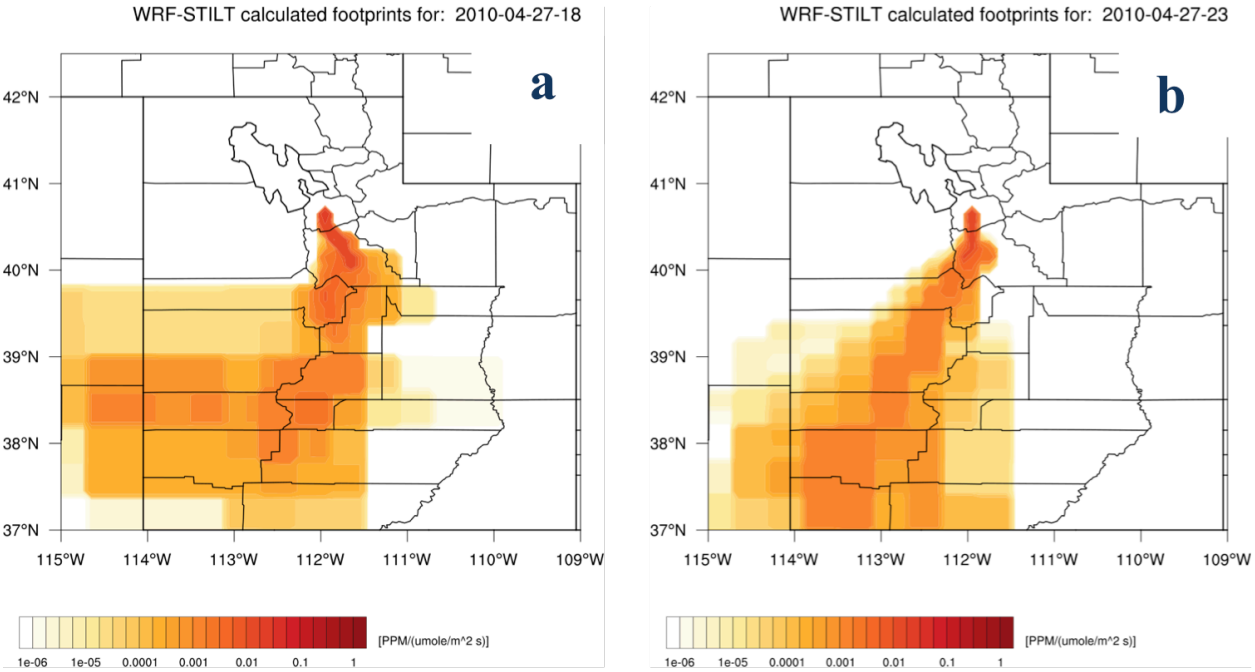

Figure 17. WRF-STILT footprints for (a) 2300 and (b) 0300 UTC on April 27th and 28th, respectively.

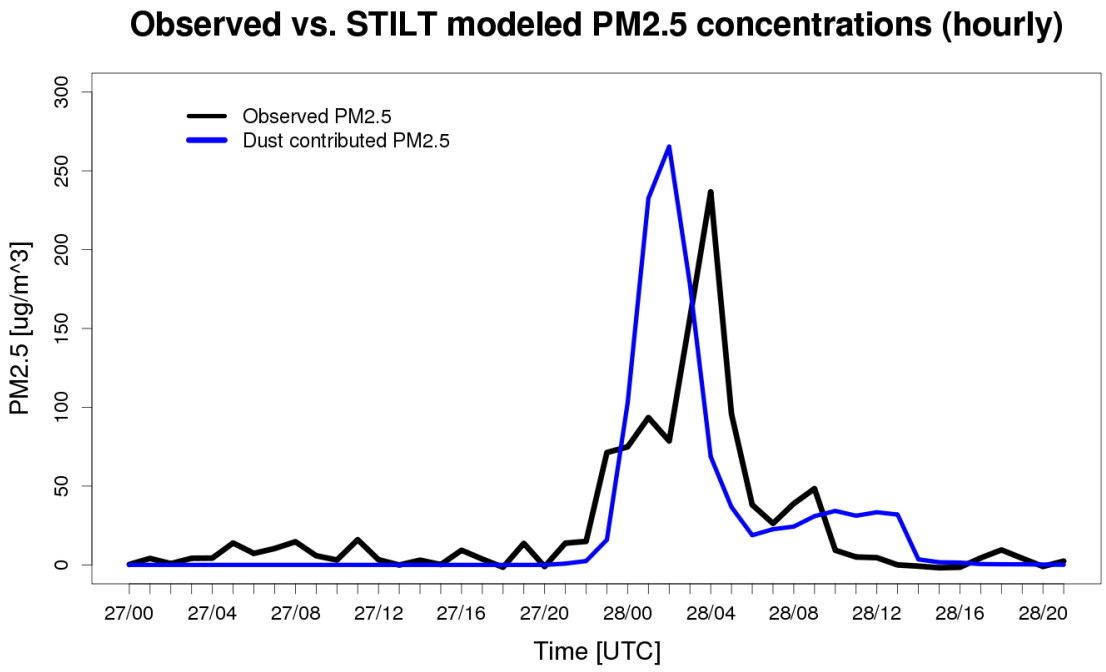

Figure 18. WRF-STILT modeled $PM_{2.5}$ dust contributions vs. observed $PM_{2.5}$ concentrations for Hawthorne for April 27th – 28th.

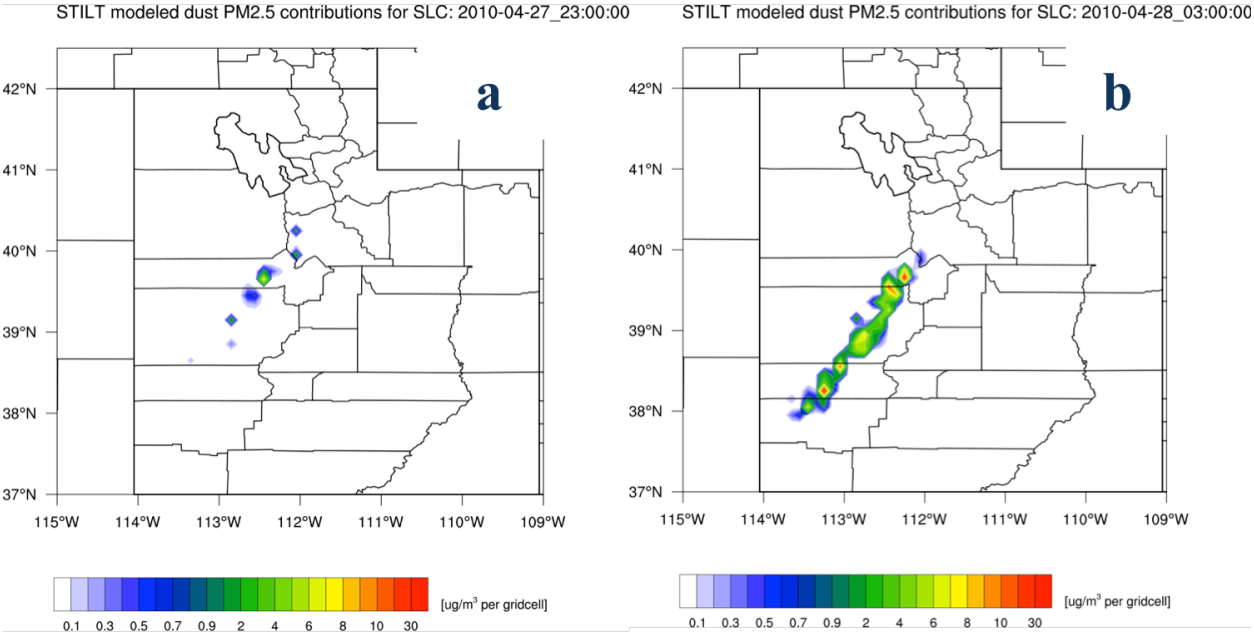

Figure 19. WRF-STILT modeled $PM_{2.5}$ dust contributions to the SLC receptor at (a) 2300 and (b) 0300 UTC.

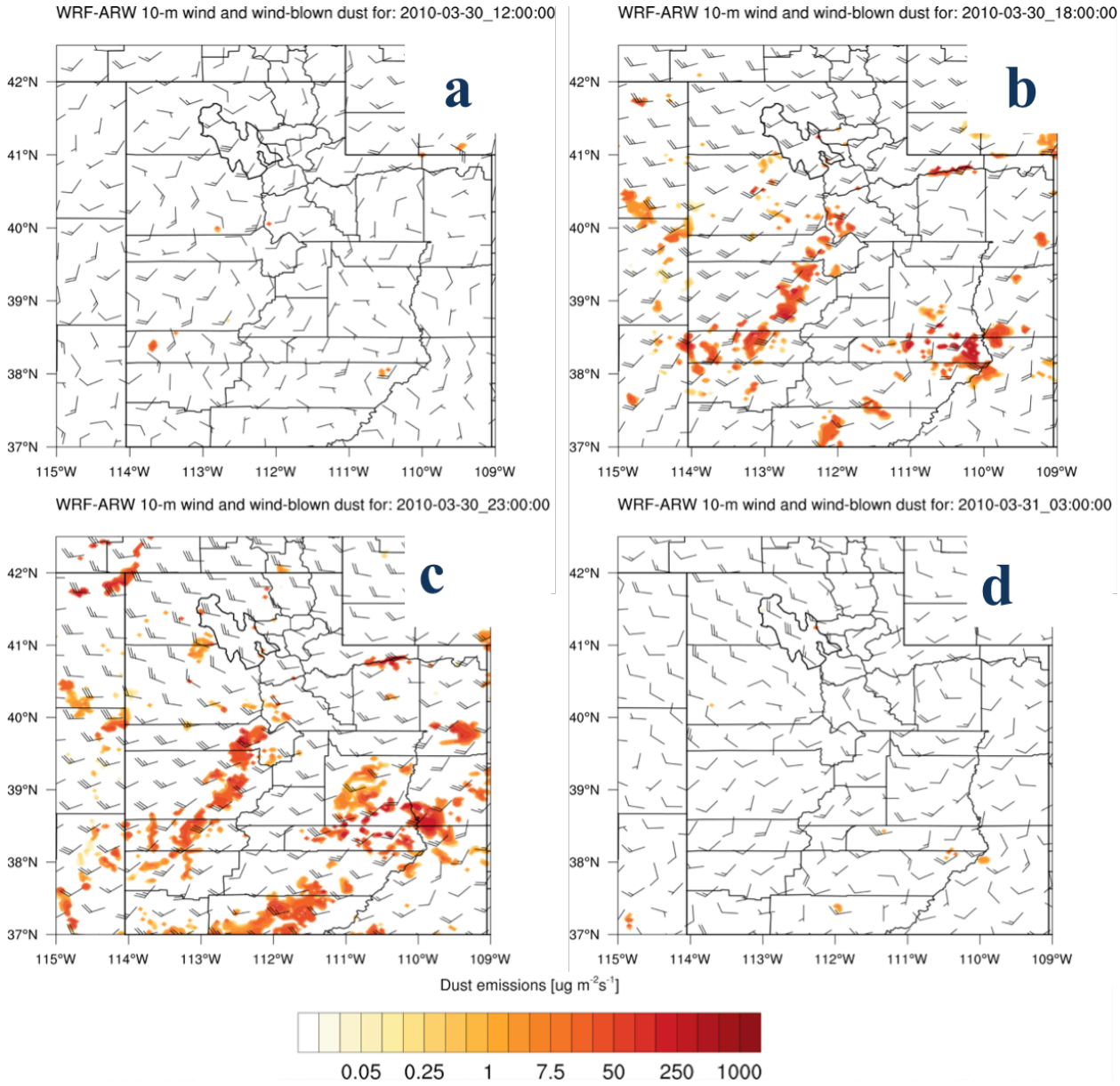

Figure 20. Dust emissions of $PM_{2.5}$ and WRF 10-m surface winds (kts) for the March 30th 2010 high wind event. Simulations for (a) 1200 UTC, (b) 1800 UTC, (c) 2300 UTC, and (d) 0300 UTC.

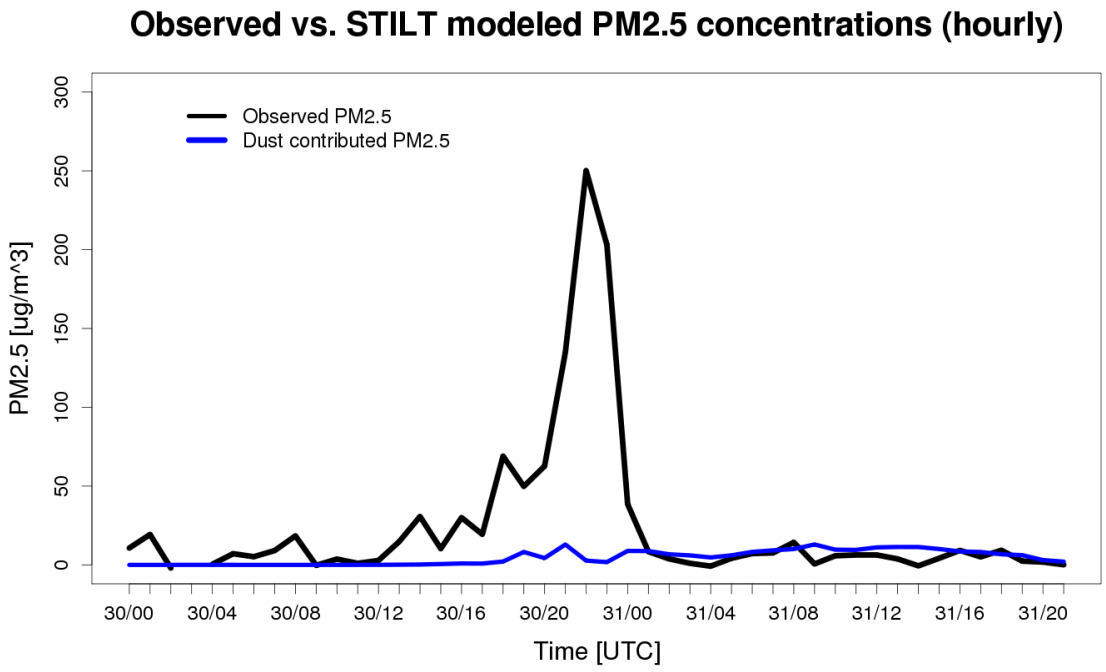

Figure 21. WRF-STILT modeled $PM_{2.5}$ dust contributions vs. observed $PM_{2.5}$ concentrations for Hawthorne for March 30th – 31st.

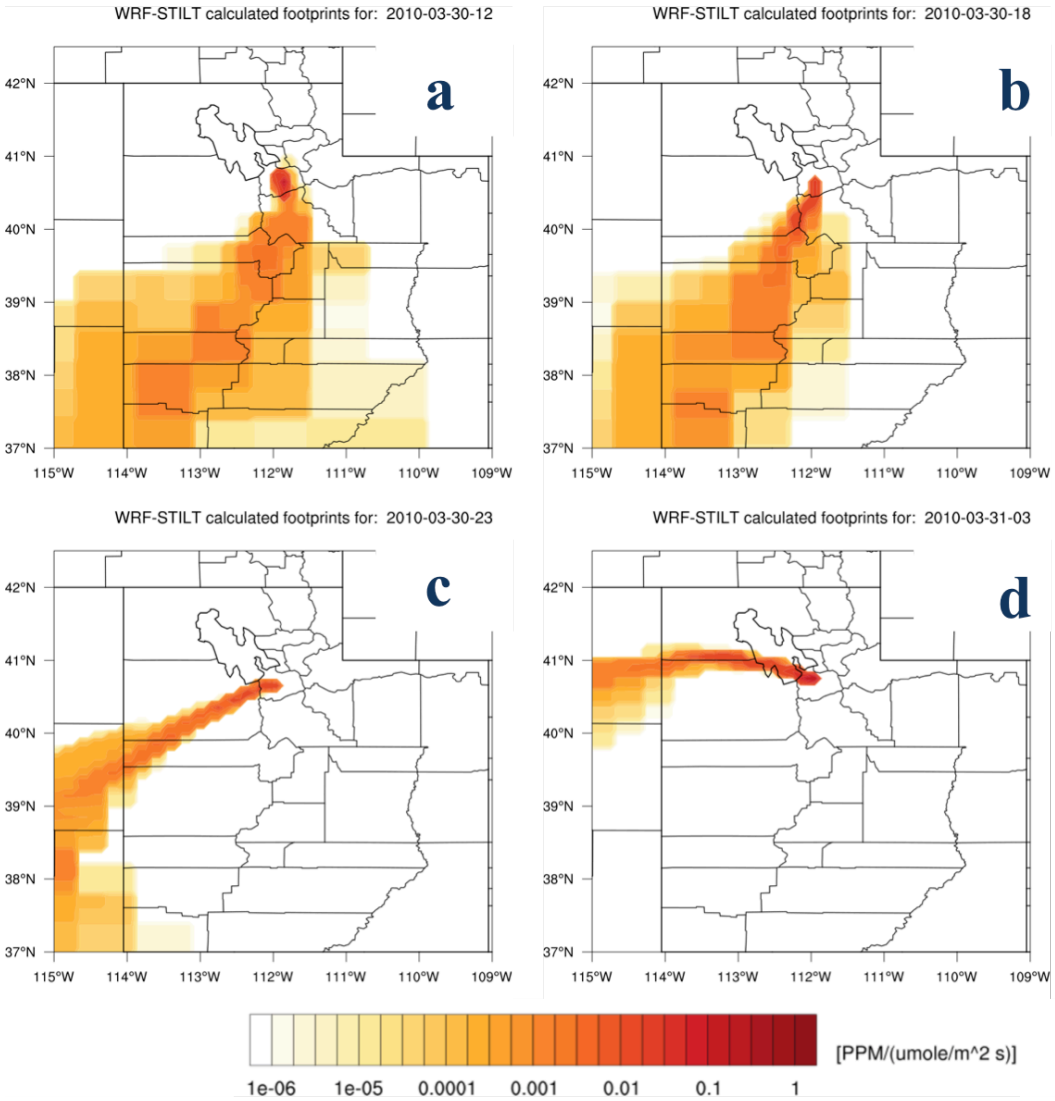

Figure 22. STILT footprints for (a) 1200 and (b) 1800 UTC, (c) 2300, and (d) 0300 UTC for March 30th and 31st.

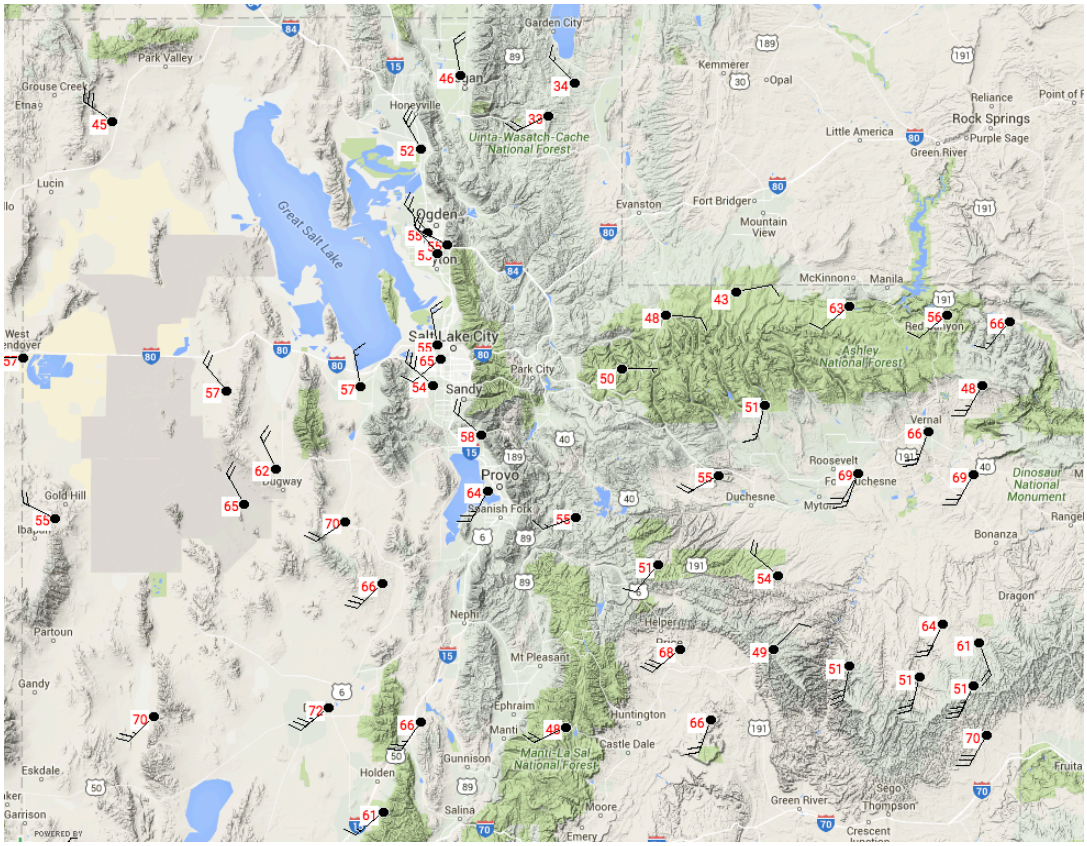

Figure 23. Mesowest surface observations centered over SLC at 2300 UTC.

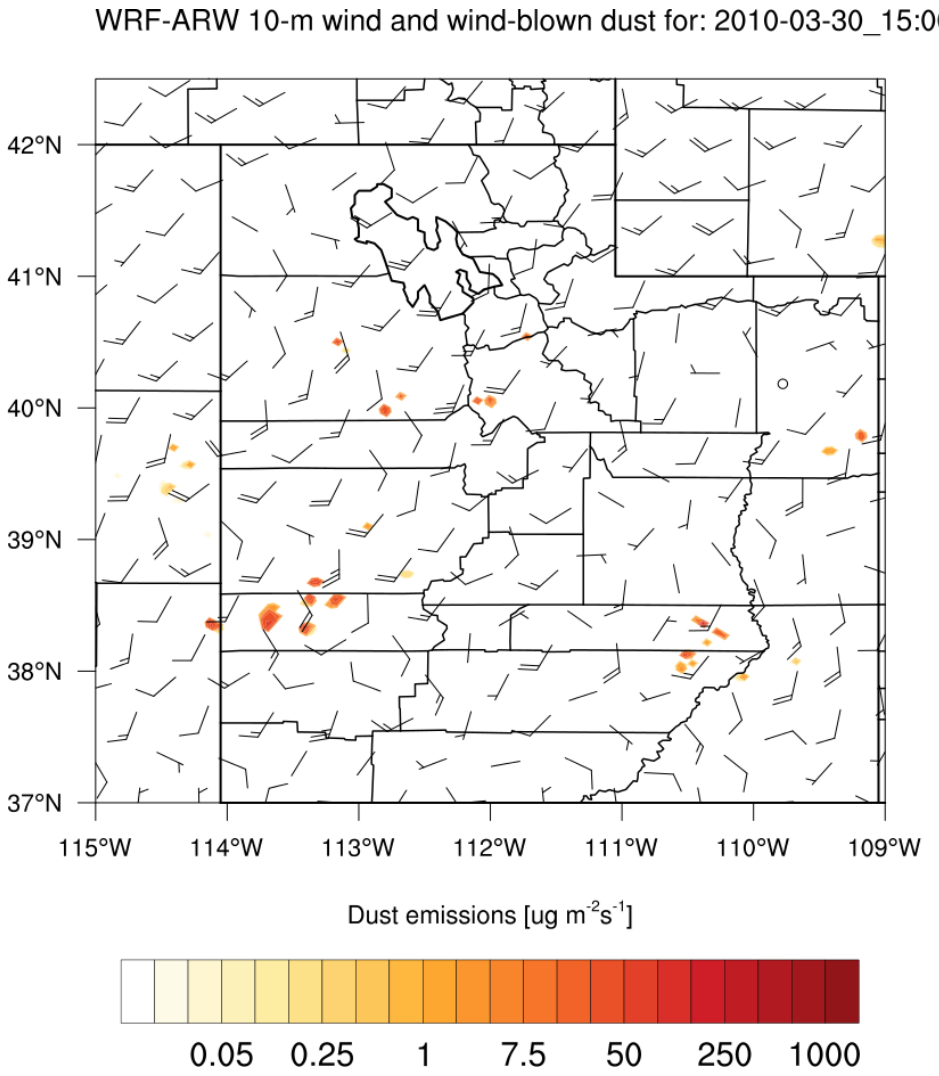

Figure 24. Dust emissions of $PM_{2.5}$ and WRF 10-m surface winds (kts) for the March 30th at 1400 UTC.

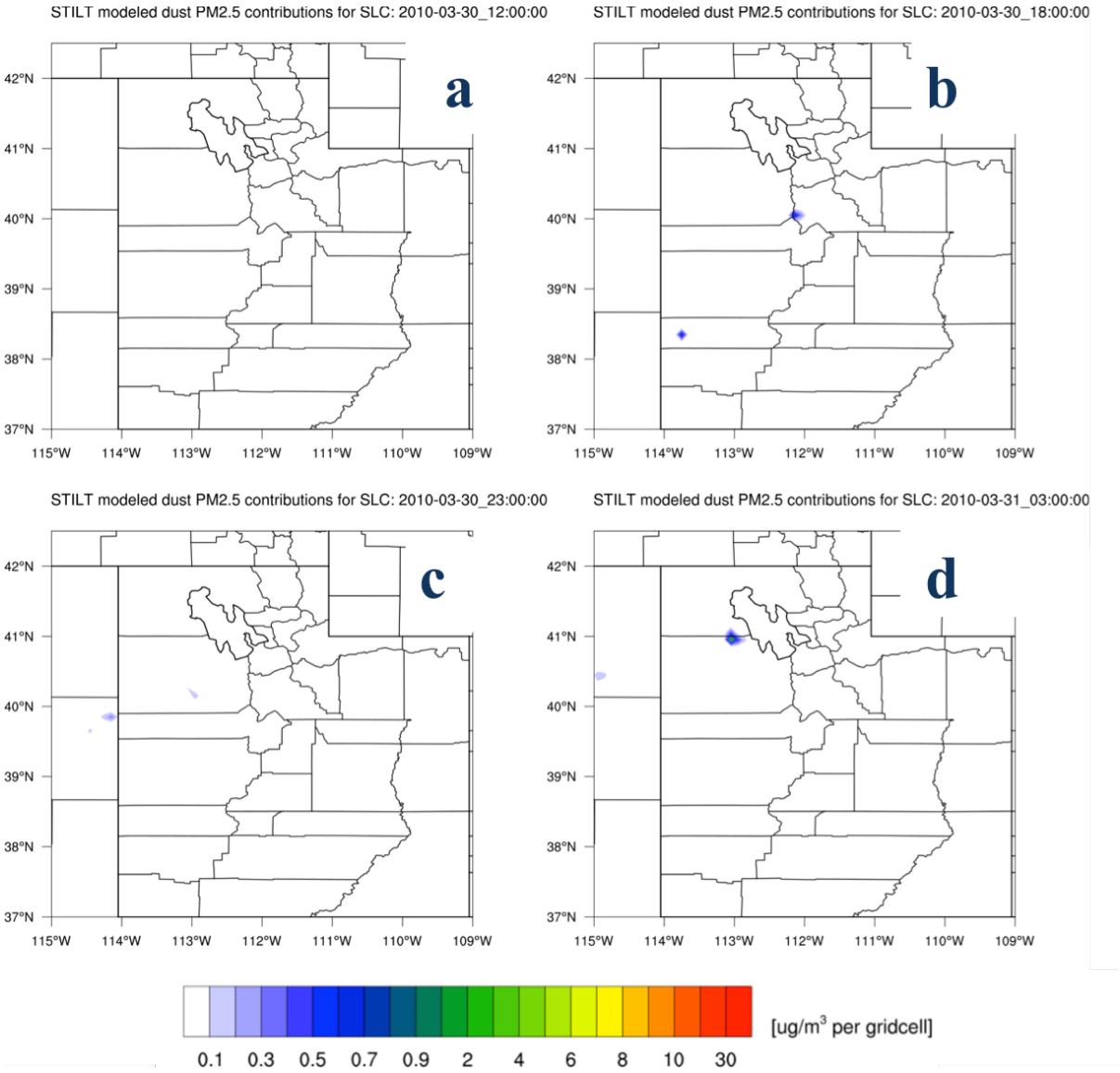

Figure 25. WRF-STILT modeled $PM_{2.5}$ dust contributions at (a) 1200, (b) 1800, (c) 2300, (d) 0300 UTC.

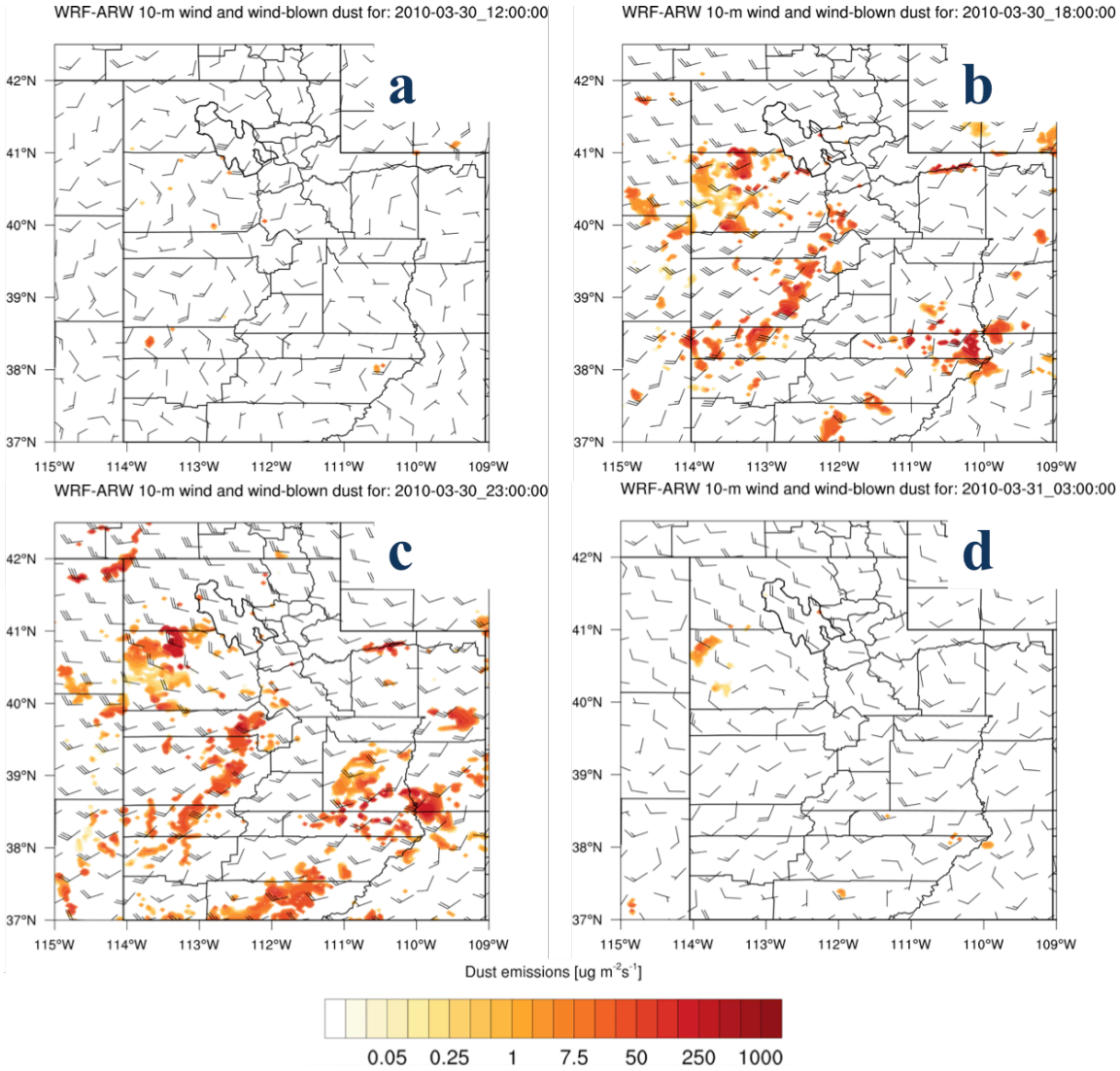

Figure 26. Modified dust emissions of $PM_{2.5}$ using an improved threshold friction velcoity formulation and WRF 10-m surface winds (kts) for the March 30th 2010 high wind event. Simulations for (a) 1200 UTC, (b) 1800 UTC, (c) 2300 UTC, and (d) 0300 UTC.

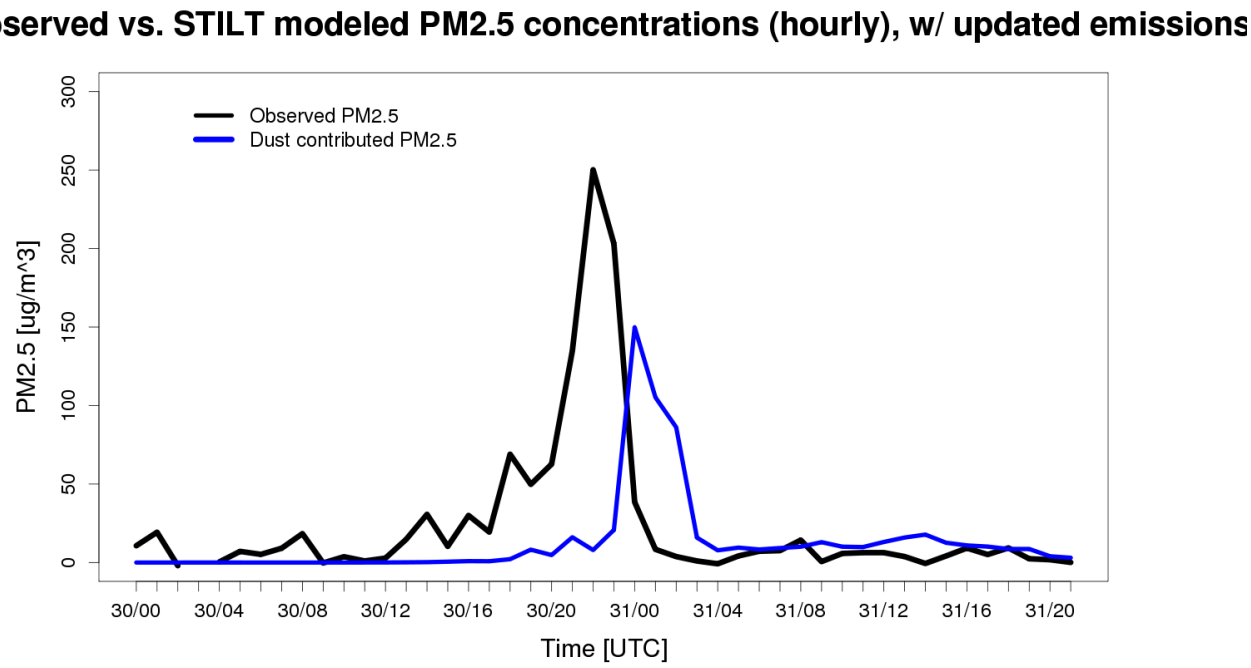

Figure 27. WRF-STILT modeled $PM_{2.5}$ dust contributions using the modified dust emissions inventory vs. observed $PM_{2.5}$ concentrations for Hawthorne for March 30th – 31st, 2010.

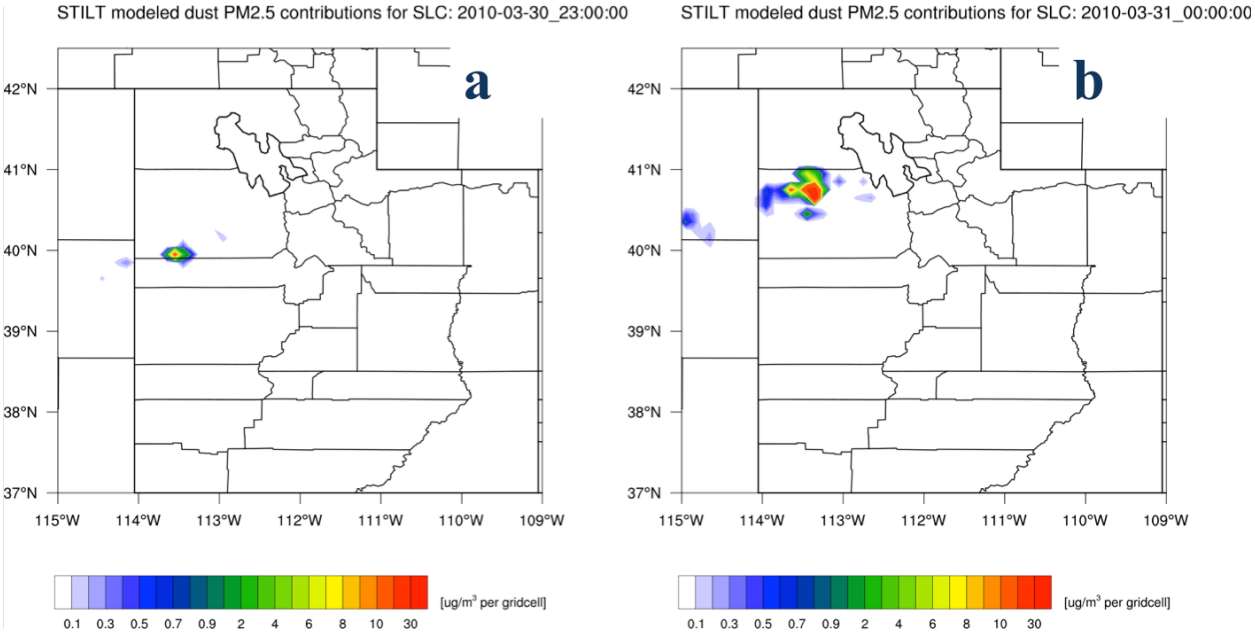

Figure 28. WRF-STILT modeled $PM_{2.5}$ dust contributions at (a) 2300 and (b) 0000 UTC.

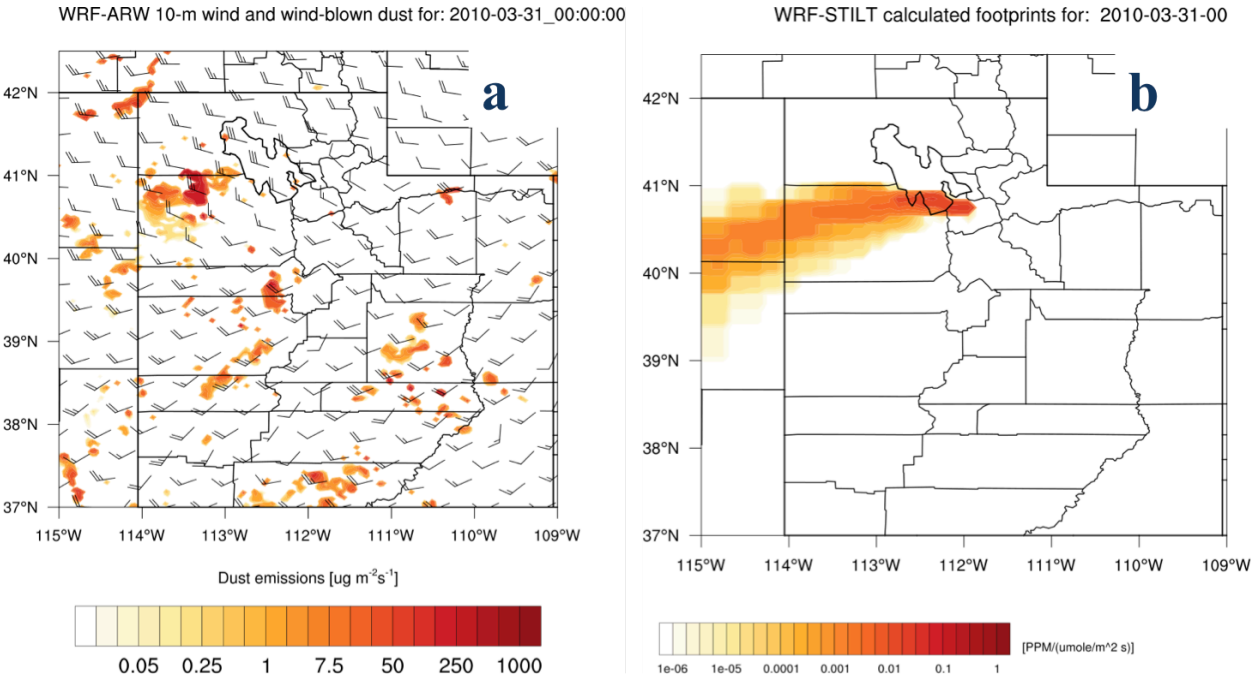

Figure 29. (a) Modified dust emissions and 10-m winds derived from WRF over Utah and (b) WRF-STILT footprint for SLC at 0100 UTC on March 31st.

AGU PUBLICATIONS

JGR

Journal of Geophysical Research: Atmospheres

RESEARCH ARTICLE
10.1002/2014JD022472

Key Points:
- WRF-STILT model used to determine impacts of wildfire emissions
- Wildfire emissions had episodic impacts in Salt Lake City
- Impacts of wildfires confirmed by observations

Correspondence to:
D. V. Mallia,
Derek.Mallia@utah.edu

Citation:
Mallia, D. V., J. C. Lin, S. Urbanski, J. Ehleringer, and T. Nehrkorn (2015), Impacts of upwind wildfire emissions on CO, CO_2, and $PM_{2.5}$ concentrations in Salt Lake City, Utah, *J. Geophys. Res. Atmos.*, *120*, doi:10.1002/2014JD022472.

Received 26 AUG 2014
Accepted 30 NOV 2014
Accepted article online 3 DEC 2014

Impacts of upwind wildfire emissions on CO, CO_2, and $PM_{2.5}$ concentrations in Salt Lake City, Utah

D. V. Mallia[1], J. C. Lin[1], S. Urbanski[2], J. Ehleringer[3], and T. Nehrkorn[4]

[1]Department of Atmospheric Sciences, University of Utah, Salt Lake City, Utah, USA, [2]Missoula Fire Sciences Laboratory, Rocky Mountain Research Station, United States Forest Service, Missoula, Montana, USA, [3]Department of Biology, University of Utah, Salt Lake City, Utah, USA, [4]Atmospheric and Environmental Research Inc., Lexington, Massachusetts, USA

Abstract Biomass burning is known to contribute large quantities of CO_2, CO, and $PM_{2.5}$ to the atmosphere. Biomass burning not only affects the area in the vicinity of fire but may also impact the air quality far downwind from the fire. The 2007 and 2012 western U.S. wildfire seasons were characterized by significant wildfire activity across much of the Intermountain West and California. In this study, we determined the locations of wildfire-derived emissions and their aggregate impacts on Salt Lake City, a major urban center downwind of the fires. To determine the influences of biomass burning emissions, we initiated an ensemble of stochastic back trajectories at the Salt Lake City receptor within the Stochastic Time-Inverted Lagrangian Transport (STILT) model, driven by wind fields from the Weather Research and Forecasting (WRF) model. The trajectories were combined with a new, high-resolution biomass burning emissions inventory—the Wildfire Emissions Inventory. Initial results showed that the WRF-STILT model was able to replicate many periods of enhanced wildfire activity observed in the measurements. Most of the contributions for the 2007 and 2012 wildfire seasons originated from fires located in Utah and central Idaho. The model results suggested that during intense episodes of upwind wildfires in 2007 and 2012, fires contributed as much as 250 ppb of CO during a 3 h period and 15 $\mu g/m^3$ of $PM_{2.5}$ averaged over 24 h at Salt Lake City. Wildfires had a much smaller impact on CO_2 concentrations in Salt Lake City, with contributions rarely exceeding 2 ppm enhancements.

1. Introduction

Fires from biomass burning are responsible for emitting large quantities of CO_2, CO, and $PM_{2.5}$ into Earth's atmosphere. Biomass burning has been suggested to account for as much as 15–30% of global CO emissions [*Galanter et al.*, 2000; *Intergovernmental Panel on Climate Change* (*IPCC*), 2013]. In the western U.S. during active years, wildfire emissions of CO and $PM_{2.5}$ can account for up to 20% and 40% of total annual emissions, respectively [*Urbanski et al.*, 2011]. On average, CO_2 emission from wildfires in the United States comprises 4–6% of anthropogenic emissions [*Wiedinmyer and Neff*, 2007].

In addition to gaseous species such as CO_2 and CO, fires can also release large quantities of particulate matter [*Davies and Unam*, 1999; *Sapkota et al.*, 2005; *Park et al.*, 2007]. Particulate matter with an aerodynamic dynamic diameter < 2.5 μm ($PM_{2.5}$) is a criteria pollutant that is regulated by the U.S. Environmental Protection Agency (EPA) [*U.S. Environmental Protection Agency* (*EPA*), 2011]. EPA has established national ambient air quality standards (NAAQS) for both short-term and long-term exposure to $PM_{2.5}$. Compliance with the short-term standard of 35 $\mu g/m^3$ is evaluated as the 3 year average of the 98th percentile of the daily maximum 24 h average concentration, and compliance with the long-term standard of 12 $\mu g/m^3$ is evaluated as the 3 year average of the annual mean $PM_{2.5}$ concentration [*EPA*, 2011]. High concentrations of $PM_{2.5}$ can have adverse effects on human health, as these particulates can be easily inhaled enabling them to penetrate deep into the lungs [*EPA*, 2011]. The elderly, young children, and people with lung and heart diseases are the most susceptible to increased concentrations of $PM_{2.5}$ [*EPA*, 2011; *Beard et al.*, 2012]. In urban areas of the Intermountain West, NAAQS for $PM_{2.5}$ and ozone continue to be violated [*EPA*, 2011; *Chen et al.*, 2012; *Lareau et al.*, 2013; *Silcox et al.*, 2012].

The western U.S. is the primary source of wildfire emissions in the U.S., due to arid conditions, the abundance of needleleaf forests, and a dry season [*Westerling et al.*, 2006; *Wiedinmyer and Neff*, 2007]. The greatest

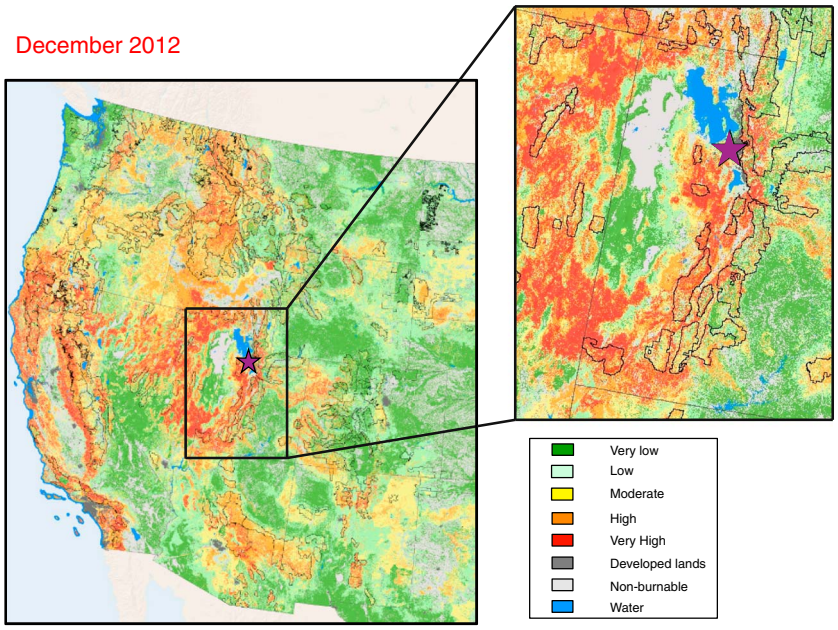

Figure 1. The Wildland Fire Potential product for the western U.S [*Missoula Fire Laboratory*, 2013]. The shaded values represent the wildfire potential risk beyond 2012 while the purple star represents the location of downtown SLC.

wildfire emissions occur between the months of June and October, with maximum emissions occurring in August [*Wiedinmyer and Neff*, 2007; *Urbanski et al*., 2011]. *Dennison et al*. [2014] noted a general increase in large wildfires (>405 ha) across the western U.S. from 1984 through 2011. Annual western U.S. burned areas have also been on the increase since the 1970s according to observed and reconstructed databases that span from 1916 to 2004 [*Littell et al*., 2009]. These changes have been attributed to higher annual mean temperatures that result in earlier snowmelt and land use changes that prolong the wildfire season [*Westerling et al*., 2006; *Dennison et al*., 2014; *Riley et al*., 2013]. This trend is likely to continue with the average maximum air temperature and drought severity increasing for these regions under the Intergovernmental Panel on Climate Change's moderate emission scenario A1B [*IPCC*, 2013].

This study focuses on wildfires in the western United States and their impacts on CO, CO_2, and $PM_{2.5}$ concentrations in Salt Lake City (SLC), in the state of Utah. SLC is one of the major urban centers located in the Intermountain West with a population that is projected to double in size by the year 2050 [*Utah Foundation*, 2014]. The area surrounding SLC is also prone to wildfire activity, as indicated by the Wildland Fire Potential product, from the Fire Program Analysis system (Figure 1) [*Missoula Fire Laboratory*, 2013; *Finney et al*., 2011]. Concentrations of CO, CO_2, and $PM_{2.5}$ can become further amplified in regions like the SLC valley due to strong surface inversions that are influenced by the surrounding topography. While CO_2 does not have any direct impacts on air quality, it is an inert gas that is a suitable tracer for atmospheric transport, thereby allowing us to evaluate the validity of simulated transport [*Pataki et al*., 2006].

Wildfires have the potential to enhance concentrations of pollutants regulated by the EPA in downwind regions, e.g., CO, $PM_{2.5}$, and O_3 [*Clinton et al*., 2006; *Bravo et al*., 2002; *Davies and Unam*, 1999; *Debell et al*., 2004; *Sapkota et al*., 2005; *Dempsey*, 2013]. For example, wildfires in Quebec during the summer of 2002 injected large quantities of CO and $PM_{2.5}$ into the mixed layer of the atmosphere that were later transported by midlevel winds to the northeastern U.S [*Debell et al*., 2004; *Sapkota et al*., 2005]. During this period, CO and $PM_{2.5}$ monitoring stations across the Northeast noted elevated concentrations, which occurred during the passage of the smoke plumes originating from the Quebec wildfires [*Debell et al*., 2004; *Sapkota et al*., 2005]. A similar situation was observed when smoke from wildfires in northern Saskatchewan was transported over Toronto, resulting in elevated levels of $PM_{2.5}$ and O_3 [*Dempsey*, 2013]. If the passage of a smoke plume occurs in an urban area during the morning or afternoon rush hours, when traffic emissions are maximized, very high CO concentrations can be observed [*Debell et al*., 2004; *Sapkota et al*., 2005; *Dempsey*, 2013].

Previous studies have determined the influences of wildfire emissions on downwind locations using qualitative methodologies [*Debell et al*., 2004; *Sapkota et al*., 2005; *Dempsey*, 2013]. However, these studies have been unable to quantify the direct influences from these fires. Cities across the western U.S. have often exceeded the NAAQS for $PM_{2.5}$ and O_3 during the summer months due to increased wildfire activity [*EPA*, 2010; *Utah's Division of Air Quality* (*UDAQ*), 2013, 2012b; *Jaffe et al*., 2013; *Jaffe and Wigder*, 2012]. However, as of 2007, the EPA has adopted a new regulation, the Treatment of Data Influenced by Exceptional Events (EER), which allows every state to flag data in EPA's Air Quality System database for events that are not reasonably controllable or preventable and are natural. For an event to be considered "exceptional" by the definitions set forth by EPA [*EPA*, 2013], it has to be demonstrated that the event meets the following criteria: (1) associated with measured concentrations in excess of historical fluctuations, (2) a clear relationship between the flagged measurements and the event, and (3) no exceedance would have taken place had the exceptional even not occurred. Here we will use a source apportionment modeling method that will attempt to separate the impacts of nonwildfire emissions from wildfire-emitted CO_2, CO, and $PM_{2,5}$. This modeling framework will make use of state-of-the-art Lagrangian and Eulerian atmospheric models along with the latest wildfire emission inventories in order to determine the influences of upwind wildfire emissions on SLC. Going forward, this modeling framework has the potential to allow air quality managers to quantify the impact of wildfire events on air quality.

2. Methodology

The Weather Research and Forecasting (WRF) model was coupled with the Stochastic Time-Inverted Lagrangian Transport (STILT) particle dispersion model to determine the impacts of upwind wildfire emissions on CO, CO_2, and $PM_{2.5}$ concentrations in SLC [*Skamarock et al*., 2008; *Lin et al*., 2003]. WRF is a Eulerian nonhydrostatic atmospheric model equipped with a large suite of physical parameterizations. Backward trajectory ensembles arriving at SLC used to model CO, CO_2, and $PM_{2.5}$ were generated using the STILT model driven by the WRF wind fields. A Lagrangian framework like STILT offers several benefits over Eulerian tracer models in the Lagrangian formulation's physical realism, numerical stability, lack of numerical diffusion, adherence to mass conservation, and computational efficiency [*Lin et al*., 2013; *Wohltmann and Rex*, 2009; *Shin and Reich*, 2009; *Smolarkiewicz and Pudykiewicz*, 1992; *McKenna et al*., 2002].

Surface flux footprints $f(x_r, t_r|x_i, y_j, t_m)$ for a receptor at location x_r and time t_r to an upwind source at (x_i, y_j) and prior time t_m can be estimated from the WRF-STILT backward trajectories [*Lin et al*., 2003; *Nehrkorn et al*., 2010; *Skamarock et al*., 2008]. The footprint is simply the measure of the upwind surface influences for a receptor as determined by the STILT backward trajectories. The footprint is a function of the number of Lagrangian particles within the planetary boundary layer (PBL) for some upwind location and has units of mixing ratio per unit surface flux as seen in the equation below:

$$f\left(x_r, t_r \middle| x_i, y_j, t_m\right) = \frac{m_{\text{air}}}{h\overline{\rho}\left(x_i, y_j, t_m\right)} \frac{1}{N_{\text{tot}}} \sum_{p=1}^{N\text{tot}} \Delta t_{p,i,j,k} \tag{1}$$

where m_{air} is the molecular weight of air, h is the height of the volume in which the surface fluxes are diluted over (surface influence volume), ρ is the average density for all particles, N_{tot} is the total number of particles, and $\Delta t_{p,i,j,k}$ is the amount of time a particle p spends within the surface influence volume at location (x_i, y_j) and time t_m [*Lin et al*., 2003; *Wen et al*., 2012; *Kim et al*., 2013; *Lin et al*., 2013]. Any surface fluxes that occur within the PBL are assumed to be rapidly mixed within the surface influence volume, which is taken to extend from the surface to a height of 0.5 z_i (one half of the PBL height). Previous studies have indicated that simulated STILT footprints were insensitive to the exact value of the column height "h" as long as h was between 10 and 100% of the PBL height [*Lin et al*., 2003; *Gerbig et al*., 2003].

Multiplying the footprint field with fluxes of CO, CO_2, and $PM_{2.5}$ allows us to determine the direct contribution of upwind source regions on the total concentration of CO, CO_2, and $PM_{2.5}$ arriving at the receptor. Simulations were carried out for the 2007 and 2012 wildfire seasons, which were characterized by significant emissions in the western U.S. (see section 3) The wildfire season is defined as the months of June through October [*Westerling et al*., 2006].

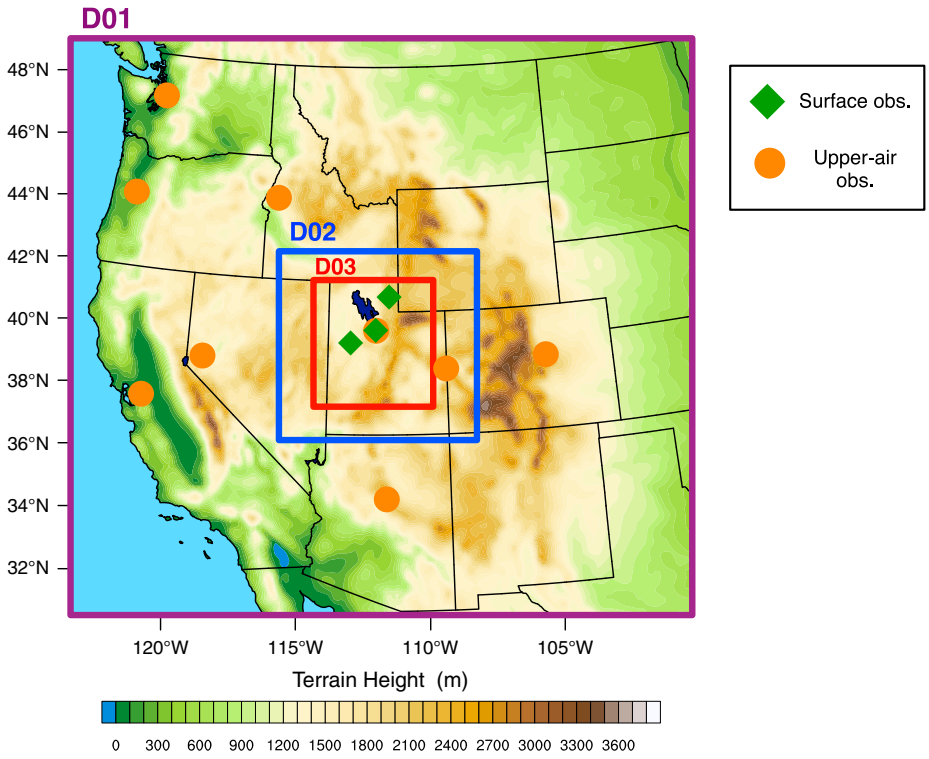

Figure 2. The WRF domain used for this study with surface and upper air observations used for our WRF run comparisons. The horizontal grid spacing is 12 km for D01, 4 km for D02, and 1.333 km for D03.

2.1. WRF-STILT Model Configuration

The Advanced Research version of the WRF model (ARW, version 3.4.1) [*Skamarock et al.*, 2008] was used to drive the backward trajectories created by the STILT model. Boundary conditions were provided by the North American Regional Reanalysis (NARR) which is available at a horizontal grid spacing of 32 km with 30 vertical levels every 3 h [*Mesinger et al.*, 2006]. Our WRF simulations consisted of three domains at 12, 4, and 1.33 km resolution with two-way nesting (Figure 2). Outside of the WRF domain (Figure 2), the Global Data Assimilation System final analysis (FNL) (1° resolution every 6 h) was used to drive STILT.

Time-averaged, mass coupled winds from the WRF model were used to improve mass conservation and the temporal representation of wind variation [*Nehrkorn et al.*, 2010; *Hegarty et al.*, 2013]. The native vertical levels within STILT were selected to closely match the WRF vertical levels to further improve mass continuity. WRF simulations were carried out from the beginning of June to the end of October with hourly output for 2007 and 2012. Previous research has indicated that output frequencies higher than 3 h for high-resolution meteorology fields are needed to further reduce interpolation errors within Lagrangian particle dispersion models like STILT [*Bowman et al.*, 2013]. WRF simulations were reinitialized every 7 days and were allowed to have a spin-up time of 12 h. The first 12 h of each run were then replaced with the last 12 overlap hours from the previous WRF simulation.

WRF simulations using a variety of physical parameterizations and nudging techniques were compared against National Weather Service regional and local upper air and surface observation sites in order to determine the optimal settings (Figure 2). Ten different WRF simulations centered over SLC were carried out for the month of July 2007 using a variety of configurations involving different parameterizations and grid nudging setups (Table 1). All model runs had 41 vertical levels with 10 of these levels within 1 km of the surface in order to better resolve circulations within the PBL. The model top was located at the 50 hPa pressure level. It should be noted that certain runs used the 2006 National Land Cover Database, which is denoted as "yes" under the land use column in Table 1. Runs denoted with a "no" under the land use column in Table 1 simply used the default WRF land use database. These model runs also adopted a two-way nested

Table 1. Overview of the WRF Configurations Tested for the WRF Simulations Centered Over Salt Lake City for July 2007[a]

Run #	Nudging	Microphysical	Cumulus	PBL	Urban?	Land Use?	RMSE *u* Wind (m/s)	RMSE *v* Wind (m/s)	RMSE Temperature (°C)	BIAS *u* Wind (m/s)	BIAS *v* Wind (m/s)	BIAS Temperature (°C)
#1	Spectral nudging above PBL	New Thompson	Kain-Fritsch	YSU	No	No	3.45	3.30	1.96	0.71	−0.48	−0.13
#2	Spectral nudging at all levels	New Thompson	Kain-Fritsch	YSU	No	No	3.05	3.04	1.93	−0.06	−0.18	−0.18
#3	No nudging	New Thompson	Kain-Fritsch	YSU	No	No	3.42	4.00	2.39	1.06	−1.11	−0.48
#4	No nudging	WSM 3-class	Kain-Fritsch	MYJ	Yes	No	3.89	3.77	2.11	−0.05	−0.81	−0.81
#5	No nudging	New Thompson	Betts-Miller-Janjić	MYJ	Yes	No	3.86	3.74	2.07	0.97	−0.99	−0.49
#6	Grid nudging above PBL	Purdue Lin	Grell-Devenyi Ens.	YSU	Yes	No	2.72	2.66	1.69	0.81	−0.54	−0.27
#7	Grid nudging above PBL	Purdue Lin	Grell-Devenyi Ens.	MYJ	Yes	No	2.76	2.67	1.63	0.81	−0.50	−0.36
#8	Grid nudging above PBL	Purdue Lin	Grell-Devenyi Ens.	MYJ	Yes	Yes	2.80	2.71	2.01	0.80	−0.52	0.31
#9	Spectral nudging above PBL	Purdue Lin	Grell-Devenyi Ens.	MYJ	Yes	Yes	4.00	3.80	2.24	1.06	−1.11	−0.46
#10	No nudging	Purdue Lin	Grell-Devenyi Ens.	MYJ	Yes	Yes	3.16	3.00	1.81	0.62	−0.45	−0.20

[a]All of these simulations used the RRTMG longwave and shortwave radiation schemes, NOAH land surface model, and had a similar domain with 41 vertical levels. Also included is the averaged RMSE and model BIAS (model-observation) for all upper air and surface observations for the *u* and *v* wind components and temperature.

grid with boundary conditions obtained from the NARR [*Mesinger et al.*, 2006]. All simulations used the Rapid Radiative Transfer Model for GCMs (RRTMG) longwave and shortwave radiation schemes [*Iacono et al.*, 2008] and the NOAH land surface model [*Chen and Dudhia*, 2001].

The root-mean-square error (RMSE) and model biases (model-observation) were calculated using surface and upper air observations across the western U.S. in order to determine the errors associated with each model run (Table 1). These statistics were calculated for horizontal wind components (u, v) as well as temperature, since these variables are key determinants, respectively, of air parcel trajectories and stability within the STILT simulations. The RMSE and model bias at all observation stations were then averaged over July 2007 to arrive at an average error statistic for each WRF run as seen in Table 1.

The WRF simulations that utilized settings discussed in *Nehrkorn et al.* [2013] (WRF runs #6 and 7) exhibited the best performance when compared against surface and upper air observations. These simulations used the Purdue Lin scheme for microphysics and the Grell-Devenyi ensemble scheme for the cumulus parameterization in domain 1 only, with the urban canopy model switched on [*Grell and Devenyi*, 2002; *Lin et al.*, 1983]. Grid nudging was also switched on for the horizontal wind components and temperature for all WRF vertical levels above the PBL for domain 1 only with a nudging coefficient of 3×10^{-4} s^{-1}. WRF#6 had the lowest average RMSE for the u and v wind components (2.72 and 2.66 m/s) while WRF#7 had the lowest RMSE for temperature (1.63°C). Both of these runs also exhibited small biases for wind vectors and temperature (Table 1).

In addition to these error statistics, the vertical profiles of potential temperature (θ) from each of these runs were compared to the Salt Lake City Airport (KSLC) upper air observation site at the SLC airport (40.79°N, −111.98) at 0000 and 1200 UTC (Figure 3).

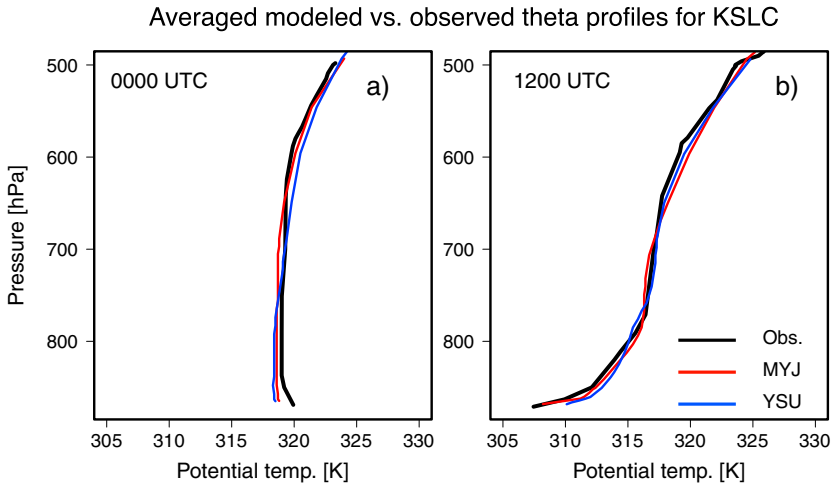

Figure 3. (a) Comparisons between the averaged 0000 UTC upper air observations and modeled potential temperature profiles for KSLC during the month of July 2007. (b) The average for the 1200 UTC potential temperature profiles. The black lines are the observed values, the red lines are the modeled values using the MYJ scheme, and the blue lines are modeled values using the YSU scheme.

STILT-simulated footprint strengths are dependent on whether the meteorological model driving STILT accurately resolves the PBL height. Resolving inversion events in mountain valleys like the SLC valley can be especially difficult for numerical weather models [*Chen et al*., 2012; *Lareau et al*., 2013; *Silcox et al*., 2012; *Reeves et al*., 2011]. Furthermore, CO_2 and CO concentrations within SLC exhibit a strong diurnal signal that is dependent on the growth/decay of the PBL, further necessitating accurate simulations of the PBL [*Strong et al*., 2011; *Nehrkorn et al*., 2013; *McKain et al*., 2012].

The θ profiles for WRF#6 and #7 were averaged for the month of July 2007 and were plotted against the KSLC upper air observation site (Figure 3). Both WRF simulations over KSLC for 0000 UTC showed a slight cool bias below the 750 hPa pressure level, with minimal differences separating the two runs (Figure 3a). However, the WRF simulation that adopted the 1.5-order-closure Mellor-Yamada-Janjić PBL scheme (MYJ; WRF#7) did a better job resolving nocturnal inversions when compared to WRF#6 which used the first-order-closure, eddy-diffusivity turbulence Yonsei-University PBL scheme (YSU) (Figure 3b) [*Mellor and Yamada*, 1982; *Hong et al*., 2006]. This is in accordance with the results found in *Nehrkorn et al*. [2013] who also concluded that WRF simulations using the MYJ PBL scheme performed the best in resolving the near-surface θ profile at SLC. Henceforth, WRF#7 was chosen as the optimal WRF configuration for all subsequent simulations.

The STILT model was run with multiple particles that traveled 72 h backward in time, with a time step of 2 min for the mean-wind component (and turbulence time steps on the order of seconds). Unlike single-trajectory models, STILT simulates backward trajectories as an ensemble to account for the random turbulence air parcels experience, particularly while traveling within the PBL [*Lin et al*., 2013]. A particle ensemble size of 2000 was chosen, following the sensitivity analysis described below. Theoretically, an extremely large number of particles are needed to represent the ensemble properties of atmospheric transport. Due to finite computational resources and lack of meteorological input that can comprehensively parameterize eddy motions, only an ensemble of limited size can be simulated. A limited number of particles can lead to incomplete sampling of particle trajectories and emissions, which can cause modeled concentrations to fluctuate depending on the size of the particle ensemble, with the fluctuation decreasing as the particle number increases [*Gerbig et al*., 2003]. To assess the magnitude of these fluctuations as a function of ensemble size, 50 STILT simulations for CO were run for each ensemble size on 15 August 2012 at 0000 UTC (Figure 4). This particular day was chosen as there were significant wildfire contributions toward SLC's CO concentrations at this time. The standard deviation of these simulations was calculated for each ensemble size in order to quantify the sensitivity of the STILT model (Figure 4). As expected, the model shows the most sensitivity to ensemble size when simulating the contributions from distant point sources, which was the case for the wildfire contributions seen in Figure 4. On the other hand, limited sensitivity to ensemble size was observed in the simulated background concentrations, likely due to its smaller spatial

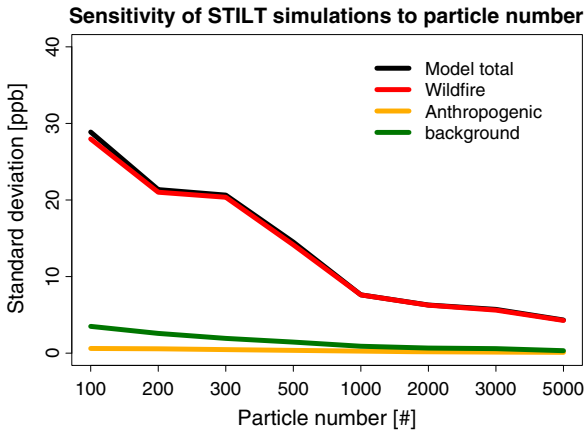

Figure 4. Fluctuations in STILT-simulated CO as a function of the particle ensemble size, i.e., number of particles. The standard deviation of 50 different STILT runs to simulate CO from different components (total, wildfire, anthropogenic, and background) arriving at SLC for 15 August 2012 is calculated for each particle ensemble size.

variability and the fact that the STILT particles are already highly dispersed at the end of the 72 h simulation. The anthropogenic contributions also exhibited a limited amount of sensitivity to the ensemble size as most of these contributions originated locally from sources within the SLC valley. An ensemble size of 2000 was chosen since model fluctuations appeared to be highly damped.

2.2. Wildfire Emissions

Wildfire CO, CO_2, and $PM_{2.5}$ emissions for the western U.S. were obtained from an updated version of the Wildland Fire Emissions Inventory (WFEI) [*Urbanski et al.*, 2011]. The updated WFEI includes new CO and $PM_{2.5}$ emission factors for forest fires [*Urbanski*, 2013]. For 2012, the Moderate Resolution Imaging Spectroradiometer (MODIS Direct Broadcast)-based burned area used in WFEI was unavailable and alternate sources of burned area maps were employed. Daily burned area was based on a combination of fire perimeter polygons collected by the U.S. Geological Survey GeoMAC (http://wildfire.usgs.gov/geomac/index.shtml) and a daily MODIS burn scar product produced by the U.S. Forest Service Remote Sensing Applications Center (http://activefiremaps.fs.fed.us/burnscar.php) using the algorithm of *Giglio et al.* [2009]. Fire perimeter area not mapped by the daily MODIS burn scar product was assigned an estimated burn date using active fire detections from the MODIS MXD14 product [*Giglio et al.*, 2003] and NOAA's Hazard Mapping System (http://www.ssd.noaa.gov/PS/FIRE/hms.html). The 2012 emission product also integrated significant updates for vegetation maps and fuel loading. Forest vegetation type and fuel loading were assigned based on a Forest Type Group map [*Ruefenacht et al.*, 2008] and the forest surface fuel classification of *Keane et al.* [2013]. The surface fuel loading was augmented with fuel loading estimates of understory fuels [*Wilson et al.*, 2013] and canopy fuels, the latter of which was estimated from canopy spatial data layers from the LANDFIRE project [*LANDFIRE*, 2014]. Area mapped as nonforest in the Forest Type Group map was assigned fuel loading from a MODIS normalized difference vegetation index-based rangeland biomass product (M. Reeves, manuscript in preparation, 2014). Forest canopy fuel consumption was taken as 50% while consumption of other fuel components was estimated using the First-Order Fire Effects Model assuming "dry" conditions (see *Urbanski et al.* [2011] for details). As in the 2007 emission data set, CO and $PM_{2.5}$ emission factors for forest fires were taken from *Urbanski* [2013]. For both 2007 and 2012 the heat flux was estimated using a heat of combustion of 18.6 MJ kg^{-1} biomass [*Susott et al.*, 1975; *Klass*, 1998]. The WFEI is available daily at 500 m grid spacing for years between 2003 and 2008, as well as 2012. Annual, domain-wide uncertainties within the WFEI range from 28 to 51% for CO emissions and 40–65% for $PM_{2.5}$ emissions [*Urbanski et al.*, 2011]. Emissions from the WFEI were regridded to latitude/longitude grids with a spatial resolution of 0.1° × 0.1° to match the WRF-STILT footprint grid. Finally, the WFEI daily emissions were scaled by time of day using daily factors obtained from the Global Fire Emissions Database v3.1 [*Mu et al.*, 2010; *van Der Werf et al.*, 2010].

2.3. Anthropogenic Emissions

Global anthropogenic CO_2 and CO emissions were obtained from the Emission Database for Global Atmospheric Research (EDGAR), which has a spatial resolution of 0.1° × 0.1° and is available from 1970 through 2010 [*European Commission*, 2009]. Previous CO_2 modeling studies for the SLC area used the VULCAN database [*Gurney et al.*, 2009] for an anthropogenic CO_2 emissions field [*Strong et al.*, 2011; *Nehrkorn et al.*, 2013; *McKain et al.*, 2012]. However, these researchers found VULCAN-derived simulations to consistently underestimate CO_2 concentrations across the SLC valley [*Nehrkorn et al.*, 2013; *McKain et al.*, 2012]. *Nehrkorn et al.* [2013] hypothesized that the systematic underprediction of CO_2 was caused by an overestimation of mixing by the WRF model and/or an underestimation in anthropogenic emissions predicted by VULCAN.

Initial findings in this study found that the systematic underestimation of CO_2 was removed when using the EDGAR data set scaled by hour of day for anthropogenic emissions (not shown). Scaling factors were needed for time of day for CO and CO_2 due to the fact that EDGAR only reports annual emissions. Hourly scaling factors for CO emissions in northern Utah were computed by dividing the Utah's Division of Air Quality (UDAQ) SMOKE emissions (hourly temporal resolution for the summer of 2007) by the annual EDGAR emissions. UDAQ SMOKE emissions were not available outside of July 2007 and were limited to northern Utah, so these emissions could not be used directly within WRF-STILT. The hourly scaling factors for CO were then applied back to the EDGAR emissions based on the time of day. This methodology was only applied to emissions for northern Utah due to domain constraints in UDAQ SMOKE inventory. This is a reasonable approximation, since we found that anthropogenic emissions beyond northern Utah only account for ~3–5% of the anthropogenic CO arriving at SLC, on average. A similar methodology was applied to the EDGAR CO_2 emissions using time-of-day scaling factors obtained from VULCAN. A simple linear trend was then calculated for EDGAR CO emissions from 2000 to 2008, in order to extrapolate CO emissions to 2012.

2.4. Biospheric Fluxes

The biospheric flux fields within CarbonTracker-2013, which utilized the Carnegie-Ames-Stanford Approach model [*Potter et al*., 1996, 1999; *Potter and Klooster*, 1997], were used to obtain biospheric CO_2 fluxes. CarbonTracker is a CO_2 assimilation system developed by NOAA in order to quantify the sources and sinks of CO_2 over the globe [*Peters et al*., 2007]. The CarbonTracker biospheric flux field is available every 3 h from 2010 through 2012 with a horizontal grid resolution of 1 × 1° for North America.

2.5. Background CO and CO_2 Concentrations

CarbonTracker-2013's 3-D fields of CO_2 were applied as background concentrations by taking the endpoints of the 2000 particle ensemble members and interpolating them to the corresponding grid cell 72 h backward in time. The background concentrations at the trajectory endpoints are then simply advected to the receptor location. The global CarbonTracker-2013 data set has a gridded resolution of 3 × 2° at the global scale and 1 × 1° for North America with a temporal resolution of 3 h. For CO, the Model for Ozone and Related Chemical Tracers (MOZART-4) database [*Emmons et al*., 2010] was used to obtain background concentrations using the same methodology described for CO_2 with the exception that oxidation with OH is applied throughout the STILT trajectory pathways (discussed in the next section). The MOZART-4 model has a global domain with a gridded resolution of 2.8 × 2.8° with a temporal resolution of 6 h. Uncertainties in background CO concentrations as simulated by MOZART are approximately 15 ppb [*Emmons et al*., 2010].

2.6. Chemical and Depositional Losses

Chemically reactive species such as CO and $PM_{2.5}$ undergo transformations as they are transported through the atmosphere. Using the methodology described in *Miller et al*. [2008], we applied a first-order chemical loss due to reactions with OH to the CO simulations. Six-hourly OH concentrations were obtained from MOZART-4. The loss of CO due to the presence of OH in the atmosphere can be described by the following equation:

$$\frac{\partial[\mathrm{CO}]}{\partial t} = -k[\mathrm{OH}][\mathrm{CO}] \tag{2}$$

where k is the oxidation rate constant obtained from the *NASA's Jet Propulsion Laboratory*'s [2011] chemical kinetics publication. This reaction was applied to each STILT particle at 2 min time steps.

$PM_{2.5}$ is influenced by dry/wet deposition (sink) and secondary formation from chemical reactions with other species (source). Dry deposition survival rates were obtained by applying a size-segregated particle dry deposition scheme developed by *Zhang et al*. [2010] to the STILT trajectories. Dry deposition was only applied to particles that dipped below the STILT model PBL height. The diameter and particle density of wildfire-emitted $PM_{2.5}$ used in this scheme were assumed to be 0.25 μm and 1.3 g/cm^3, respectively [*Reid et al*., 2005]. The wet deposition rates for $PM_{2.5}$ along each trajectory path were calculated using an adaption of the GEOS-Chem wet deposition scheme, which assumes that aerosols are hydrophilic [*Liu et al*., 2001]. Both dry and wet deposition were calculated every 2 min along each trajectory. The secondary

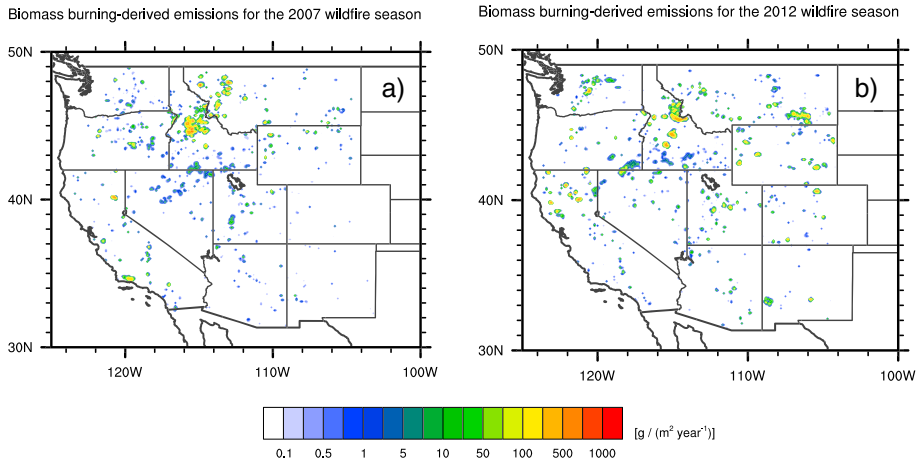

Figure 5. Total wildfire emissions for the (a) 2007 and (b) 2012 western U.S. wildfire season as derived from the updated WFEI.

formation of $PM_{2.5}$ was excluded from the WRF-STILT model framework due to the complexity of $PM_{2.5}$ reactions with other chemical species. Incorporating the secondary formation of $PM_{2.5}$ will be part of a future study.

2.7. Observation Networks

Near-surface CO_2 concentrations have been measured continuously since 2001 across much of Salt Lake valley using a network of infrared gas analyzers [*Pataki et al.*, 2003, 2006; *Ehleringer et al.*, 2008, 2009]. This particular study focused on the Sugarhouse site, which is approximately 3 miles equals 5 km (approximation) to the southeast of downtown SLC (40.73°N, −111.86°W).

CO and $PM_{2.5}$ measurements were obtained from the UDAQ's Hawthorne site (40.73°N, −111.87°W) in SLC, which is maintained by UDAQ and is approximately 1 km to the west of the Sugarhouse CO_2 monitoring site. The Tapered Element Oscillating Microbalance Filter Dynamic Measuring System was used to obtain hourly $PM_{2.5}$ concentration while CO measurements were obtained using the Instrumental Gas Phase Correlation [*UDAQ*, 2012a]. Measurements of potassium ion and organic carbon concentrations were

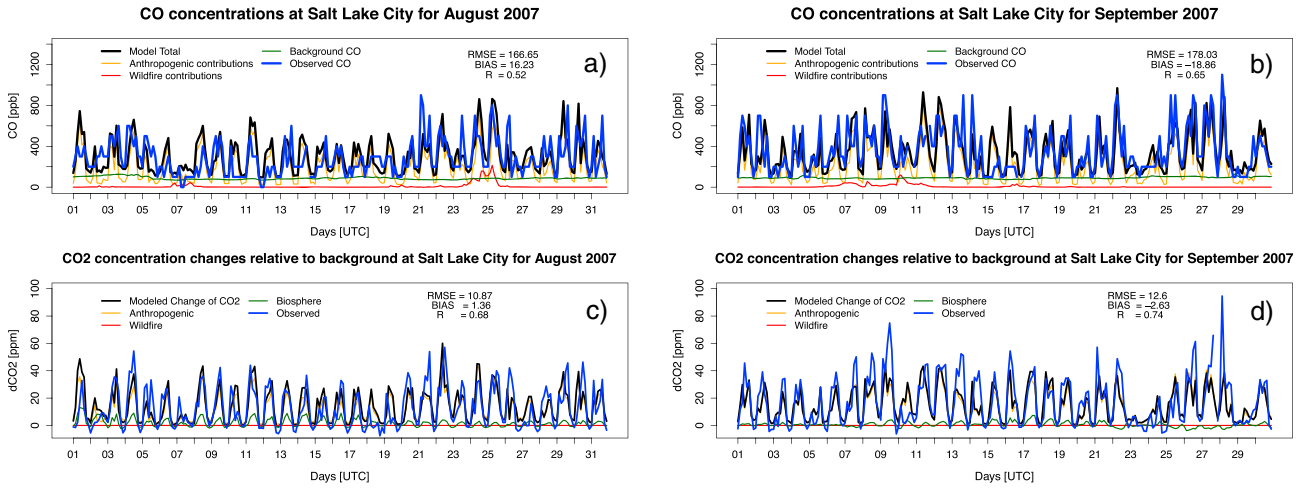

Figure 6. (a and b) STILT-simulated and observed CO concentrations at SLC during August and September 2007. The black line is modeled total CO, while the orange, red, and green lines are contributions from anthropogenic and fire emissions and the background CO. The blue line is the observed CO concentrations at SLC. (c and d) STILT-simulated and observed CO_2 concentrations at SLC during August and September 2007. The black line is the modeled total CO_2 while the orange, red, and green lines represent the source contributions.

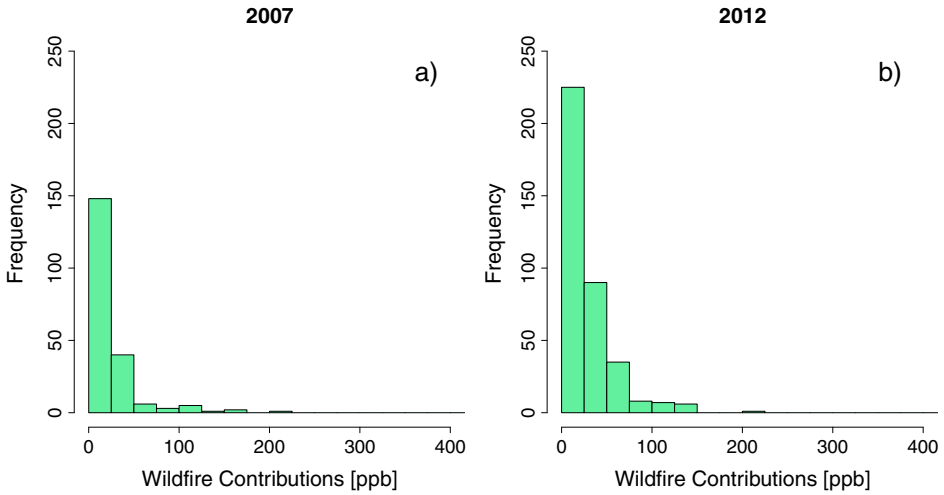

Figure 7. Frequency of 3-hourly wildfire contributions to SLC CO concentrations for the (a) 2007 and (b) 2012 western U.S. wildfire seasons. Wildfire contributions ≥5 ppb are included in the lowest bin.

obtained from UDAQ. The Hawthorne observation site is one of three urban $PM_{2.5}$ chemical speciation monitors that are part of EPA's Speciation Trends Network [*UDAQ*, 2012a]. Potassium ion and organic carbon are considered good biomarkers for wood smoke and were later used to verify periods of increased wildfire activity simulated by the STILT model [*Pachon et al.*, 2013; *Zhang et al.*, 2010; *Cheng et al.*, 2013; *Park et al.*, 2007].

3. Results

3.1. Wildfire Season of 2007

The summer of 2007 was the first wildfire season analyzed for wildfire contributions toward SLC. Western U.S. wildfires emitted a total of 76 Tg of CO_2 and 5.6 Tg of CO which exceeded the 2004–2008 season average of 44 Tg of CO_2 and 3.1 Tg of CO, according to the updated version of WFEI. The majority of the emissions

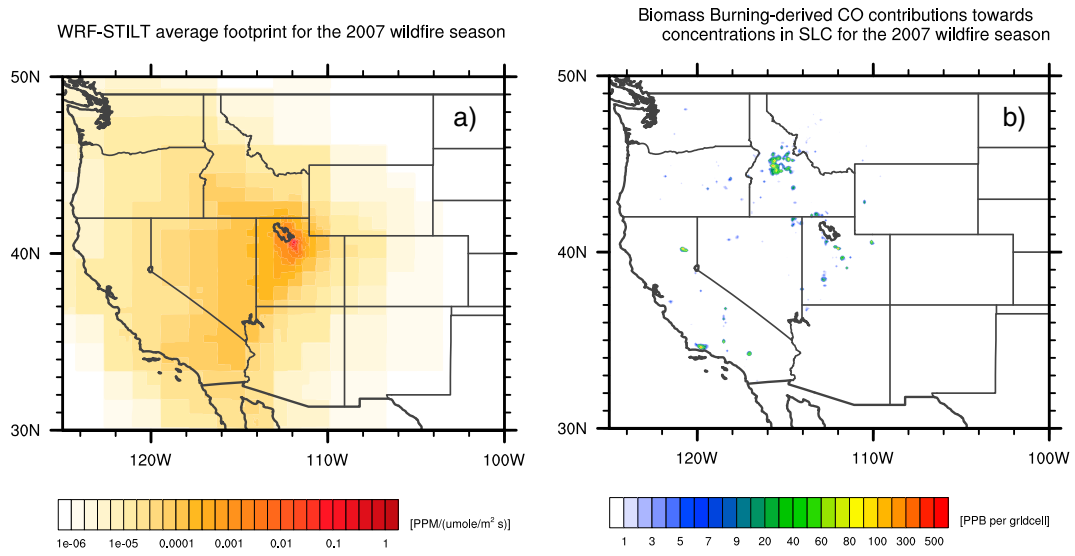

Figure 8. (a) STILT-generated average footprints for the 2007 wildfire season. (b) Wildfire-derived contributions to CO concentrations at SLC, integrated over the 2007 wildfire season.

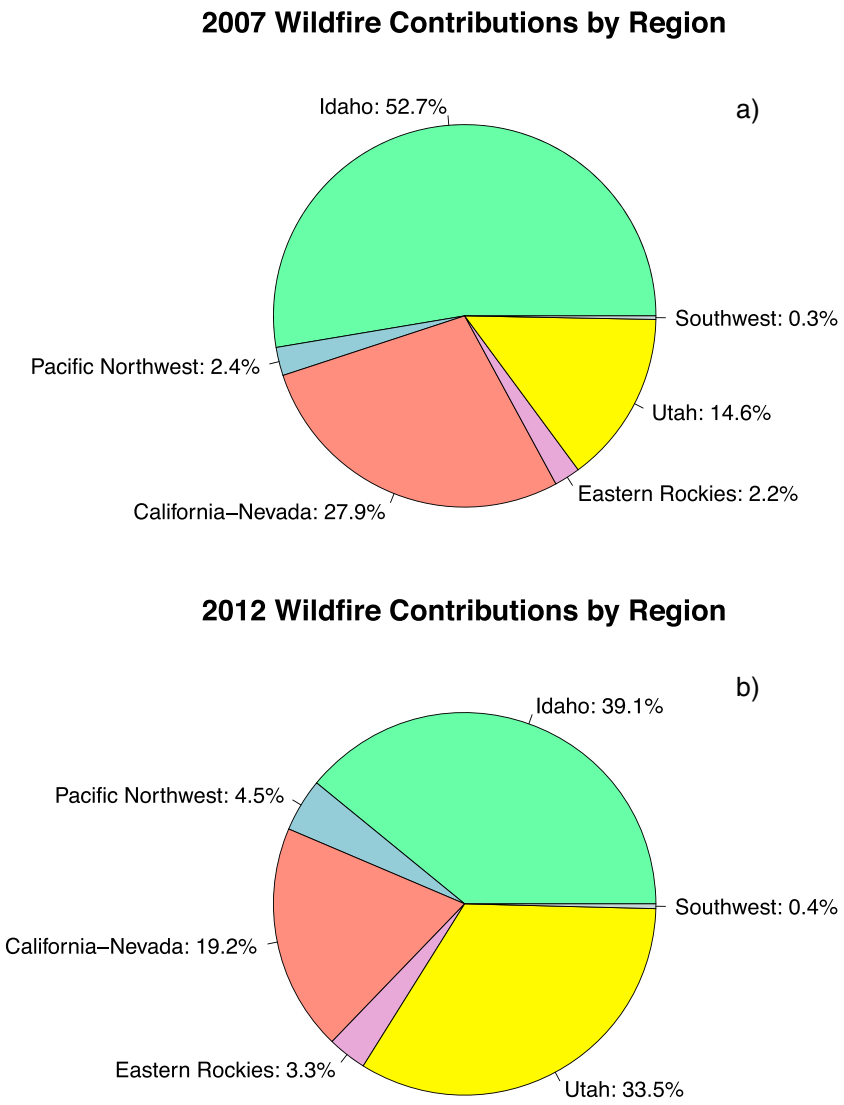

Figure 9. The contribution from each of the source regions to wildfire-derived CO enhancements at SLC for the (a) 2007 and (b) 2012 western U.S. wildfire seasons.

forthe 2007 wildfire season occurred in central Idaho, upwind of SLC (Figure 5a). A large portion of this wildfire activity occurred during the months of August and September.

Simulations for CO and CO_2 were carried out from June through October to determine the influences that upwind wildfires had on SLC air quality. STILT-simulated CO concentrations for SLC showed reasonable agreement with the measured values as the timing and magnitude of the diurnal cycle were well captured by the model (Figures 6a and 6b). Anthropogenic emissions were the dominant source of CO for SLC when integrated across the months of August and September. Northern Utah accounted for the majority (95–97%) of the anthropogenic contributions to SLC with sources outside of the state accounting for only 3–5%. Despite the significant wildfire activity across northern Idaho, the overall impact of these fire emissions on the SLC's CO concentrations was limited to a few days during the fourth week of August and third week of September (Figures 6a and 6b). Minimal wildfire contributions were observed in the modeled CO concentrations during June, July, and October (not shown).

Significant wildfire contributions toward elevated 3-hourly CO concentrations in SLC were sporadic for the 2007 western U.S. wildfire season (Figure 7a). Only a handful of these episodes contributed more than 50 ppb toward hourly CO concentrations. The mean of the "nonnegligible" wildfire episodes (defined as

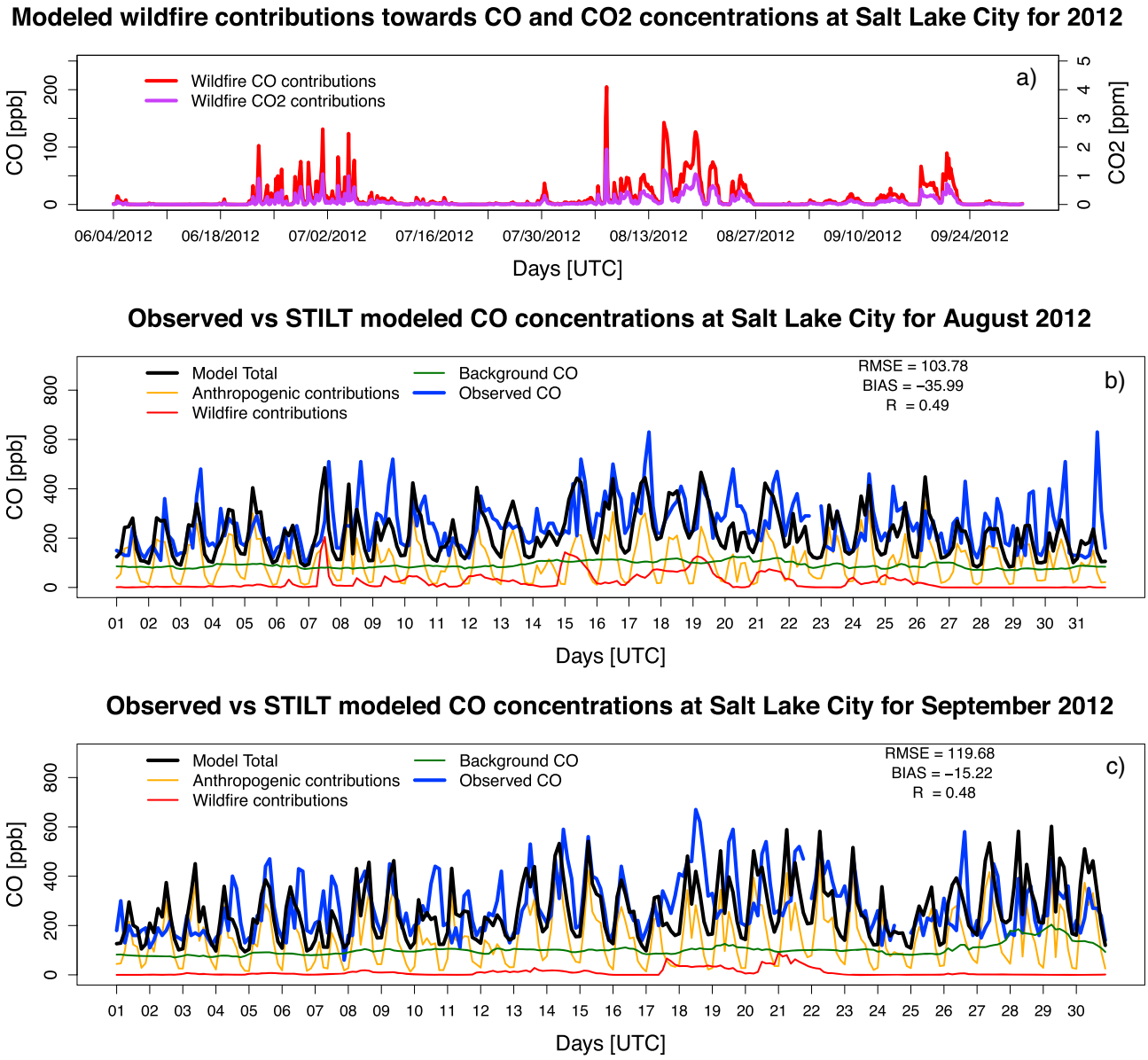

Figure 10. (a) Modeled wildfire CO contributions for the entire 2012 western U.S. wildfire season. (b and c) STILT-simulated and observed CO concentrations for SLC, zoomed in on August and September 2012. The black line is model total while the orange, red, and dark green lines are contributions from anthropogenic and fire emissions and the background CO, respectively. The blue line is the observed CO concentrations for SLC.

enhancements ≥ 5 ppb) was 23.4 ppb, while the median was much lower at 12.6 ppb. Major episodic wildfire events (>95% percentile) for the 2007 wildfire season elevated SLC's CO concentrations in excess of 86.4 ppb, with a median of 118.9 ppb.

The spatial distribution of these contributions suggested that wildfires in northern Idaho were responsible for much of the wildfire-derived CO enhancements in SLC (Figure 8). CO contributions from wildfires were aggregated by source region, as seen in Figure 8, which included the Pacific Northwest (Washington and Oregon), California + Nevada, Idaho, Utah, the Southwest (Arizona and New Mexico), and the eastern Rockies (Colorado, Wyoming, and Montana). Overall, the majority of the wildfire source contributions toward CO enhancements in SLC for 2007 came from Idaho (52.7%), with California + Nevada contributing an additional 27.9% (Figure 9a). Wildfires within Utah only contributed 14.6%, while the Southwest and the eastern Rockies had wildfire source contributions that were under 3% (Figure 9a). The Pacific Northwest contributed the remaining 2.4%.

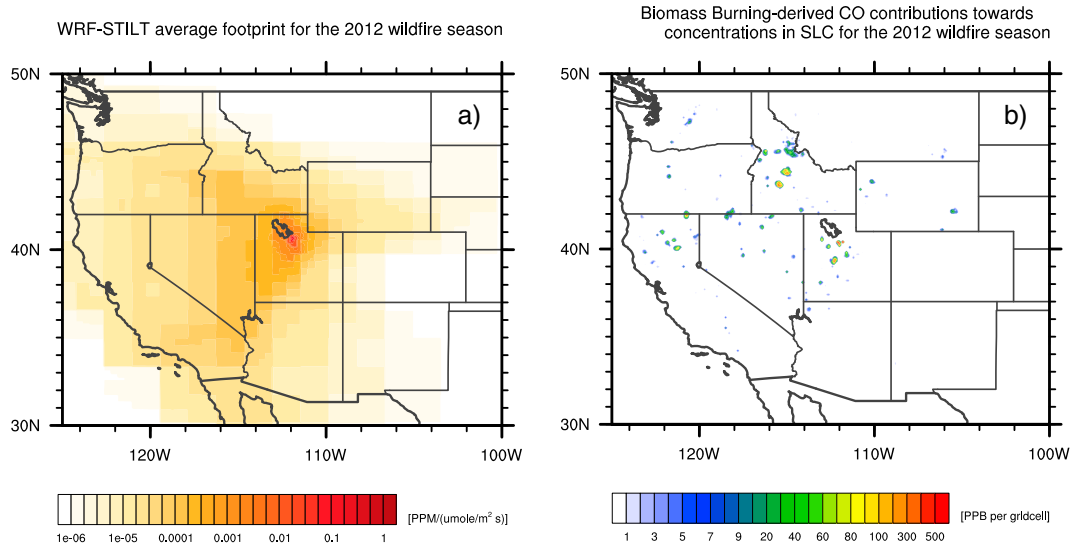

Figure 11. The same plots as in Figure 8 but for the 2012 western U.S. wildfire season.

CO_2 emitted by wildfires had a much smaller impact on SLC, as seen in Figures 6c and 6d. As with CO, the anthropogenic emissions coupled with the shallow nocturnal PBL were the strongest driver of CO_2 enhancements. Overall, wildfires played a negligible role throughout August and September (Figures 6c and 6d) despite the increased wildfire activity during 24–26 August and 6–12 September as seen in the STILT CO simulations. Anthropogenic emissions in SLC were the dominant contributor to local elevated CO_2 concentrations, with biospheric fluxes having a second-order effect. WRF-STILT CO_2 simulations were in reasonable agreement with observations. The SLC CO_2 simulations had a bias of only −1.3 ppm and a RMSE of ~11 ppm (Figures 6c and 6d). This improves upon previous WRF-STILT studies for the SLC valley [*Nehrkorn et al*., 2013; *McKain et al*., 2012], which found that the model generally underestimated CO_2 concentrations during the night. The difference here may be the enhanced capability of WRF in resolving the nocturnal inversion better (Figure 3a).

Taken as a whole, the CO_2 simulations suggest that the WRF-STILT model is performing reasonably, albeit the comparisons did not necessarily provide an indication of whether wildfire-derived CO_2 was captured by the model, due to its minor impact on elevating CO_2 values.

3.2. Wildfire Season of 2012

The 2012 wildfire season was another active year for the western U.S., with over 6 Tg of CO and 80 Tg of CO_2 emitted, according to the updated WFEI. This was nearly double the average emission for the 2004–2008 wildfire seasons over western U.S. Similar to the 2007 western U.S. wildfire season, the 2012 fires were primarily located across Idaho with additional wildfire activity located across the eastern Rockies (Figure 5b). There was also increased local wildfire activity within Utah that was absent in 2007. Simulations for the 2012 wildfire season were carried out for June through September. October 2012 was excluded from consideration since no major wildfires were present. Simulations for the 2012 wildfire season showed frequent wildfire impact on CO concentrations at SLC (Figure 10a). There were three distinct episodes of prolonged wildfire impacts: 24 June to 5 July, 6–24 August, and 19–24 September (Figure 10a). Wildfire contributions toward CO_2 concentrations in SLC were also observed during these times (Figure 10a), though these contributions were insignificant ($<$2 ppm) when changes in CO_2 concentrations in SLC generally exceed 35 ppm from local anthropogenic and biospheric sources.

The time-integrated wildfire contribution toward CO enhancement in SLC was greater in 2012 than in 2007 by a factor of 2.3. The 2012 wildfire season was characterized by more frequent episodes of wildfire-derived enhancements that often lasted longer than those in 2007 (Figure 7b). The mean CO enhancement from nonnegligible episodes ($\geq$5 ppb) was 28.6 ppb, with a median of 17.2 ppb. This was greater than the 2007

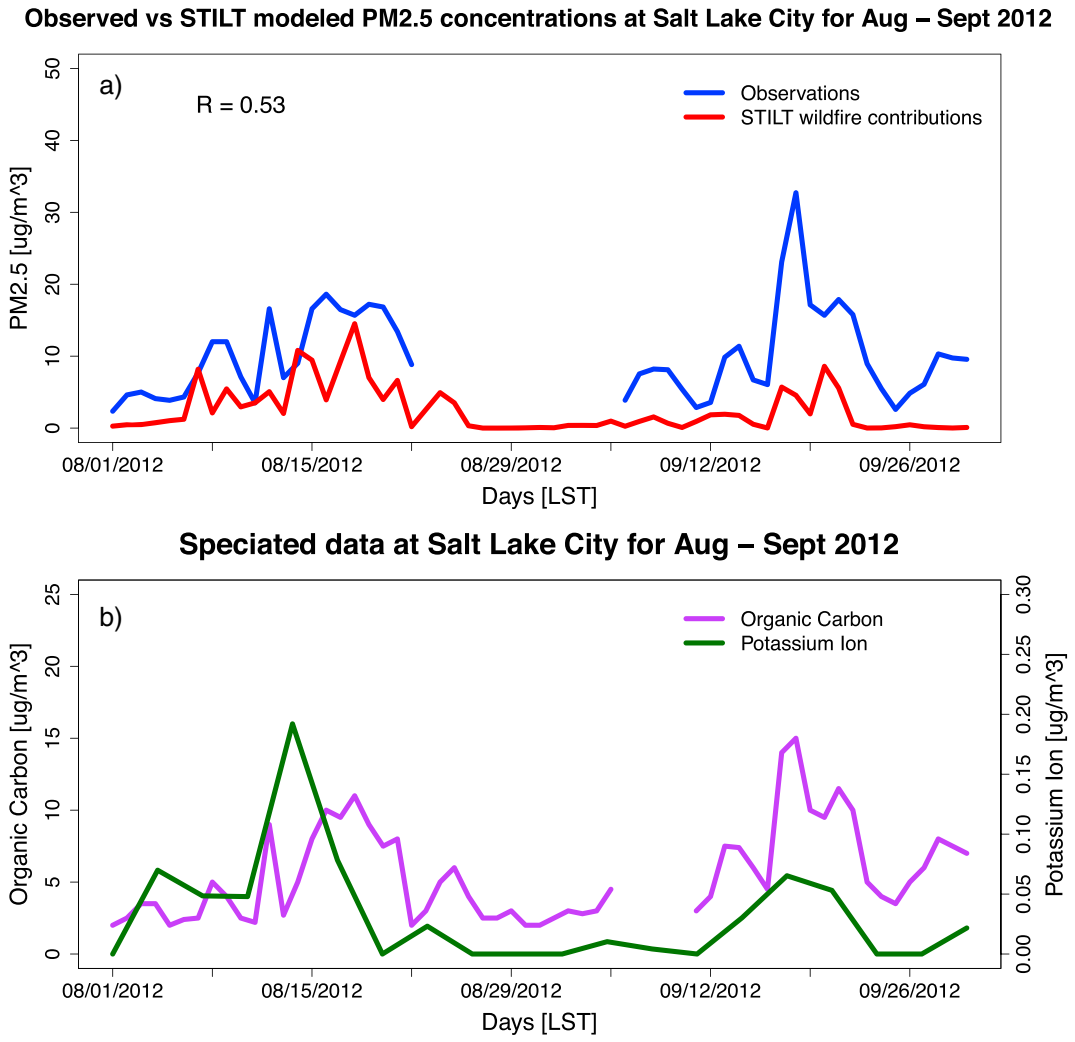

Figure 12. (a) Modeled and observed daily averaged $PM_{2.5}$ concentrations at SLC. (b) Measured values of organic carbon (daily) and speciated potassium ion concentrations (every 3 days) at SLC.

western U.S. wildfire season, which reported a mean and median of 23.4 and 12.6 ppb, respectively. The most intense wildfire episodes (>95% percentile) had enhancements with a median of 122.3 ppb (Figure 7b), which was also higher than the value in 2007.

Wildfires in Utah had a much larger impact on SLC in 2012 than in 2007, contributing 33.5% of the CO enhancements over the entire season (Figures 9b and 11), versus only 14.6% in 2007 (Figure 9a). Wildfires in Idaho continued to play a large role, with 39.1% of the contributions coming from this source region in 2012 (Figure 9b). Contributions from California + Nevada were moderate role (19.2%) while the impacts from the wildfires in the Pacific Northwest and eastern Rockies were minimal, with only 4.5% and 3.3%, respectively (Figure 9b). Contributions from the southwestern U.S. were considered negligible, with contributions under 1%.

WRF-STILT simulations for CO performed reasonably well when compared against observed values in SLC for August and September (Figures 10b and 10c). Increased wildfire activity started around 6 August and was fairly persistent through 25 August (Figures 10a and 10b). The daily averaged $PM_{2.5}$ concentrations (both modeled and observed) are shown in Figure 12a for SLC. The enhancements seen in the observed $PM_{2.5}$ correspond roughly with increases in modeled wildfire contributions to $PM_{2.5}$, with a correlation coefficient of 0.53 (Figure 12a).

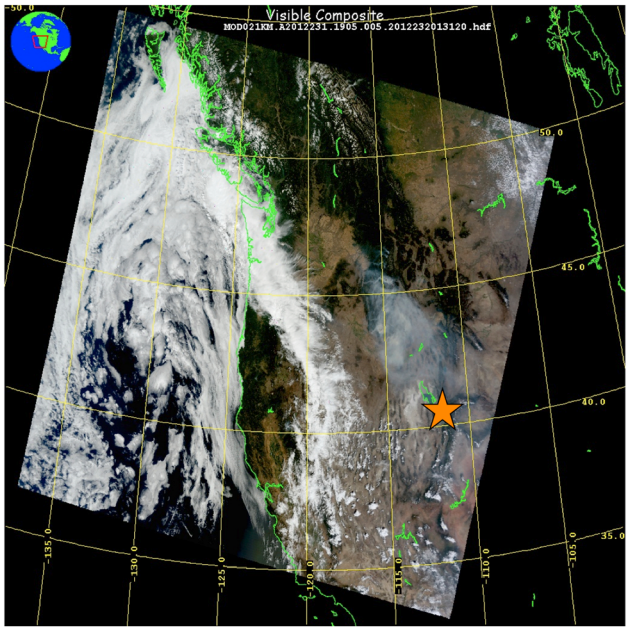

Figure 13. MODIS scan from the TERRA polar-orbiting satellite of the visible light spectrum on 18 August 2012 at 1905 UTC. The star indicates the location of SLC. Credit: NASA.

While the WRF-STILT model appeared reasonable in resolving periods of increased wildfire contributions for August and September 2012, it is difficult to determine from CO and $PM_{2.5}$ concentrations alone whether enhancements can be directly attributed to increased wildfire contributions. Therefore, speciated particulate matter observations were used as an additional means to verify days of wildfire contributions.

The increased wildfire contributions as suggested by WRF-STILT match up, in general, with the elevated concentrations of speciated organic carbon and potassium ions (Figure 12b) between 8–25 August and for 13–23 September. The correspondence between modeled $PM_{2.5}$ from wildfires against the observed $PM_{2.5}$, organic carbon, and potassium ions suggests that modeled wildfire contributions are likely realistic. However, the exact contributions suggested by the WRF-STILT to enhancements of $PM_{2.5}$ cannot be regarded as quantitative, due to the lack of consideration of chemical reactions that affect $PM_{2.5}$. This could also explain the discrepancies between the modeled wildfire contributions and the observed $PM_{2.5}$ contributions.

NASA satellite remote sensing products were also used to verify periods of increased wildfire contributions. The strongest and most persistent wildfire activity found in the WRF-STILT simulations occurred from 14 through 21 August. The MODIS Terra polar-orbiting satellite made a direct pass over western U.S. on 18 August at 1905 UTC (Figure 13). Large wildfires were present over central Idaho during this time, with smoke advected in a southward direction toward SLC (Figure 13). The aerosol optical depth (AOD) product was also available for this time (Figure 14). A higher AOD indicates that more aerosols are present in the atmospheric column [*Schaap et al.*, 2009; *Natunen et al.*, 2010; *UDAQ*, 2013]. Widespread areas across the Intermountain West with high AOD (>0.4) are colocated with the wildfires and smoke shown in Figure 13. While SLC is in a region of missing data, surrounding and upwind regions have AOD values that exceed 0.5. The cause of the missing data to the west of SLC can likely be attributed to the nearby Salt Flats. The nearest available data point to SLC was located over Ogden, UT. This point had an AOD of 0.6 (Figure 14), which loosely corresponds with a $PM_{2.5}$ mass

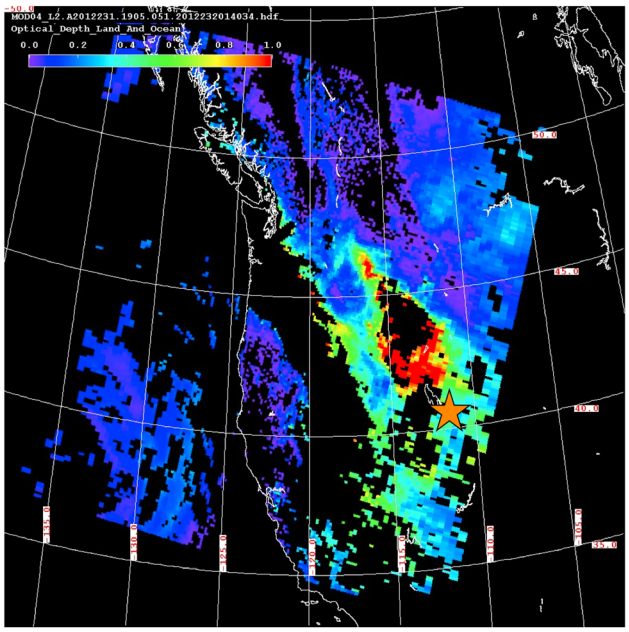

Figure 14. Aerosol optical depth as retrieved from MODIS-TERRA, observed at the same time as shown in Figure 12. The star indicates the location of SLC. Credit: NASA.

concentration of 36 $\mu g/m^3$ [*Schaap et al.*, 2009; *Natunen et al.*, 2010]. The SLC site measured $PM_{2.5}$ concentrations between 15 and 20 $\mu g/m^3$ for the same time while the STILT-modeled $PM_{2.5}$ wildfire contributions had a similar magnitude.

4. Discussion

The WRF-STILT model was used to estimate the impact of upwind wildfires on SLC's CO_2, CO, and $PM_{2.5}$ concentrations for two major western U.S. wildfire seasons. The modeling framework incorporated a variety of sources/sinks for each species in order to determine the wildfire contributions relative to the other sources/sinks. Through the analyses shown earlier in this study, the WRF model was able to adequately resolve the growth/decay of the PBL and the wind fields over northern Utah resulting in realistic meteorological drivers to derive the STILT backward trajectories. Additionally, the simulated CO_2 and CO values compare reasonably against observations in SLC.

WRF-STILT model results for CO_2 in 2007 indicate that wildfires play a negligible role toward enhancements in CO_2 concentrations within the SLC valley. As already shown by *Strong et al.* [2011], anthropogenic emissions were a dominant source of CO_2 with biospheric fluxes playing a minor role in CO_2 variability at SLC. The diurnally varying anthropogenic emissions, in combination with the growth and decay of the PBL in the SLC valley, were responsible for the strong diurnal cycles seen in CO_2, resulting in changes of 20–40 ppm for CO_2 that dominate over the <2 ppm maximum wildfire signal. This, combined with transport uncertainties associated with the WRF-STILT model (see below), likely makes the wildfire contribution to CO_2 difficult to separate out.

The simulations indicate that wildfire contributions to CO enhancements in SLC were also fairly minimal for the 2007 wildfire season, with the exception of a 2 day wildfire episode toward the end of August and another minor wildfire period in the middle of September. The 25 August event contributed substantial CO, such that concentrations increased by a factor of ~1.5 during the afternoon. Despite these large contributions, anthropogenic emissions during the nighttime led to the largest CO enhancements, due to trapping of these emissions by the nocturnal inversion. The 2012 wildfire season was characterized by more numerous wildfire contributions to CO within the SLC valley. There were several instances in which wildfire-derived CO enhancements actually exceeded those from anthropogenic emissions. Large contributions were especially prevalent across the months of August and September 2012. With the exception of a local fire on 6–8 August, most of the wildfire contributions during these months came from large wildfires in central Idaho, which were over 400 km away from SLC. Despite the increased wildfire contributions for the 2012 western U.S. wildfire season, these events were transient in nature.

Similar to CO_2, errors in modeled CO concentrations exist due to uncertainties in PBL mixing, advection, and background values. Uncertainties in the background CO concentrations as simulated by MOZART are approximately 15 ppb [*Emmons et al.*, 2010]. Errors due to advection for wildfire sources for CO are around 50%, while PBL mixing represents a relative uncertainty of 35%, following roughly the error statistics derived for CO_2 in *Lin and Gerbig* [2005] and *Gerbig et al.* [2008]. These error sources result in a ~60% uncertainty in the wildfire-derived CO enhancement (assuming statistical independence between different errors). It should be noted that significant effort in testing different WRF configurations centered over the SLC region and in assessing the veracity of the simulated meteorology (Table 1 and Figure 3) suggests that these uncertainties may be conservative.

Primary $PM_{2.5}$ contributions from wildfires were substantial for August and September for the 2012 wildfire season. Most of the increases in observed $PM_{2.5}$ concentrations corresponded with increased wildfire contributions, as suggested by the WRF-STILT model with the exception of a few days. Speciated data from SLC for August and September were consistent with times when wildfires were burning in the upwind source region, as identified by the model. Furthermore, remote sensing products from MODIS were also used to verify the source of increased levels of $PM_{2.5}$. The MODIS visible and aerosol optical depth products clearly showed large smoke plumes originating over central Idaho that fanned out over SLC. The WRF-STILT model output coupled with remote sensing images confirmed that western U.S. wildfires had a substantial impact on SLC's air quality during August to September 2012.

While the study makes a good first estimate of wildfire contributions toward $PM_{2.5}$ concentrations in SLC, more work needs to be done to account for the additional chemical production of $PM_{2.5}$ due to secondary

formation. Previous studies have indicated that the secondary production of $PM_{2.5}$ is sensitive to many environmental factors and can account for 20–80% of total $PM_{2.5}$ [*Zhang et al*., 2013; *Particulate Matter Science for Policy Makers*, 2003]. Future work will use the STILT-Chem model [*Wen et al*., 2012], which simulates chemical transformations along STILT—backward trajectories that will allow the model to explicitly calculate the secondary production of $PM_{2.5}$. This model can also be used to determine the contributions of wildfires to chemically active species such as O_3, which often exceed regulatory limits across the Intermountain West due to upwind wildfires [*Jaffe et al*., 2013; *Jaffe and Wigder*, 2012].

While the WRF-STILT model performed adequately in capturing the wildfire activity for the summer of 2012, it should be noted that the model assumed wildfire emissions took place at the surface and were only diluted initially within the PBL. Although this is likely a valid assumption for many cases in this study, significant wildfires dominated by crown burning are generally associated with higher heat fluxes and buoyancy, which may be able to inject smoke plumes directly into the free troposphere [*Freitas et al*., 2007; *Sessions et al*., 2011; *Lavouè et al*., 2000; *Cofer et al*., 1996; *Generoso et al*., 2007]. This is especially relevant for wildfires across Northern Canada that occur in boreal forests where crown burning is more prevalent. Future work will be needed to parameterize smoke plumes within Lagrangian particle dispersion models in order to reduce the uncertainty in simulating wildfire contributions.

SLC and other urban centers across the western U.S. will continue to be susceptible to a higher risk of wildfires in the coming years. Previous studies have shown a steady increase in wildfire frequency and intensity that is expected to continue as virtually all climate model projections indicate that warmer springs will continue to promote longer wildfire seasons due to earlier snowmelt [*Westerling et al*., 2006; *Dennison et al*., 2014]. The increased frequency and intensity of western U.S. wildfires will only increase the vulnerability of the population in this region to pollutants such as O_3 and $PM_{2.5}$ from wildfires.

While this study represents a first step toward quantifying the impact of wildfires on air quality for urban systems in the Intermountain West, additional model development is needed to reduce its uncertainties along with continued improvement in the wildfire emission inventories. Accounting for additional chemistry and fire plume rises will yield better understanding of the exact impacts of wildfires on western U.S. urban systems. In addition, a formal quantification of the uncertainties originating from the WRF-STILT model and wildfire emissions inventories will be included in a future study. We envision that the Lagrangian modeling framework represented by WRF-STILT could serve as a valuable tool for air quality managers, for understanding wildfire events that lead to pollutant levels exceeding the NAAQS and for potentially demonstrating exceptional events.

Acknowledgments

This study was made possible by NOAA grant NA130AR4310087 and funding from the Utah Division of Air Quality. We would like to thank the Utah Division of Air Quality for carrying our observations at the Hawthorne site (downloaded from http://www.epa.gov/ttn/airs/airsaqs/) and for providing emission data used in this study. D. Mallia gratefully acknowledges the support of the University of Utah's Global Change and Sustainability Center Graduate Fellowship during his first year of graduate studies. The Salt Lake Valley CO_2 observation network was supported by the Office of Science (BER), U.S. Department of Energy, grants DEFG0206ER64309 and DESC0005266 (http://co2.utah.edu). The authors also thank Joshua Benmergui for providing scripts that calculate depositional loss and valuable input from Logan Mitchell, Court Strong, Erik Crosman, John Horel, Adam Kochanski, Deyong Wen, Munkhbayar Baasandorgj, and the University of Utah WRF Users Group. The support and resources from the Center for High Performance Computing at the University of Utah are gratefully acknowledged. The data used to produce the results in this study are available from the corresponding author upon request. Lastly, the authors would like to thank the three anonymous reviewers for their comments and suggestions.

References

Beard, J. D., C. Beck, R. Graham, S. C. Packham, M. Traphagan, R. T. Giles, and J. G. Morgan (2012), Winter temperature inversions and emergency department visits for asthma in Salt Lake County, Utah, 2003–2008, *Environ. Health Perspect.*, *120*(10), 1385–1390, doi:10.1289/ehp.1104349.

Bowman, K. P., J. C. Lin, A. Stohl, R. Draxler, P. Konopka, M. Bourqui, A. Andrews, and D. Brunner (2013), Input data requirements for Lagrangian trajectory models, *Bull. Am. Meteorol. Soc.*, *94*, 1051–1058.

Bravo, A. H., E. R. Sosa, A. P. Sánchez, P. M. Jaimes, and R. M. Saaverde (2002), Impacts of wildfires on the air quality in Mexico City, 1992–1999, *Environ. Pollut.*, *117*(2), 243–253.

Chen, F., and J. Dudhia (2001), Coupling an advanced land-surface–hydrology model with the Penn State–NCAR MM5 modeling system. Part I: Model implementation and sensitivity, *Mon. Weather Rev.*, *129*, 569–586.

Chen, L.-W. A., J. G. Watson, J. C. Chow, M. C. Green, D. Inouye, and K. Dick (2012), Wintertime particulate pollution episodes in an urban valley of the Western US: A case study, *Atmos. Chem. Phys.*, *12*, 10,051–10,064, doi:10.5194/acp-12-10051-2012.

Cheng, Y., G. Engling, K. B. He, F. K. Duan, Y. L. Ma, Z. Y. Du, J. M. Liu, M. Zheng, and R. J. Weber (2013), Biomass burning contribution to Beijing aerosol, *Atmos. Chem. Phys. Discuss.*, *13*, 8387–8434, doi:10.5194/acp-13-7765-2013.

Clinton, N., P. Gong, and K. Scott (2006), Quantification of pollutants emitted from very large wildland fires in Southern California, USA, *Atmos. Environ.*, *40*, 3686–3695, doi:10.1016/j.atmosenv.2006.02.016.

Cofer, W. R., E. L. Winstead, B. J. Stocks, L. W. Overbay, J. G. Goldammer, and D. Cahoon (1996), Emissions from boreal forest fires: Are the atmospheric impacts underestimated?, in *Biomass Burning and Global Change*, edited by J. S. Levine, pp. 834–839, MIT Press, Cambridge, Mass.

Davies, S. J., and L. Unam (1999), Smoke-haze from the 1997 Indonesian forest fires: Effects on pollution levels, local climate, atmospheric CO_2 concentrations, and tree photosynthesis, *For. Ecol. Manage.*, *124*, 137–144.

Debell, L. J., R. W. Talbot, J. E. Dibb, J. W. Munger, E. V. Fischer, and S. E. Frolking (2004), A major regional air pollution event in the northeastern United States caused by extensive forest fires in Quebec, Canada, *J. Geophys. Res.*, *109*, D19305, doi:10.1029/2004JD004840.

Dempsey, F. (2013), Forest fire effects on air quality in Ontario: Evaluation of several recent examples, *Bull. Am. Meteorol. Soc.*, *94*, 1059–1064.

Dennison, P. E., S. C. Brewer, J. D. Arnold, and M. A. Moritz (2014), Large wildfire trends in the western United States, 1984–2011, *Geophys. Res. Lett.*, *41*, 2928–2933, doi:10.1002/2014GL059576.

Ehleringer, J., A. J. Schauer, C.- T. Lai, D. R. Bowling, D. E. Pataki, and B. B. Stephens (2008), Long-term carbon dioxide monitoring in Salt Lake City, Eos Trans. AGU, Fall Meet. Suppl., Abstract B43D-0466.

Ehleringer, J., A. Moyes, C. Cook, D. Pataki, C.-T. Lai, and A. Schauer (2009), Long-term results from an urban CO_2 monitoring network, Eos Trans. AGU, Fall Meet. Suppl., Abstract B33D-0414.

Emmons, L. K., et al. (2010), Description and evaluation of the Model of Ozone and Related Chemical Tracers, version 4 (MOZART-4), *Geosci. Model Dev.*, *3*, 43–67.

European Commission (2009), Joint Research Centre/Netherlands Environmental Assessment Agency, Emission Database for Global Atmospheric Research (EDGAR), release version 4.0.

Finney, M. A., C. W. McHugh, I. C. Grenfell, K. L. Riley, and K. C. Short (2011), A simulation of probabilistic wildfire risk components for the continental United States, *Stochastic Environ. Res. Risk Assess.*, *25*, 973–1000.

Freitas, S. R., K. M. Longo, R. Chatfield, D. Latham, M. A. F. Silva Dias, M. O. Andreae, E. Prins, J. C. Santos, R. Gielow, and J. A. Carvalho Jr. (2007), Including the sub-grid scale plume rise of vegetation fires in low resolution atmospheric transport models, *Atmos. Chem. Phys.*, *7*, 3385–3398, doi:10.5194/acp-7-3385-2007.

Galanter, M., H. Levy, and G. R. Carmichael (2000), Impacts of biomass burning on tropospheric CO, NO_x, and O_3, *J. Geophys. Res.*, *105*(D5), 6633–6653, doi:10.1029/1999JD901113.

Generoso, S., I. Bey, J.-L. Attie, and F.-M. Breon (2007), A satellite- and model-based assessment of the 2003 Russian fires: Impact on the Arctic Region, *J. Geophys. Res.*, *112*, D15302, doi:10.1029/2006JD008344.

Gerbig, C., et al. (2003), Toward constraining regional-scale fluxes of CO_2 with atmospheric observations over a continent: 2. Analysis of COBRA data using a receptor-oriented framework, *J. Geophys. Res.*, *108*(D24), 4757, doi:10.1029/2003JD003770.

Gerbig, C., S. Korner, and J. C. Lin (2008), Vertical mixing in atmospheric tracer transport models: Error characterization and propagation, *Atmos. Chem. Phys.*, *8*, 591–602.

Giglio, L., J. Descloitres, C. O. Justice, and Y. J. Kaufman (2003), An enhanced contextual fire detection algorithm for MODIS, *Remote Sens. Environ.*, *87*, 273–282.

Giglio, L., T. Loboda, D. P. Roy, B. Quayle, and C. O. Justice (2009), An active-fire based burned area mapping algorithm for the MODIS sensor, *Remote Sens. Environ.*, *113*, 408–420.

Grell, G. A., and D. Devenyi (2002), A generalized approach to parameterizing convection combining ensemble and data assimilation techniques, *Geophys. Res. Lett.*, *29*(14), 1693–1696, doi:10.1029/2002GL015311.

Gurney, K. R., D. L. Mendoza, Y. Zhou, M. L. Fischer, C. C. Miller, S. Geethakumar, and S. de la Rue du Can (2009), High resolution fossil fuel combustion CO_2 emission fluxes for the United States, *Environ. Sci. Technol.*, *43*(14), 5535–5541, doi:10.1021/es900806c.

Hegarty, J., et al. (2013), Evaluation of Lagrangian particle dispersion models with measurements from controlled tracer releases, *J. Appl. Meteorol. Climatol.*, *52*, 2623–2637.

Hong, S.-Y., Y. Noh, and J. Dudhia (2006), A new vertical diffusion package with an explicit treatment of entrainment processes, *Mon. Weather Rev.*, *134*, 2318–2341.

Iacono, M. J., J. S. Delamere, E. J. Mlawer, M. W. Shephard, S. A. Clough, and W. D. Collins (2008), Radiative forcing by long- lived greenhouse gases: Calculations with the AER radiative transfer models, *J. Geophys. Res.*, *113*, D13103, doi:10.1029/2008JD009944.

Intergovernmental Panel on Climate Change (IPCC) (2013), *Climate Change 2013: The Physical Science Basis. Contribution of Working Group I to the Fifth Assessment Report of the Intergovernmental Panel on Climate Change*, edited by T. F. Stocker et al., 1535 pp., Cambridge Univ. Press, Cambridge, U. K., and New York.

Jaffe, D. A., and N. L. Wigder (2012), Ozone production from wildfires: A critical review, *Atmos. Environ.*, *51*, 1–10.

Jaffe, D. A., N. L. Wigder, N. Downey, G. Pfister, A. Boynard, and S. B. Reid (2013), Impact of wildfires on ozone exceptional events in the western, *U.S. Environ. Sci. Technol.*, *47*, 11,065–11,072.

Keane, R. E., J. M. Herynk, C. Toney, S. P. Urbanski, D. C. Lutes, and R. D. Ottmar (2013), Evaluating the performance and mapping of three fuel classification systems using Forest Inventory and Analysis surface fuel measurements, *For. Ecol. Manage.*, *305*, 248–263.

Kim, S., D. Millet, L. Hu, M. Mohr, T. Griffis, D. Wen, J. C. Lin, S. Miller, and M. Longo (2013), Constraints on carbon monoxide emissions in the United States based on tall tower measurements, *Environ. Sci. Technol.*, *47*, 8316–8324, doi:10.1021/es4009486.

Klass, D. L. (1998), *Biomass for Renewable Energy, Fuels, and Chemicals*, 651 pp., Academic Press, San Diego, Calif.

LANDFIRE (2014), LANDFIRE. [Available at http://www.landfire.gov/.]

Lareau, N. P., E. Crosman, C. D. Whiteman, J. D. Horel, S. W. Hoch, W. O. J. Brown, and T. W. Horst (2013), The persistent cold-air pool study, *Bull. Am. Meteorol. Soc.*, *94*, 51–63.

Lavouè, D., C. Liousse, H. Cachier, B. J. Stocks, and J. G. Goldammer (2000), Modeling of carbonaceous particles emitted by boreal and temperate wildfires at northern latitudes, *J. Geophys. Res.*, *105*(D22), 26,871–26,890, doi:10.1029/2000JD900180.

Lin, J. C., and C. Gerbig (2005), Accounting for the effect of transport errors on tracer inversions, *Geophys. Res. Lett.*, *32*, L01802, doi:10.1029/2004GL021127.

Lin, J. C., C. Gerbig, S. C. Wofsy, A. E. Andrews, B. C. Daube, K. J. Davis, and C. A. Grainger (2003), A near-field tool for simulating the upstream influence of atmospheric observations: The Stochastic Time-Inverted Lagrangian Transport (STILT) model, *J. Geophys. Res.*, *108*, D03161, doi:10.1029/2002JD003161.

Lin, J. C., D. Brunner, C. Gerbig, A. Stohl, A. Luhar, and P. Webley (2013), Lagrangian modeling of the atmosphere, *AGU Geophys. Monogr.*, *200*, 349.

Lin, Y.-L., F. D. Farley, and H. D. Orville (1983), Bulk parameterization of the snow field in a cloud model, *J. Appl. Meteorol.*, *22*(6), 1065–1092.

Liu, H., D. J. Jacob, I. Bey, and R. M. Yantosca (2001), Constraints from ^{210}Pb and ^{7}Be on wet deposition and transport in a global three-dimensional chemical tracer model driven by assimilated meteorological fields, *J. Geophys. Res.*, *106*(D11), 12,109–12,128, doi:10.1029/2000JD900839.

McKain, K., S. C. Wofsy, T. Nehrkorn, J. Eluszkiewicz, J. R. Ehleringer, and B. B. Stephens (2012), Assessment of ground-based atmospheric observations for verification of greenhouse gas emissions from an urban region, *Proc. Natl. Acad. Sci. U.S.A.*, *109*, 8423–8428, doi:10.1073/pnas.1116645109.

McKenna, D. S., P. Konopka, J.-U. GrooB, G. Gunther, and R. Muller (2002), A new Chemical Lagrangian Model of the Stratosphere (CLaMS) 1. Formulation of advection and mixing, *J. Geophys. Res.*, *107*(D16), 4309, doi:10.1029/2000JD000.

Mellor, G. L., and T. Yamada (1982), Development of a turbulence closure model for geophysical fluid problems, *Rev. Geophys. Space Phys.*, *20*, 851–875.

Mesinger, F., et al. (2006), North American regional reanalysis, *Bull. Am. Meteorol. Soc.*, *87*, 343–360.

Miller, S. M., et al. (2008), Sources of carbon monoxide and formaldehyde in North America determined from high-resolution atmospheric data, *Atmos. Chem. Phys.*, *8*, 7673–7679, doi:10.5194/acp-8-7673-2008.

Missoula Fire Laboratory (2013), Wildland fire potential. [Available at http://www.firelab.org/fmi/data-products.]
Mu, M., et al. (2010), Daily and 3-hourly variability in global fire emissions and consequences for atmospheric model predictions of carbon monoxide. *J. Geophys. Res.*, *116*, D24303, doi:10.1029/2011JD016245.
NASA's Jet Propulsion Laboratory (2011), Chemical kinetics and photochemical data for use in atmospheric studies. [Available at http://jpldataeval.jpl.nasa.gov/pdf/JPL%2010-6%20Final%2015June2011.pdf.]
Natunen, A., A. Arola, T. Mielonen, J. Huttunen, M. Komppula, and K. E. Lehtinen (2010), A multi-year comparison of $PM_{2.5}$ and AOD for the Helsinki region, *Boreal Environ. Res.*, *15*, 544–552.
Nehrkorn, T., J. Eluszkiewicz, S. C. Wofsy, J. C. Lin, C. Gerbig, M. Longo, and S. Freitas (2010), Coupled Weather Research and Forecasting-Stochastic Time-Inverted Lagrangian Transport (WRF-STILT) model, *Meteorol. Atmos. Phys.*, *107*, 51–64.
Nehrkorn, T., J. Henderson, M. Leidner, M. Mountain, J. Eluszkiewicz, K. McKain, and S. Wofsy (2013), WRF simulations of the urban circulation in the Salt Lake City area for CO_2 modeling, *J. Appl. Meteorol. Climatol.*, *52*, 323–340.
Pachon, J., R. Weber, X. Zhang, J. A. Muholland, and A. G. Russell (2013), Revising the source apportionment of $PM_{2.5}$, *Atmos. Pollut. Res.*, *4*, 14–21.
Park, R. J., D. J. Jacob, and J. A. Logan (2007), Fire and biofuel contributions to the annual mean aerosol mass concentrations in the United States, *Atmos. Environ.*, *41*, 7389–7400, doi:10.1016/j.atmosenv.2007.05.061.
Particulate Matter Science for Policy Makers (2003), A NARSTO Assessment. Parts 1 and 2. NARSTO Management Office. [Available at http://www.narsto.org/pm_science_assessment.]
Pataki, D. E., D. R. Bowling, and J. R. Ehleringer (2003), Seasonal cycle of carbon dioxide and its isotopic composition in an urban atmosphere: Anthropogenic and biogenic effects, *J. Geophys. Res.*, *108*(D23), 4735, doi:10.1029/2003JD003865.
Pataki, D. E., D. R. Bowling, J. R. Ehleringer, and J. M. Zobitz (2006), High resolution monitoring of urban carbon dioxide sources, *Geophys. Res. Lett.*, *33*, L03813, doi:10.1029/2005GL024822.
Peters, W., et al. (2007), An atmospheric perspective on North American carbon dioxide exchange: CarbonTracker, *Proc. Natl. Acad. Sci. U.S.A.*, *104*, 18,925–18,930, doi:10.1073/pnas.0708986104.
Potter, C. S., and S. A. Klooster (1997), Global model estimates of carbon and nitrogen storage in litter and soil pools: Response to change in vegetation quality and biomass allocation, *Tellus*, *49*, doi:10.1034/j.1600-0889.49.issue1.1.x.
Potter, C. S., E. A. Davidson, and L. Verchot (1996), Estimation of global biogeochemical controls and seasonality in soil methane consumption, *Chemosphere*, *32*(11), 2219–2246.
Potter, C. S., S. A. Klooster, and V. Brooks (1999), Interannual variability in terrestrial net primary production: Exploration of trends and controls on regional to global scales, *Ecosystems*, *2*, 36–48, doi:10.1007/s100219900056.
Reeves, H. D., K. L. Elmore, G. S. Manikin, and D. J. Stensrud (2011), Assessment of forecasts during persistent valley cold pools in the Bonneville basin by the North American Mesoscale model, *Weather Forecasting*, *26*, 447–467.
Reid, J. S., R. Koppmann, T. F. Eck, and D. P. Eleuterio (2005), A review of biomass burning emissions. Part II: Intensive physical properties of biomass burning particles, *Atmos. Chem. Phys.*, *5*, 799–825, doi:10.5194/acp-5-799-2005.
Riley, K. L., J. T. Abatzoglou, T. G. John, C. Isaac, A. E. Klene, and F. A. Heinsch (2013), The relationship of large fire occurrence with drought and fire danger indices in the western USA, 1984–2008: The role of temporal scale, *Int. J. Wildland Fire*, *22*(7), 894–909.
Ruefenacht, B., et al. (2008), Conterminous U.S. and Alaska forest type mapping using forest inventory and analysis data, *Photogramm. Eng. Remote Sens.*, *74*, 1379–1388.
Sapkota, A., J. M. Symons, J. Kleissl, L. Wang, M. B. Parlange, J. Ondov, P. N. Breysse, G. B. Diette, P. A. Eggleston, and T. Buckley (2005), Impacts of the 2002 Canadian forest fires on particulate matter air quality in Baltimore City, *Environ. Sci. Technol.*, *39*(1), 24–32.
Schaap, M., A. Apituley, R. M. Timmermans, R. B. Koelemeijer, and G. de Leeuw (2009), Exploring the relation between aerosol optical depth and $PM_{2.5}$ at Cabauw, the Netherlands, *Atmos. Chem. Phys.*, *9*, 909–925, doi:10.5194/acp-9-909-2009.
Sessions, W. R., H. E. Fuelberg, R. A. Kahn, and D. M. Winker (2011), An investigation of methods for injecting emissions from boreal wildfires using WRF-Chem during ARCTAS, *Atmos. Chem. Phys.*, *11*, 5719–5744, doi:10.5194/acp-11-5719-2011.
Shin, S., and S. Reich (2009), Hamiltonian particle-mesh simulations for a non- hydrostatic vertical slice model, *Atmos. Sci. Lett.*, *10*, 233–240.
Silcox, G. D., K. E. Kelly, E. T. Crosman, C. D. Whiteman, and B. L. Allen (2012), Wintertime PM2.5 concentrations in Utah's Salt Lake valley during persistent, multi-day cold-air pools, *Atmos. Environ.*, *46*, 17–24.
Skamarock, W., J. B. Klemp, J. Dudhia, D. O. Gill, D. M. Barker, M. G. Duda, X. Y. Huang, W. Wang, and J. G. Powers (2008), A description of the Advanced Research WRF Version 3, NCAR Technical Note, 126-126.
Smolarkiewicz, P., and J. A. Pudykiewicz (1992), A class of semi-Lagrangian approximations for fluids, *J. Atmos. Sci.*, *49*, 2082–2096.
Strong, C., C. Stwertka, D. R. Bowling, B. B. Stephens, and J. R. Ehleringer (2011), Urban carbon dioxide cycles within the Salt Lake Valley: A multiple-box model validated by observations, *J. Geophys. Res.*, *116*, D15307, doi:10.1029/2011JD015693.
Susott, R. A., W. F. DeGroot, and F. Shafizadeh (1975), Heat content of natural fuels, *J. Fire Flammability*, *6*, 311–325.
U. Foundation (2014), A snapshot of 2050: An Analysis of the projected population change in Utah, Research report 720.
U.S. Environmental Protection Agency (EPA) (2010), Review of evidence regarding claimed exceptional events leading to 24-hour $PM_{2.5}$ exceedances. [Available at http://www.epa.gov/ttn/analysis/docs/EPA%20technical%20support%20document%2033010.pdf.]
U.S. Environmental Protection Agency (EPA) (2011), National Ambient Air Quality Standards (NAAQS). [Available at www.epa.gov/air/criteria.html.]
U.S. Environmental Protection Agency (EPA) (2013), Interim guidance to implement requirements for the treatment of air quality monitoring data influenced by exceptional events. [Available at http://www.epa.gov/ttn/analysis/exevents.htm.]
Urbanski, S. P. (2013), Combustion efficiency and emission factors for wildfire-season fires in mixed conifer forests of the northern Rocky Mountains, U.S., *Atmos. Chem. Phys.*, *13*, 7241–7262.
Urbanski, S. P., W. M. Hao, and B. Nordgren (2011), The wildland fire emission inventory: Western United States emission estimates and an evaluation of uncertainty, *Atmos. Chem. Phys.*, *11*, 12,973–13,000, doi:10.5194/acp-11-12973-2011.
Utah's Division of Air Quality (UDAQ) (2012a), Utah 2012 air monitoring network plan. [Available at http://www.airmonitoring.utah.gov/network/2012AirMonitoringNetworkPlan.pdf.]
Utah's Division of Air Quality (UDAQ) (2012b), Exceptional event demonstration ozone exceedances at Beach, Brigham City, Harrisville and Hawthorne monitoring stations. [Available at http://www.airquality.utah.gov/Public-Interest/Public-Commen-Hearings/Docs/2013/10Oct/81212ozonereportv1.pdf.]
Utah's Division of Air Quality (UDAQ) (2013), Exceptional events—$PM_{2.5}$ from wildfire. [Available at http://www.airquality.utah.gov/Public-Interest/Public-CommenHearings/Docs/2013/08Aug/Septpmreport.pdf.]
van der Werf, G. R., J. T. Randerson, L. Giglio, G. J. Collatz, M. Mu, P. S. Kasibhatla, D. C. Morton, R. S. DeFries, Y. Jin, and T. T. van Leeuwen (2010), Global fire emissions, and the contribution of deforestation, savanna, forest, agricultural, and peat fires (1997–2009), *Atmos. Chem. Phys.*, *10*, 11,707–11,735, doi:10.5194/acp-10-11707-2010.

Wen, D., J. C. Lin, D. Millet, A. Stein, and R. Draxler (2012), A backward-time stochastic Lagrangian air quality model, *Atmos. Environ.*, *54*, 373–386, doi:10.1016/j.atmosenv.2012.02.042.

Westerling, A. L., H. G. Hidalgo, D. R. Cayan, and T. W. Swetnam (2006), Warming and earlier spring increases western U.S. forest fire activity, *Science*, *313*, 940–943.

Wiedinmyer, C., and J. C. Neff (2007), Estimates of CO_2 from fires in the United States: Implications for carbon management, *Carbon Balance Manage.*, *2*(10), doi:10.1186/1750-0680-2-10.

Wilson, B. T., C. W. Woodall, and D. M. Griffith (2013), Imputing forest carbon stock estimates from inventory plots to a nationally continuous coverage, *Carbon Balance Manage.*, *8*, doi:10.1186/1750-0680-8-1.

Wohltmann, I., and M. Rex (2009), The Lagrangian chemistry and transport model ATLAS: Validation of advective transport and mixing, *Geosci. Model Dev.*, *2*, 153–173.

Zhang, R., et al. (2013), Chemical characterization and source apportionment of $PM_{2.5}$ in Beijing: Seasonal perspective, *Atmos. Chem. Phys.*, *13*, 7053–7074, doi:10.5194/acp-13-7053-2013.

Zhang, X., A. Hecobian, M. Zheng, N. H. Frank, and R. J. Weber (2010), Biomass burning impact on PM $_{2.5}$ over the southeastern US during 2007: Integrating chemically speciated FRM filter measurements, MODIS fire counts and PMF analysis, *Atmos. Chem. Phys.*, *10*, 6839–6853, doi:10.5194/acp-10-6839-2010.